RELIABILITY OF MARINE STRUCTURES IN THE CONTEXT OF RISK BASED DESIGN

by

Ângelo Manuel Palos Teixeira

Thesis submitted for the Degree of Master of Science in the

Faculty of Engineering in Glasgow University

Department of Naval Architecture and Ocean Engineering

University Glasgow

November, 1997

ProQuest LLC.
789 East Eisenhower Parkway
P.O. Box 1346
Ann Arbor, MI 48106 – 1346

To the memory of my father

Amândio

DECLARATION

Except where reference is made to the work of others,
this thesis is believed to be original

ACKNOWLEDGEMENTS

This work was carried out at the Department of Naval Architecture and Ocean Engineering, University of Glasgow and at the Instituto Superior Técnico, Universidade Técnica de Lisboa.

This study has been undertaken as a part of the projects SHIPREL "Reliability Methods for Ship Structural Designs and OFSOS "Optimized Fire Safety of Offshore Structures", which have been partially funded by the European Commission under the BRITE/EURAM program. The technical contribution of all partners is gratefully acknowledged.

I wish to express my sincere gratitude to Professor C. Guedes Soares and Dr. P.K. Das for their valuable guidance, advice and support throughout the duration of my study.

Thanks are also given to Mr. J.M. Gordo for his generous help at various levels of my research.

I also would like to thank the Junta Nacional de Investigação Científica, who provided me with the necessary financial support during my research.

Finally, I would like to express my gratitude to all my family members, especially to my wife Marta Teixeira.

CONTENTS

LIST OF FIGURES

LIST OF TABLES

SUMMARY

The aim of this thesis is to establish the suitability of the theory of structural reliability as the appropriate tool to establish the notional probability of failure for different structural designs with respect to the same adverse state in the context of risk based design.

In chapter 1 the problem is introduced by a brief presentation of some accident statistical data on total losses of the world merchant fleet. The analysis of this data shows that only an overall risk model can explain the difference between the real and the notional safety levels, which are estimated from the structural reliability theory.

Although a safety index can make no claim of representing an absolute measure of the probability of failure, it can be included in an overall risk model providing an efficient mean of comparing the safety levels of different structures. In this context, two examples of integration between risk and reliability analysis are then presented.

Chapter 2 reviews the development of the methods suggested by a number of writers in recent years for the calculation of an "index of reliability" and the associated estimates of failure probability.

In chapter 3 the methods of structural reliability are used to assess the reliability of the primary ship structure of four tankers with respect to the ultimate collapse moment. The stochastic model of still water bending moment is defined for one individual voyage based on available data from general ship statistics. The evaluation of the wave induced load effects that occur during long-term operation of the ship in the seaway is carried out for the North Atlantic.

A more rigorous formulation of the reliability problem is defined by requiring that the structure is safe under the combined maximum of still water and wave induced bending moment that occurs in a reference period. The reliability results using these two formulations are compared showing that these formulations can be related to each other and the choice of one or the other is a matter of standardisation in order to allow the ship structures to be compared.

The results of the reliability analyses are used to assess the partial safety factors that can be applied in a probabilistic based design rule for a defined target safety level. As an example, the design formula is used to redesign the midship section of one of the sample

ships in order to meet the target failure probability considered in the rule development process.

The reliability formulation is also applied to different ship types with the objective of achieving indications in the safety levels of the different designs. The reliability results of one containership and two different designs of a bulk carrier are compared with the ones obtained for tankers.

Additionally, the variability in notional reliability levels that result from the ships being subjected to different wave environments in European coastal waters is quantified.

In chapter 4 a reliability formulation is proposed for thermally insulated plates subjected to pool fires. The basic features of the fire model, of the heat transfer through the passive protection and of the collapse temperature of plates are described.

A systematic study on plate collapse under heat loads with uniform distribution in the plate was performed using a non-linear finite element code that accounts for the elasto-plastic behaviour and for the changes in the material properties. The load-shortening behaviour of plates with different aspect ratios, slenderness and initial imperfections are presented.

Since plate elements are part of a structure, its boundary conditions are far from being fixed. This effect is studied using elastic supports as well as localised heat loads.

The basic mechanisms that influence the shape of the flame of a pool fire are described and a first order second moment approach is used to quantify the uncertainty of the heat loads and to describe the importance of the governing variables in the limit state function. The limit state function is defined in terms of steel temperature and the reliability index is determined by a time independent first order method. An example of the reliability analysis of a fire wall protected with insulation is provided.

A different reliability formulation is defined when the heat load is not applied to the whole plate surface, but instead is localised in area. In this case the plates are able to sustain additional in-plane compressive loads before collapse. Therefore, it is appropriate to formulate the reliability problem in terms of stresses because this is the condition that will govern collapse. Calculations are presented concerning the effect of the different parameters on the reliability of plates, and in particular the effect of the size of the heated area is quantified.

CHAPTER 1
INTRODUCTION

During the last decade, structural reliability methods have found a wide range of applications to designs governed by quantities that exhibit variability or uncertainty by nature. Most of the developments in the methods of assessing the structural reliability have occurred in the civil engineering field. However, the modelling and the type of analysis have been applied to ship and offshore structures.

In the marine field, the reliability theory has been applied for the prediction of structural safety of various types of vessels and installations. Two different approaches to structural reliability can be identified. On one hand, there are attempts to assess the overall levels of failure rate of the structures based on the analysis of accident data. On the other hand, the reliability theory has been applied to derive indications of the notional safety levels of structural components and systems.

The analyses of the ship accident statistics have shown that the majority of the accidents can be traced to human or organisational errors. Only about 20% of the catastrophic accidents are caused by structural or mechanical failures of the vessel under extreme environmental conditions exceeding the life design loads.

In fact only in recent years it became clear that the formulation of the safety problem should take into account accident scenarios in order to improve the safety of the ship operations as well as to explain the difference between the notional and the real safety levels.

Risk analysis is the common designation within the marine industry to indicate the reliability studies that account for all possible failure modes. This is intended to distinguish them from the structural reliability studies, which consider only failures of the structure resulting from the excessive service loads or from too low structural strength.

In fact, a unified fully probabilistic model for marine safety can be achieved by integrating Quantified Risk Analysis that uses all the available statistical data with the modern methods of structural reliability analysis. This approach to total risk analysis is easy to state but difficult to implement when dealing with a large number of failure modes.

1.1 ACCIDENT STATISTICS

The analysis of the statistical data on total losses of the world merchant fleets allows the quantification of the real safety levels for different ship types as well as the main modes of failure.

Several organisations conduct analyses and publish regular statistical updates of maritime casualties. For instance, the Lloyds Maritime Information Services (LMIS) publishes "World Maritime Casualty Statistics", a statistical update of all major maritime casualties in the world. Agencies such as the UK Department of Transport's Maritime Accident Investigation Branch (MAIB) and the Institute of London Underwriters (ILU) issue such updates based on data collected by them. Other than Lloyds Register, classification societies such as Det norske Veritas conduct their own statistical updates of maritime casualties, which they use mostly for their own internal purposes. The use of bulk carrier casualty statistics to support the recent guidelines of the International Maritime Organisation (IMO) and of the International Association of Classification Societies (IACS) on bulk carrier safety is one example.

In this section, a brief overview of ship safety is presented based on the analysis of the description of all accidents between 1983 and 1993 reported by Lloyds Register of Shipping.

From 1983 to 1993, there has been a very welcome drop in the number of marine accidents as illustrated in figure 1.1. In fact, ship safety standards have been raised by a common effort of ship owners, insurers, classification societies as well as regulatory bodies.

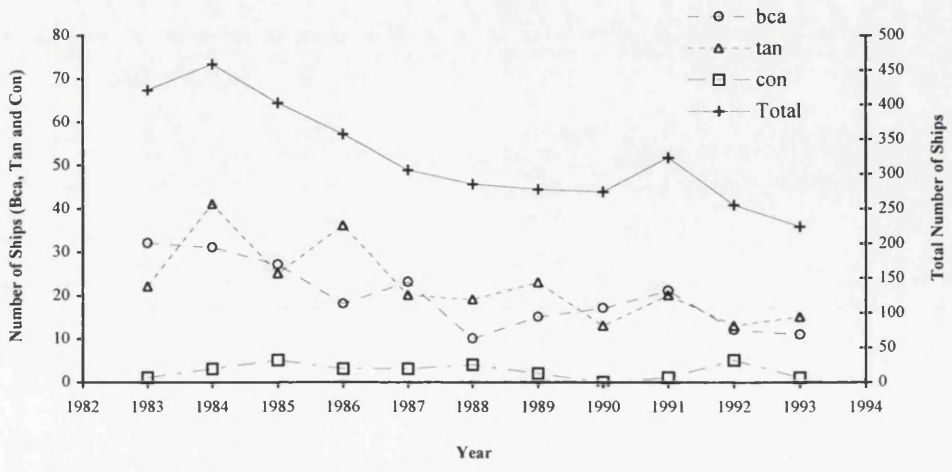

Figure 1.1: Total number of ship accidents

It can be also seen that the number of marine accidents with tankers (tan) and bulk carriers are larger than the number of accidents with containerships (con). However, bulk carriers have typically a very high number of lives lost in fatal accidents, which indicate that the consequences of bulk carrier casualties are more severe than for other ship types.

In order to investigate whether the ship type influences the probability of having an accident, data on the composition of the world fleet is required. Figure 1.3 shows the frequency of occurrence of accidents for different ship types calculated based on the information of the size and composition of the world fleet illustrated in figure 1.2 for tankers, bulk carriers and containerships.

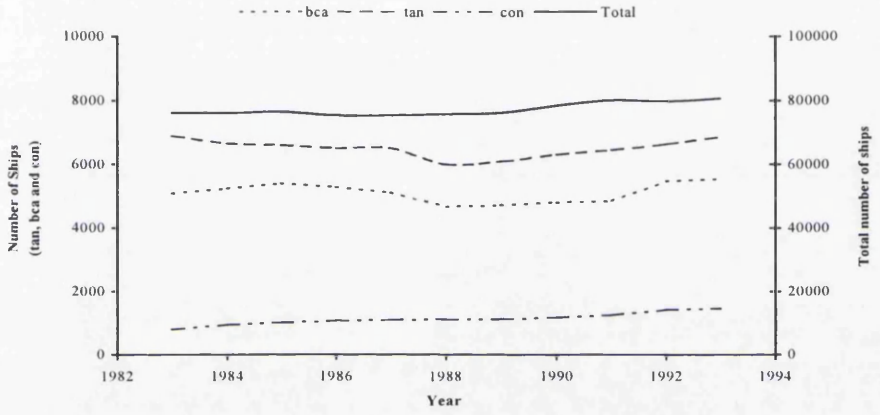

Figure 1.2: Composition of the world fleet

From figure 1.3, it can be seen that the annual accident frequencies have varied considerably, which must be expected due to the low number of accidents per year. However, there is a trend of decreasing rates of accidents in the period under consideration. In 1993 the annual rates of accidents are 0.0022 and 0.0020, respectively for tankers and bulk carriers while for containerships this value is around 0.0007.

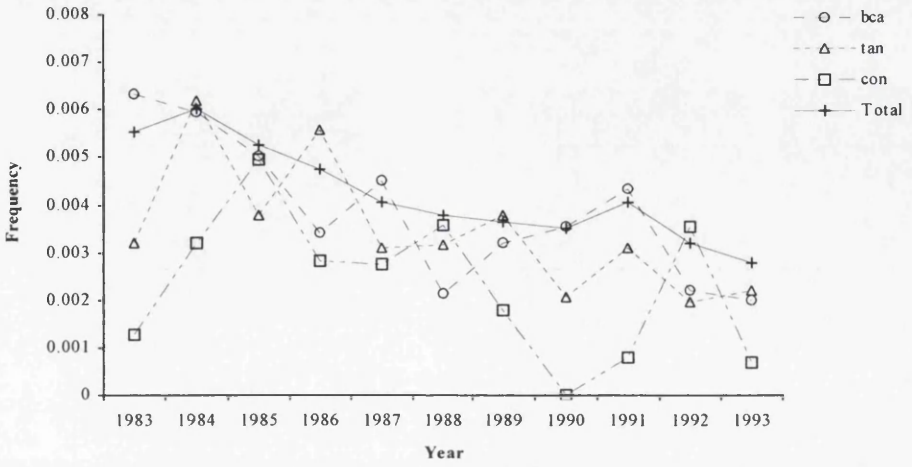

Figure 1.3: Frequency of occurrence of accidents for different ship types

The analysis of the dependency of marine accidents on ship age is illustrated in figure 1.4. As would be expected the age of the vessel influences her probability of being involved in an accident. The number of accidents steadily grow with the ship age from the 0-4 year category to the > 20 years of age.

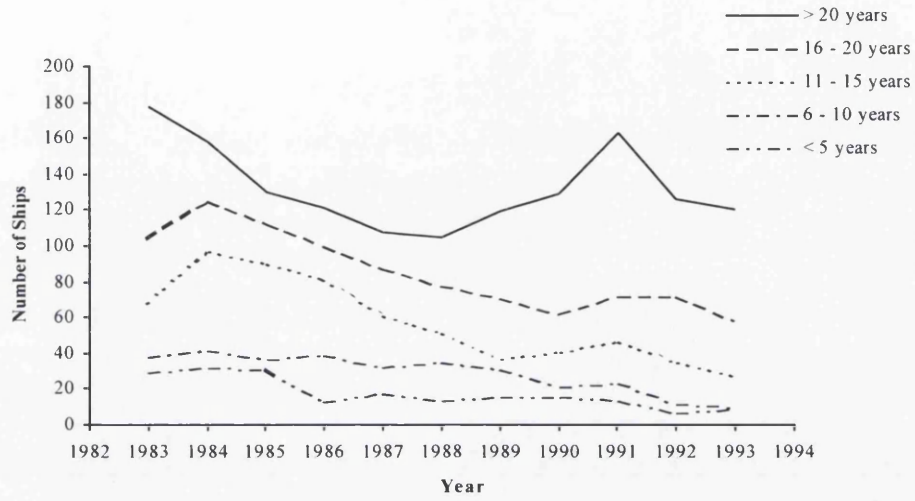

Figure 1.4: Distribution of number of accidents by ship age

In addition to the quantification of the safety levels for different ship types, the analysis of accident statistics allows the distribution of the accidents by the most common type of accidents. In the present analysis, an accident is described by the first and the last event. The former event is important due to its proximity to the cause of the accident, while the latter event basically describes the consequence of the accident.

Figure 1.5 presents the distribution of first and last event by the type of accident. The most common type of first events are grounding, fire/explosion and foundering followed by contact/collision. Most of the accidents end up with foundering.

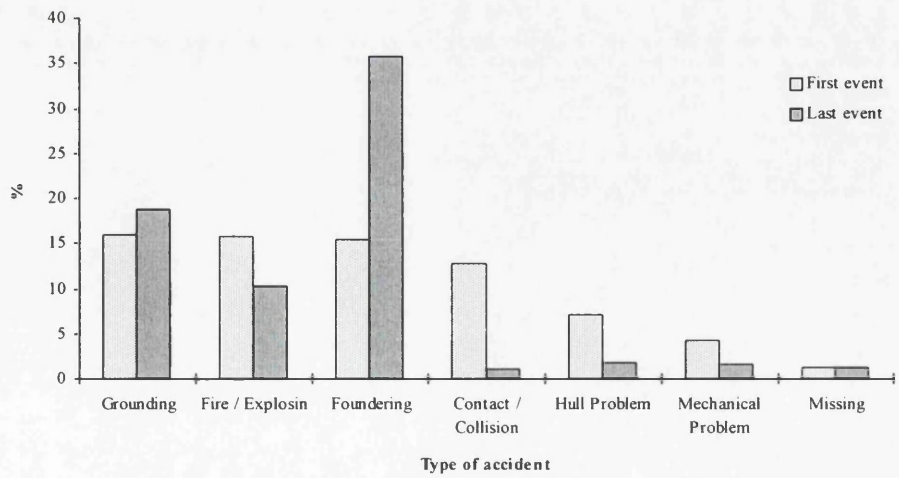

Figure 1.5: Distribution of first and last events by the type of accident

It should be noted that the initial cause "hull problem" is strictly related to structural failure, which is not a consequence of other accidental situations such as collision or grounding. The accident code "hull problem" includes the events "broke", "broke in two/three", "burst", "corroded", "cracked" and "damaged".

Figure 1.6 illustrates the evolution of the first event, which can be considered the main cause of the accident. These smoothed curves were obtained by interpolation of the annual frequencies of accidents.

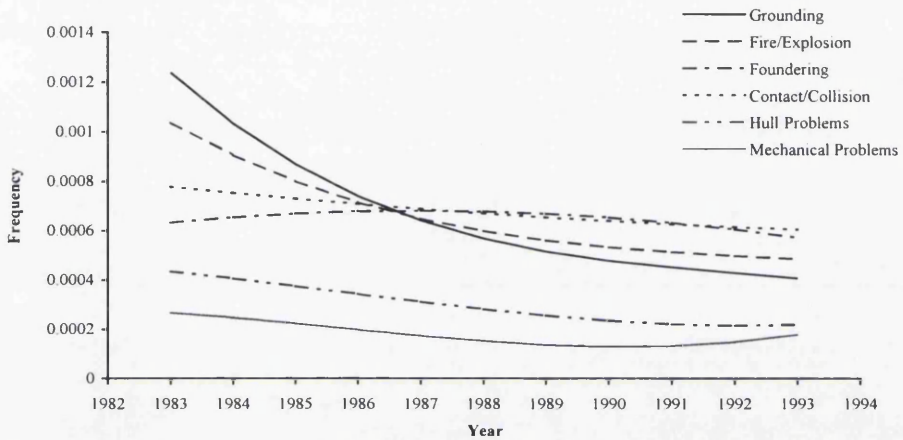

Figure 1.6: Evolution of the frequency of occurrence of the first event

As one can see there is a trend of decreasing rate of accidents due to grounding and fire/explosion. The frequencies of accidents caused by mechanical and hull problems have also decreased but not as much. Additionally, the accident rates due to contact and collision are almost constant from 1983 to 1993.

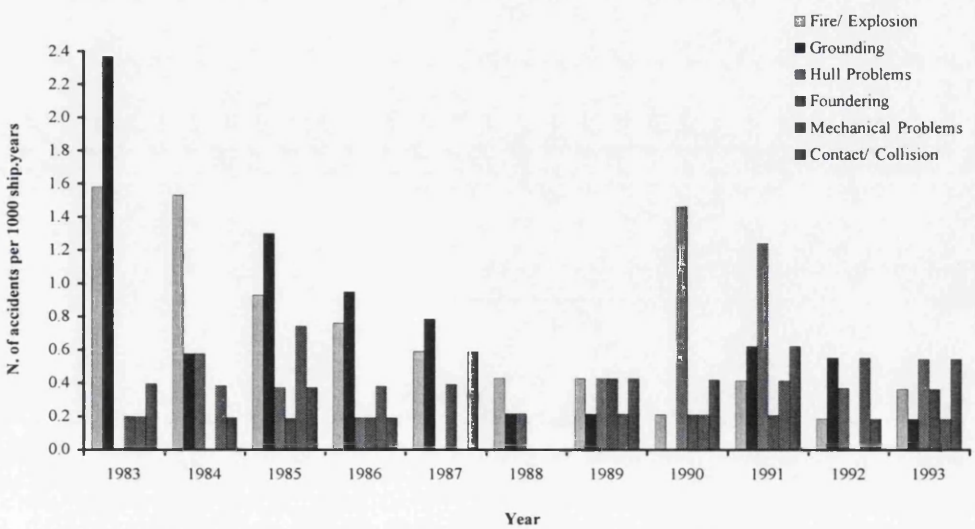

Figure 1.7: Annual rate of accidents for bulk carriers

From the reliability point of view, the statistics of interest are the number of the different initial causes of accidents that have occurred for a particular class of ships. This information is presented in figures 1.7 and 1.8 for bulk carriers and tankers, respectively.

It can be seen that grounding and fire/explosion were the most common type of first events in the period from 1983 to 1988. However in the nineties, hull problems in bulk carriers have been identified as the dominant cause of accidents.

From the analysis of figure 1.8, one can conclude that fire/explosion is by far the most important initial cause of accidents in tankers which has probability of occurrence of 1.0×10^{-3}/year for the first three years of the nineties.

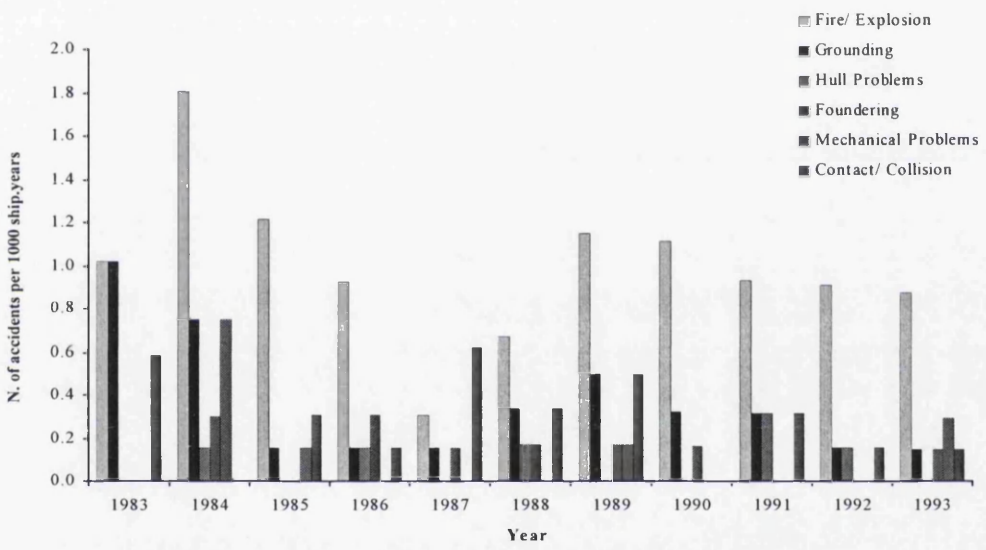

Figure 1.8: Annual rate of accidents for tankers

Table 1.1 and figure 1.9 show the average rate of the different initial causes of accidents for bulk carriers, containerships and tankers. These values were estimated based on the annual frequencies in the period from 1983 to 1993. Fire/explosion is the dominant mode of failure for tankers, while grounding, fire/explosion and hull problems are important initial causes of accidents for bulk carriers.

Table 1.1
Distribution of the annual average rate of accidents by ship type

Initial Event	Annual average rate of accidents per 1000 ships		
	Bulk Carriers	Containerships	Tankers
Fire/ Explosion	0.6728	0.4300	0.9922
Contact/ Collision	0.3565	0.2657	0.2809
Grounding	0.7042	0.2124	0.3620
Foundering	0.1969	0.1686	0.1272
Mechanical Problems	0.2968	0.1777	0.1237
Hull Problems	0.4892	0.1265	0.0848

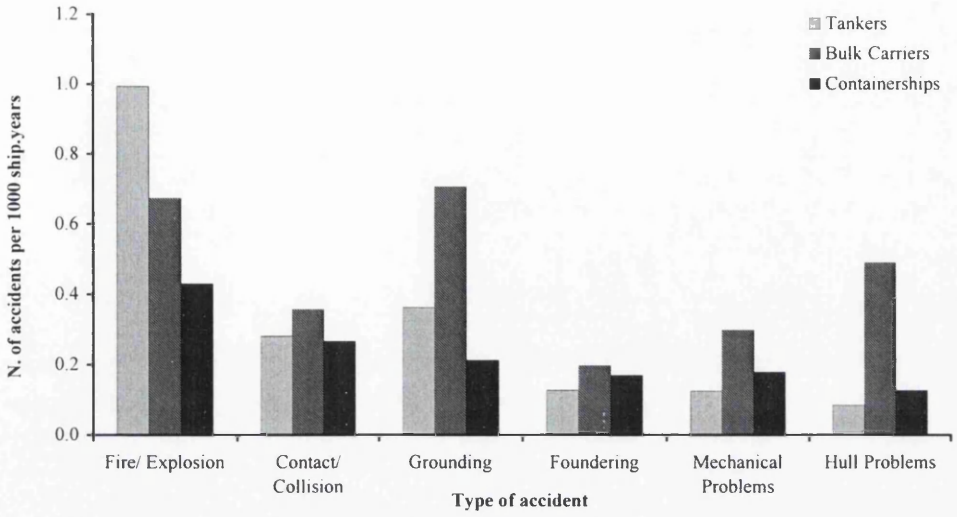

Figure 1.9: Distribution of annual average rate of the first event by ship type

It should be noted that the annual rate of accidents due to fire/explosion and grounding have decreased from 1983 to 1993 as illustrated in figure 1.6. Therefore, the average annual rate for these two initial causes of accidents given in table 1.1 can be overestimated when compared to current values. This fact increases the importance of other initial causes such as contact/collision for all ship types and hull problems especially in bulk carriers.

1.2 STRUCTURAL RELIABILITY WITHIN A RISK BASED METHODOLOGY

1.2.1 Risk Analysis

Risk analysis can be defined as a systematic approach to the identification and evaluation of factors that may lead to accidents. Furthermore, risk analysis can provide an overall picture of the hazards within a system as well as quantitative measures of certain types of risks that can be used for comparative studies.

To emphasise that an analysis is quantitative, the terms Probabilistic Risk Analysis (PRA) or Quantitative Risk analysis (QRA) are frequently used. In these cases the risk is estimated by combining the probability of occurrence of an undesired event and its consequences.

Although the subject risk analysis has began to take increased importance in the later half of the 1970's, nowadays the term risk analysis is not well established and the interpretations of what an analysis should consist of may vary.

In the marine industry, risk analysis is the designation that has become common to indicate the reliability studies that account for all possible failure modes. This is intended to distinguish them from the structural reliability studies, which consider only failures of the structure resulting from excessive service loads or from too low structural strength.

The risk analysis has been more commonly applied to offshore structures than to ship structures. This is probably a result of the fact that offshore structures made their appearance at a time when the profession was more aware of probabilistic concepts.

A Risk analysis is not a single activity, but consists of a number of co-ordinated steps, which jointly make up a procedure. Figure 1.10 provides one example of the main steps involved in the risk analysis.

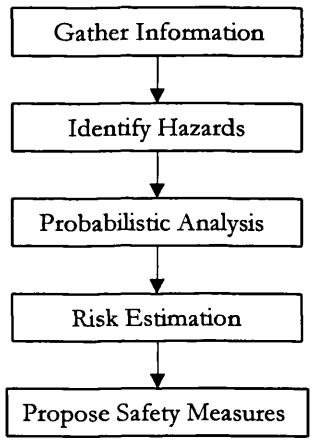

Figure 1.10: Stages of risk analysis

The first step involves the collection of information about the system. This applies to its technical design, how the system functions and which activities are undertaken. Various types of information on the problem can be utilised. Historical information, possibly obtained by consultation of databases, or interviews with people involved, may be useful. Within a probabilistic analysis, data on the frequencies of failure for system and components are also needed.

Identification of hazards that might lead to accidents is a central component of most risk analysis. One aim should be to discover the major sources of danger and failure modes that might trigger off an accident based on all the information available.

In the conventional Probabilistic Risk Analysis (PRA), methods of reliability engineering, including fault tree or event tree analysis, are used to quantify the probabilities of accidental scenarios.

The frequencies of the majority of the events in the logic tree are estimated based on statistical data that ensures that all relevant failure modes are included if the data is sufficiently extensive. However, this approach can not be applicable to structures for which historical data is not available. In this case, the structural reliability analysis can be used to estimate the probability of failure of the failure modes of each structural component. Furthermore, it is often required to continue the analysis from the component to the system level.

Finally risk measures should be obtained by combining the probability of occurrence of the hazard with its consequences. On the basis of these values, an evaluation is then made to decide whether the risk is acceptable or safety measures are necessary.

In general by acting on either the probability of occurrence of the hazard or the consequent damages, the risk level can be reduced. To achieve this aim, potential strategies may be followed (Ferry Borges, 1991):

- eliminating or avoiding the possible occurrence of the hazard at the origin,
- avoiding the hazard acting in the system, e.g. by modifying the project concept,
- controlling or reducing the losses, e.g. by adopting safety measures,
- adopting a design which corresponds to a sufficiently small risk,
- accepting the possibility of occurrence of the losses and preparing to reduce its consequences.

In the marine field several examples of strategies to reduce risk can be identified. The safety of offshore structures against fire is one example. The probability of the occurrence of a significant fire can be influenced by installing sprinklers and detection devices. However if the fire is already developed, the structure will be exposed to severe heating, causing its temperature to rise and its strength to decrease in a short time. At this stage a passive fire protection (PFP) should be used to limit the temperature in the structural members in order to prevent the total collapse of the structure in the period of evacuation.

1.2.2 Examples of integration between risk and reliability analysis

Safety of shipping

Analyses of accident statistics for all ship types have shown that the risk to shipping results from the contribution of different hazards such as collision, grounding, fires, structural failures and others.

In general the major events occur because of failure to comply with established procedures often during the operation of the structure but also during its design and construction.

The overall objective of risk analysis in this field is to increase the safety of shipping by analysing the underlying factors that contribute to the accident risk levels. This can be achieved by detailed evaluation of a range of critical functions defined for those who are involved in the shipping activity.

The risk assessment can be performed on the basis of accident statistics, which allows the quantification of the overall safety levels and of the main mode of failure. However there is also a need to quantify the effect of new actions, rules and regulations in the safety levels of shipping before accident data become available.

As concerned to ship operation, simulators can be used as a laboratory to establish the safety effects of training schemes, new bridge equipment, communication procedures and manoeuvring capabilities. While that the structural reliability methods are capable of assessing the effect on the safety levels that result from different ship types as well as different actual concepts.

In addition, the structural reliability can be used to quantify the changes in the notional risk for different operational scenarios. This information is particularly useful in the definition of an overall risk model that accounts for the different sources of accidents as well as their geographical variability.

Fire safety

The regulations in force in Norway and UK concerning the operation of offshore platforms in the North Sea, have adopted a goal-setting approach which leaves the operators with the task to demonstrate that their installations have a risk level as low as reasonably practicable. Furthermore the Cullen report on the 1988 Piper Alpha accident

(Department of Energy, 1990) raised the awareness of the community about the risks that fire represents for an offshore platform.

As a direct result of the subsequent accident inquiry, the offshore safety case regulations SI 2885 (Offshore Installations (Safety Case) Regulations, 1992) were introduced in May'93. The regulations require that, for the hazards of explosion, fire heat, smoke, toxic gas and fumes, the risk to people on the installation should be reduced to as low as reasonably practicable. To determine whether or not the risks are as low as reasonably practicable, a quantified risk analysis should be made. This process is concerned with identifying all the potential major accident events, and analysing them so as to determine their frequencies and consequences in order to assess the risks involved (Shetty et al., 1996).

The initiation event normally generates the link between classical risk and reliability analysis. In this way risk analysis may be the appropriate tool to assess the probability of a special loading event such as a pool fire, jet fire or an explosion.

The event tree is then used to identify and quantify the probabilities of accident scenarios by tracing the possible sequences of events by which an initiating event could develop into a major accident with considerable consequences.

The consequences of such accidental events are usually represented by an event tree, which has many different types of components that can fail. Some of them are clearly structural elements, whose failure will allow the propagation of the fire to adjacent compartments.

In the modelling of escalation events, probabilities of failure of a number of components and systems such as module support frame and fire/ballast walls need to be evaluated. At this stage the structural reliability can be used to evaluate the probabilities of those events for which historical data are not available.

In fact, the theory of structural reliability is the appropriate tool to assess the probability of failure of structural components by taking into account the uncertainties in the fire and heat transfer models as well in the methods of non-linear structural analysis.

CHAPTER 2
STRUCTURAL RELIABILITY THEORY

Until about 1960, the structural engineering profession was dominated by deterministic thinking and the pioneering work in the theory of structural reliability was largely ignored. Several reasons can explain the lack of interest in probabilistic design. First, deterministic design was enough to absorb the attention of the engineers, the structural failures were few and when they occurred they could be attributed to human error as a matter of routine. Moreover, probabilistic design seemed cumbersome; the theory was intractable mathematically and numerically. Finally, few data were available, certainly not enough to define the distributions of load and strength.

During the period from 1966 to 1974, there was a rapid growth of academic interest in structural reliability theory and a growing acceptance by engineers of probability based structural design.

The major contribution to structural reliability is due to Freudenthal et al. (1966). The basic aspects of the proposed formulation is that the strength of the structure is made dependent on only one load (L) and one resistance variable (R) that are described by their probability density functions. The measure of safety is provided by the probability of failure:

$$P_f = \int_0^\infty \int_0^l f_R(r) f_L(l)\, dr\, dl = \int_0^\infty F_R(l) f_L(l)\, dl \qquad (2.1)$$

where f and F are the density and the cumulative distribution functions of the variables.

The real structural systems are usually modelled in terms of n basic variables $X=(x_1, x_2, \ldots x_n)$. For a considered limit state $G(x_1, x_2, \ldots x_n) = 0$, the possible realisations of X can be separated in two sets, namely the safety set $G(X)>0$ and the failure set $G(X)<0$. The hypersurface, which divides the n-dimensional space in two, is called the "limit state surface" or "failure surface". Without using excessive numerical effort, it is necessary to assess the failure probability,

$$P_f = \int_{G(X)\le 0} f_{x_1,\ldots,x_n}(x_1,\ldots,x_n)\, d\, x_1,\ldots,x_n \qquad (2.2)$$

The generalisation to several load and resistance variables only implies one additional integration for each variable. However, the computational problems in the numerical evaluation of these multiple integrals remained unsolvable for about 20 years. These difficulties have only recently been solved by using approximate integration methods generally called advanced Level II methods that involve iterative procedures to obtain an approximation to the failure probability.

2.1 THE CORNELL RELIABILITY INDEX

The initial development of Level II methods is due to Cornell (1969). He proposed a reliability measure for linear failure functions and independent normal basic variables. The principal idea is that each basic variable in a limit state equation can be characterised in terms of its expected values and covariances, i.e., the first and second moments of the their probability distributions. The measure of safety is provided by the reliability index:

$$\beta = \frac{\mu_G}{\sigma_G} \tag{2.3}$$

where μ_G and σ_G are the expectation and the standard deviation of the safety margin G.

If the basic variables are independent normally distributed and the failure surface is a hyperplane the probability of failure is defined by:

$$P_f = \Phi\left(-\frac{\mu_G}{\sigma_G}\right) = \Phi(-\beta) \tag{2.4}$$

where Φ is the normal distribution function.

This definition is geometrically illustrated in figure 2.1 for a limit state equation $G(R,L) = R - L$, where R is the resistance of a structure and L is the load. With each variable being normally distributed, the corresponding limit state will be normally distributed. The mean and variance of the limit state can be calculated by:

$$\mu_G = \mu_R - \mu_L \tag{2.5}$$

$$\sigma_G^2 = \sigma_R^2 - \sigma_L^2 \tag{2.6}$$

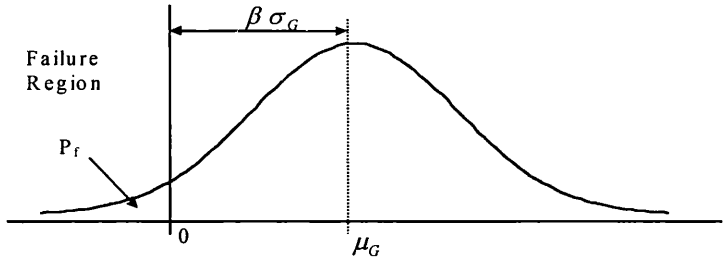

Figure 2.1: Illustration of the Cornell reliability index β

2.2 PROBLEM OF INVARIANCE

A common problem in the reliability measure defined by Cornell is the 'lack of invariance'. This phenomenon occurs due to relationship between load and resistance variables. A given limit state equation expressed in different ways can lead to different measures of reliability index for exactly the same problem.

The reliability index defined by Cornell in equation 2.3 is not invariant with respect to the choice of failure function (Ditlevsen, 1973). Cornell's estimate of reliability index for a non-linear failure function requires a linearization assumption about a given point. The most straightforward idea, which has been used repeatedly in the reported reliability investigations, was to linearize at the mean point of the basic variables.

The choice of linearization point is of vital importance to the validity of the reliability index. An alternative expansion point on the failure surface, where $G(X) = 0$, is sought to reduce this 'lack of invariance'.

2.3 THE HASOFER AND LIND RELIABILITY INDEX

Hasofer and Lind (1974) extended the concept of reliability index to the multi-variable case and solved the invariance problem.

They proposed a nonhomogeneous linear mapping of the set of basic variables into a set of normalized and uncorrelated variables X'. The transformation can be written as:

$$x_i' = \frac{x_i - \mu_i}{\sigma_i} \tag{2.7}$$

In standard normal space, the Hasofer and Lind reliability index β_{HL}, is defined as the shortest distance from the origin to a point on the failure surface. This point x'^* is referred to as the 'design' or 'failure' point, and is illustrated in figure 2.2.

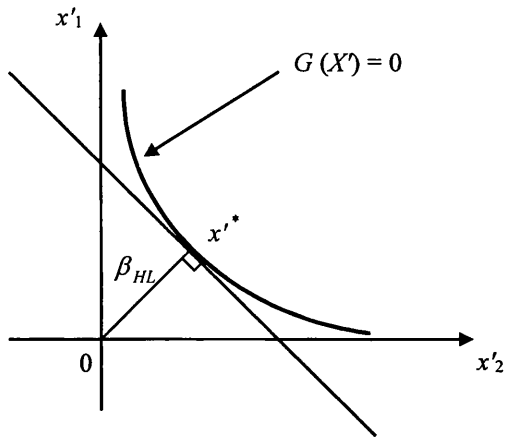

Figure 2.2: Definition of the Hasofer and Lind reliability index in standard normal space

The Hasofer and Lind reliability index is therefore defined by the equation:

$$\beta_{HL} = \frac{\mu_{G_{HL}}}{\sigma_{G_{HL}}} = \frac{-\sum_{i=1}^{n}\left(x_i'^{*}\right)\left(\frac{\delta G(X)}{\delta x_i'}\right)_{x_i'^{*}}}{\sqrt{\sum_{i=1}^{n}\left(\frac{\delta G(X)}{\delta x_i'}\right)^2_{x_i'^{*}}}} \tag{2.8}$$

The characteristics of this first order reliability approach prove advantageous in terms of sensitivity analysis of the variables. The measure of sensitivity indicates the relative importance of each variable within a given limit state function. Thus, sensitivity factors α_i^* are defined such as:

$$\beta_{HL} = -\sum_{i=1}^{n} x_i'^{*}\alpha_i^{*} \tag{2.9}$$

$$\alpha_i^{*} = \frac{\left(\frac{\delta G(X)}{\delta x_i'}\right)_{x_i'^{*}}}{\sqrt{\sum_{i=1}^{n}\left(\frac{\delta G(X)}{\delta x_i'}\right)^2_{x_i'^{*}}}} \tag{2.10}$$

The design point $x_i'^{*}$, which corresponds to the minimum distance from the origin to a point on the failure surface, is determined solving the minimisation problem:

$$\beta_{HL} = \min\left(\sum_{i=1}^{n}\left(x_i'\right)^2\right)^{1/2} \text{ with the constrain } G\left(x_i'\right) = 0 \tag{2.11}$$

2.4 COMPARATIVENESS IN RELIABILITY ESTIMATION

One of the crucial properties of reliability estimation should be the comparativeness. The concept of a reliability index allows comparisons to be made between the reliabilities of various and different structures. Structures can be ordered in terms of their reliability indices, and it is important that this ordering is consistent

Whenever the limit surfaces are not hyperplanes, the Hasofer-Lind index will not distinguish limit surfaces that have the same minimum distance to the origin, which was called lack of comparativeness (Ditlevsen, 1979). Figure 2.3 illustrates different failure surfaces obtained for structures *a*, *b*, *c* and *d*. The Hasofer-Lind index is illustrated clearly as the distance between the origin in standard normal space and the failure surface.

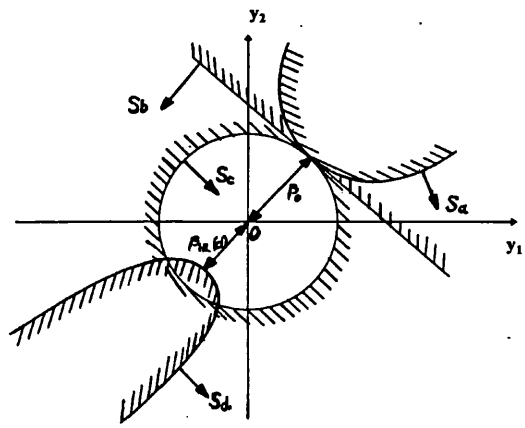

Figure 2.3: Illustration of the lack of comparativeness

Structures *a*, *b*, *c* and *d* have failure sets S_a, S_b, S_c and S_d, respectively. For the structures *a*, *b* and *c* the Hasofer and Lind reliability index maintains the same value. Simply by observing the limit state failure surfaces it can be seen that structure *a* is more reliable than structure *b*, which in return is more reliable than structure *c*.

Hasofer and Lind's safety index estimate is independent of the curvature of the failure surface. Therefore, a more selective definition of reliability index is required.

2.5 THE GENERALIZED RELIABILITY INDEX

An alternative reliability index was proposed by Ditlevsen (1979). By introducing a weight function $\psi_n(x)$ in standard-normal space, a measure of the reliability γ is then obtained by integrating this weight function over the safe set *S*,

$$\gamma = \int_S \psi_n(x)\, dS \tag{2.12}$$

For convenience Ditlevsen chose the standardised n-dimensional normal probability density function:

$$\psi_n(x_1, x_2 \ldots\ldots, x_n) = \phi(x_1)\phi(x_2)\ldots\ldots\ldots\phi(x_n) \tag{2.13}$$

The generalized reliability index β_G is defined as a monotonically increasing function of γ:

$$\beta_G = \Phi^{-1}(\gamma) = \Phi^{-1}\left(\int_S \phi(x_1)\phi(x_2)\ldots\ldots\ldots\phi(x_n) \right) \tag{2.14}$$

The normal density function is introduced purely to extend the definition of reliability index to structures with non-linear surfaces, thus allowing for a more consistent selective measure of reliability. However, the evaluation of the generalized reliability index is much more involved than the evaluation of β_{HL}. Furthermore, the numerical values of β_{HL} and β_G are almost coinciding in most cases of practical relevance.

2.6 NORMAL TAIL APPROXIMATION

The formulation of the generalized reliability index is based only on a second moment description of normally distributed design variables. In reality, for a given number of n-variables, additional data may be available concerning the nature of some or all of these variable distributions.

If the design variables are not normally distributed, there are significant differences in the reliability index as a result of the differently shaped tails of the distributions. Whenever additional information is available about the distribution type of design variables, it can be incorporated in the analysis by an approximate procedure that adjusts the distribution in the tails.

The procedure that has received widespread acceptance, due to Rackwitz and Fiessler (1978), consists of representing the design variables by a normal distribution that has the same value of density and of distribution function as the original variable at the approximation point. This is equivalent to substituting the tail of the original distribution by a normal tail.

The original distribution function F_{xi}, with density function f_{xi}, with mean value μ_{xi} and standard deviation σ_{xi} is transformed into the equivalent normal with mean μ_{xi}^N and standard deviation σ_{xi}^N such that:

$$F_{xi}(x_i^*) = \Phi\left(\frac{x_i^* - \mu_{x_i}^N}{\sigma_{x_i}^N}\right) \tag{2.15}$$

$$f_{xi}(x_i^*) = \frac{1}{\sigma_{x_i}^N}\varphi\left(\frac{x_i^* - \mu_{x_i}^N}{\sigma_{x_i}^N}\right) \tag{2.16}$$

where φ and Φ is the standard normal density and distribution function, respectively. Solutions to the above equations yield:

$$\mu_{xi}^N = x_i^* - \sigma_{x_i}^{(N)}\Phi^{-1}\left(F_{xi}(x_i^*)\right) \tag{2.17}$$

$$\sigma_{xi}^N = \frac{\varphi\left(\Phi^{-1}\left(F_{xi}(x_i^*)\right)\right)}{f_{xi}(x_i^*)} \tag{2.18}$$

A different approach, proposed by Grigoriu and Lind (1980), consists of using various probability functions to fit the tail of the distribution. The estimated distribution function is determined by weighting the distribution with parameters whose sum equals one. The optimal values of the parameters are determined by a minimisation procedure.

An improvement of the normal tail approximation was proposed by Chen and Lind (1983). It consists of using one additional parameter in the normal tail approximation, i.e. the derivative of the probability density function at the approximation point.

Parkinson (1980) suggested a different approach to transform the variables, which is based on the knowledge of their 3rd and 4th moments instead of on assumptions about the shape of distribution function.

2.7 SECOND-ORDER RELIABILITY METHODS

The relatively simple and general form of the Hasofer-Lind reliability index makes this a useful format, but its limitations have led to various suggestions for improvements. In fact, some of the available information, particularly that on the exact form of the failure surface and on higher-order moments of the design variables, is ignored.

In addition , the index β_{HL} has the problem of lack of comparativeness that results from two limit state surfaces having quite different form, and hence implying different failure probability, being assigned identical reliability indices.

Ditlevsen (1979) has solved the comparativeness problem by defining generalized reliability index employing a density function in the space of the design variables. He defined the index as a function of the integral of this density function over the safe region. Although such an index is of considerable value in developing second moment algebra for linear failure surfaces, its application to a general, non-linear limit state problem is very expensive in terms of computing time compared with that required for simpler indices.

Fiessler et al. (1980) suggested an index that is a compromise between the simplicity of the Hasofer-Lind index and the strict comparability of Ditlevsen's generalized index. He used a quadratic approximation to the limit state surface and defined an index based on the minimum distance from the origin of the transformed space to the limit state surface and its local mean curvature at the design point. Figures 2.4 and 2.5 illustrate the relative advantages of the second-order approximation of the limit state surface.

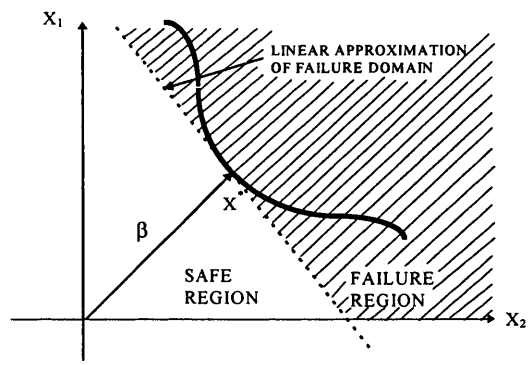

Figure 2.4: Failure domain via linear approximation about design point

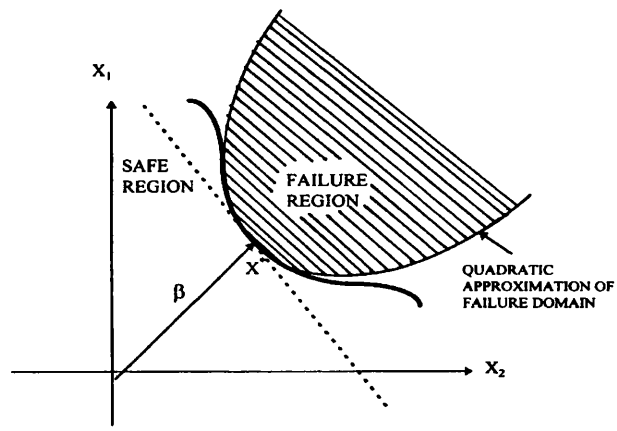

Figure 2.5: Failure domain via quadratic approximation about design point

Breitung (1984) recognised that a second-order expansion is asymptotically exact and this was the starting point of a very fruitful development in probability integration as summarised by Hohenbichler et al. (1989) and Breitung and Hohenbichler (1989).

Based on the theoretical concepts of the reliability methods, efficient computational tools for structural reliability assessment have been developed (Gollwitzer et al., 1988).

The so-called second order methods have proved to be sufficiently accurate and numerically feasible to calculate the reliability index of a multi-dimensional problem with non-normal design variables. The second moment based methods, by including information about the distribution function of the variables and by performing the integration of the probabilities over complex failure domains in many dimensions have, in a way, extended and solved the problem of the numerical calculation of the multiple integral to evaluate the probability of failure as a measure of safety (Freudenthal, Garrelts and Shinozuka, 1966).

CHAPTER 3
STRUCTURAL RELIABILITY OF THE PRIMARY SHIP STRUCTURE

3.1 PRESENT STATUS OF STUDIES OF SHIP RELIABILITY

The first references to structural safety of ships dates back to 1962 and is due to Abrahamsen (1962). However Nordenstrom (1971) is the first reported work on structural reliability. He calculated the probability of failure integrating a normally distributed resistance, a normally distributed still water load and a Weibull distributed wave induced load in the appropriate failure domain.

Mansour (1972) and Mansour and Faulkner (1973) also adopted a level three formulation to provide the first complete reliability analysis of a ship structure. They adopted Nordenstrom's model for wave induced loads and developed a probabilistic model for the ship strength; various modes of failure of the structure were considered.

Later, Mansour (1974) and Faulkner and Sadden (1979) applied the developments in the theoretical formulations and in the computational methods of structural reliability to the analysis of ship structures.

Mansour adopted the distribution of the wave induced vertical bending moment at a random point in time to calculate the reliability index of 19 merchant ships using the second order reliability methods. Faulkner and Sadden considered the most probable maximum lifetime load given by a Poisson distribution whose mean value is the most probable maximum calculated at the 10^{-8}-probability level. Using this approach, they obtained β-values in the range of 2 for warships, while the ones calculated by Mansour for merchant ships were in the range of 7.

This example showed that the results change significantly with the formulation adopted. However, recent works have shown that the various formulations can be related to each other and the choice of one or other is a matter of standardisation in order to allow the ship structures to be compared.

Many studies have been made on the system reliability analysis of structures as reviewed by Ditlevsen and Bjerager (1986). The initial applications of system reliability to ship structures have used frame models and looked at the transverse strength of ships

(Murotsu et al., 1986 and Yim et al., 1992). An approach has been presented of system reliability of ship's hull girder, which is composed of the spatial membrane elements and beam elements (Murotsu et al., 1993 and Okada et al., 1995). However, there remains much work to be done for large structures that have many failure modes. Furthermore, there are many structures that are difficult to idealise by a frame model.

Promising attempts have been made to correlate the ultimate system capacity to the strength of the most critical deck and bottom panels. A reliability analysis of the bottom and the deck panels of a typical North Sea production ship was carried out by Wang et al. (1994) considering the interaction between axial and lateral loading. However, the same still water load model was used for both panels. In (Wang and Moan, 1995) the work was extended to account different load models for bottom and deck panels as a result of different load combination factors.

Structural reliability methods have been developed to quantify time independent problems. However, on a time scale on the order of the service life of a structure, many non-stationary periods occur. In the marine field, corrosion processes and fatigue damage are examples of time dependent resistance deterioration mechanisms.

Important developments have been made to deal with time variant problems. Guedes Soares and Ivanov (1989) have proposed a model to quantify the time variation of the reliability of the primary ship structure that results from the degradation effects of corrosion. Nitta (1976) and Ivanov and Minchev (1979) treated for the first time the reliability problem related to fatigue failures. Recently, Marley and Moan (1992) used the outcrossing formulation for reliability assessment against exceedance of an ultimate capacity that decreases during service life due to a growing fatigue crack

The design of a vessel is based mainly on rules developed by the classification societies based on semi-analytical models that have not been calibrated against a uniform reliability level. Therefore, there is a need to establish a model code for ship structural design by partial safety factors, which are calibrated on the basis of a probabilistic reliability analysis.

Mansour (1984) formulated a pioneering rationale for selecting and calibrating a format of reliability-based strength standards for use in ship design. However, the partial safety factors were related to mean value of still water and wave induced bending moment, and a direct application to code values was not possible. Ostergaard (1992) extended the work towards direct application of code values by deriving a set of partial

safety factors applied to the nominal code values of still water and wave induced bending moments. However, the stochastic model of hull strength was simple a randomised model of the present code formats.

Recently, Guedes Soares et al. (1996) assessed the reliability of the primary hull structure of several tankers and containerships using a new probabilistic model for the ultimate strength of the ship as well as for the still water and wave induced bending moment. The results of the reliability analysis were the basis for the definition of a target safety level, which was used to assess the partial safety factors for a new design rules format.

3.2 FORMULATION OF STRUCTURAL RELIABILITY

In this section a reliability analysis of the primary structure of four oil tankers with respect to the ultimate collapse moment is performed using the advanced first order reliability method. Different probabilistic models of the still water and wave induced bending moment are applied in the formulation of the reliability problem. In addition, load combination factors are introduced to calculate the total vertical bending moment.

It is shown that the different approaches can be related and the choice of one or the other is a matter of standardisation in order to allow the ship structures to be compared with each other.

3.2.1 Description of the example ships

Four tankers are considered for the purposed of this study. The sample includes a small tanker, two medium size tankers and one VLCC that has failed under hogging in the harbour (Rutherford and Caldwell, 1990). Their principal dimensions are presented in table 3.1, sketches of the midship section of the ships are illustrated in figures 3.1 and 3.2 (see also appendix 1).

Table 3.1
Particulars of the ships

Ship	Year	L (m)	B (m)	D (m)	T (m)	DWT (t)	C_b
TK1	1973	133.4	18.0	9.75	7.60	10250	0.700
TK2	1979	230.0	42.0	19.8	12.70	80000	0.818
TK3	1988	236.0	42.0	19.2	13.05	88900	0.805
TK4	1970	313.0	48.2	25.2	19.60	216269	0.830

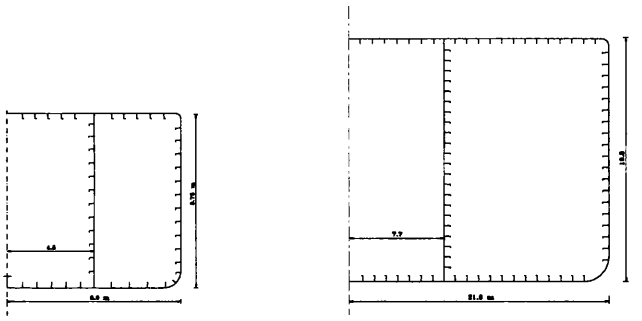

Figure 3.1: Midship section of TK1 and TK2

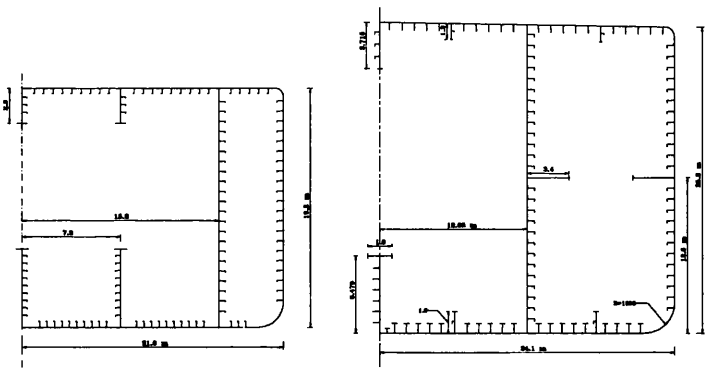

Figure 3.2: Midship section of TK3 and TK4

3.2.2 Limit state equation

To assess the reliability of structures it is necessary to compare the values of the load effects in the various components with their respective strengths. When considering the primary ship hull structure, reference is usually made to midship cross section and the two most important load effects are the still water and the wave induced bending moment.

A common limit state is related to the moment, M_e, that causes the first yield of the cross section either in the deck or in the bottom. This moment is equal to the minimum section modulus Z_e multiplied by the yield stress σ_y,

$$M_e = Z_e \, \sigma_y \tag{3.1}$$

This has been the basic approach used in the Classification Societies checking procedure and in the former reliability analysis. However, it tends to be conservative in that the material has a reserve of strength after initial yield.

Another limit state is the plastic bending moment, which is reached when the entire section becomes fully plastic. The plastic moment M_p is equal to the product of the plastic section modulus Z_p and the yield strength.

$$M_p = Z_p \, \sigma_y \tag{3.2}$$

This limit state function is generally unconservative because some of the plates that are subjected to compression may buckle locally decreasing their contribution to the overall moment.

In the present reliability assessment of the primary ship structure a more correct description of the real collapse is adopted based on the ultimate collapse moment. This moment, in general between the elastic and the plastic moment, is the sum of the contribution of all elements, taking into account their load deflection characteristics, including their post-collapse strength,

$$M_u = \sum_i^n \frac{\sigma_{ui}}{\sigma_y} d_i \, \sigma_y \tag{3.3}$$

where d_i is the distance from the centroid of the element to the neutral axis and σ_{ui} is the ultimate strength of each element.

The real collapse occurs in a mode that combines vertical and horizontal bending moments, which leads to a combined collapse of the ship hull. Thus, the collapse equation for the hull girder can be defined as,

$$1 - \left(\frac{M_s + M_{wv}}{M_{uv}} \right)^{\alpha} - \left(\frac{M_{wh}}{M_{uh}} \right)^{\alpha} \leq 0 \tag{3.4}$$

where M_s is the vertical still water bending moment; M_{wv}, M_{wh} are the wave induced vertical and horizontal bending moments, respectively; M_{uv}, M_{uh} are the ultimate vertical and horizontal bending moments; α is the exponent of the interaction equation which is between 1.5 and 1.66 for tankers (Gordo and Guedes Soares, 1995).

However, the levels of horizontal bending moments are often very small, especially in tankers, and for practical purposes it may be appropriate to deal only with the vertical bending moments. Therefore the corresponding failure equation used in the reliability analysis is given by Casella et al. (1996):

$$1-\left(\frac{M_s+\Psi\,\chi_{nl}\,\chi_W M_W}{\chi_u M_u}\right)\leq 0 \qquad (3.5)$$

where M_u is the ultimate vertical bending strength of the ship, M_s and M_w are the stochastic still water and wave induced vertical bending moment, respectively. Ψ is the combination factor between still water and wave induced bending moment; χ_u, χ_w and χ_{nl} are the uncertainties on ultimate capacity, wave load calculations and non-linear effects, respectively.

It can be noted that, in this failure equation, the effects of still water and wave induced bending moments have been separately taken into account to adopt a formulation as close as possible to a typical code formula.

3.2.3 Reference period and load conditions for reliability analysis

The one-year reliability index is considered in the formulation with respect to ultimate strength, which is an option that allows the use of time independent formulations for the reliability assessment. However, using current software packages for FORM (First Order Reliability Methods) analysis, the reliability problem can easily be extended to time dependent formulations, which can account for the effect of hull degradation (Guedes Soares and Ivanov, 1989).

For tankers three different load conditions, can be defined, i.e. Full load, Ballast and Partial load. For each load condition, a suitable percentage of ship life must be identified according to the best estimate of the operational profile. Table 3.2 shows the operational profile adopted for tankers. The voyage duration in each load condition is defined based on a statistical analysis of load duration data conducted by Guedes Soares (1990).

Table 3.2
Operational profile adopted for tankers

	Fraction of Ship Life			
Load Condition	Harbour	Full Load	Ballast Load	Partial Load
	15 %	35 %	35 %	15 %
Voyage Duration		23.5 days	23.5 days	2.0 days

The product of the fraction of ship life spent in a given condition times one-year time, gives the reference time period T_C which is used for the load evaluation in a particular load condition.

It is considered that during the one-year reference period the ship is in three complementary and exclusive situations. The probability of failure in these periods can be considered as if they were in a series system. The yearly probability of failure P_f is related to the yearly probabilities of failure under different load conditions by:

$$(1 - P_f) = (1 - P_{FL})(1 - P_{BL})(1 - P_{PL}) \tag{3.6}$$

where P_{fFL}, P_{fBL} and P_{fPL} are the failure probabilities in the different load conditions.

However, the overall probability of failure is often dominated by one load condition. In this case, a good approximation of the yearly reliability index β is obtained by:

$$\beta = \Phi^{-1}(P_{f\,BL} + P_{f\,FL} + P_{f\,PL}) \tag{3.7}$$

where Φ^{-1} is the standard normal probability distribution function.

3.2.4 Stochastic modelling of ultimate strength of the primary structure

The ultimate collapse bending moment was evaluated by the HullColl program based on the theory outlined in (Gordo et al., 1996 and Gordo and Guedes Soares, 1996). This variable is used as deterministic in the failure equation. To take into account the uncertainty on the ultimate capacity the stochastic variable χ_u was defined.

Description of the method

Broadly speaking, the assessment of a moment-curvature relationship is obtained from the imposition of a sequence of increasing curvatures to the hull's girder. For each curvature, the state of average strain of each beam-column element is determined. On entering these values in the model that represents the load-shortening behaviour of each element, the load that it sustains is calculated and consequently the bending moment resisted by the cross section is obtained from the summation of the contributions from the individual elements. The derived set of values defines the desired moment-curvature relation.

However, some problems arise in this implementation, because the discretisation of the sequence of the imposed curvatures strongly influences the convergence of the method due to the shift of the hull neutral axis. In this method, the modelling of the ship's section and the determination of the position of the neutral axis are important issues, as has already been pointed out in (Gordo, Guedes Soares and Faulkner, 1996).

The basic assumptions of the method are the following:

- the elements are composed of longitudinal stiffeners and an effective breadth of plate into which the cross section is subdivided and they are considered to act and behave independently;
- the ship cross section is assumed to remain plane during bending;
- the overall grillage collapse of the deck and bottom structures is avoided by using sufficiently strong transverse frames.

As a first step it is necessary to estimate the position of the neutral axis through an elastic analysis, because when the curvature is small the section behaves in the elastic domain. If the section is symmetric and the origin of the reference system is located on the baseline, (see fig. 3.3), the elastic neutral axis passes through a point with coordinates:

$$\begin{cases} x_n = 0 \\ y_n = \dfrac{\sum y_i A_i}{\sum A_i} \end{cases} \tag{3.8}$$

where A_i and y_i are respectively the area and the vertical position of the stiffened element under consideration.

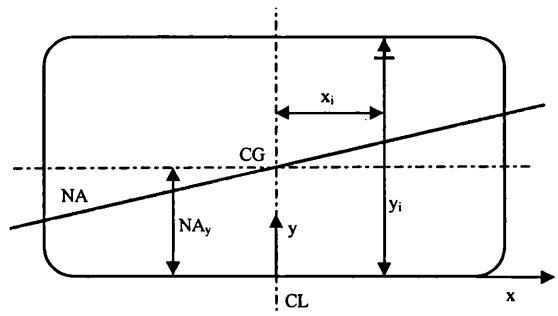

Figure 3.3: Combined bending of the hull girder

The most general case corresponds to that in which the ship is subjected to curvature in the x and y directions, respectively denoted as C_x and C_y. The global curvature C is related to these two components by:

$$C = \sqrt{C_x^2 + C_y^2} \tag{3.9}$$

or,

$$\begin{cases} C_x = C \cdot cos\theta \\ C_y = C \cdot sin\theta \end{cases} \tag{3.10}$$

adopting the right-hand rule, where θ is the angle between the neutral axis and the x axis. The strain at the centroid of an element i is ε_i which depends on its position and on the hull curvature, as given by:

$$\varepsilon_i = y_{gi} \cdot C_x - x_{gi} \cdot C_y \tag{3.11}$$

or substituting 3.10 in 3.11:

$$\varepsilon_i = C \cdot \left(y_{gi} \cdot cos\theta - x_{gi} \cdot sin\theta \right) \tag{3.12}$$

where (x_{gi}, y_{gi}) are the coordinates of the centroid of the element i (stiffener and associated effective plate) referred to the point of the intersection of the neutral axis and the center line. The relations between these local coordinates and the global coordinates are:

$$\begin{aligned} x_{gi} &= x_i - x_n \\ y_{gi} &= y_i - y_n \end{aligned} \tag{3.13}$$

Equations 3.13 are still valid if one uses any point lying on the neutral axis instead of the point used before.

Once the state of strain in each element is determined, the corresponding average stresses may be calculated according to the method described by Gordo and Guedes Soares (1993) and consequently the components of the bending moment for a curvature C are given by:

$$\begin{cases} M_x = \sum y_{gi} \cdot \Phi(\varepsilon_i) \cdot \sigma_o A_i \\ M_y = \sum x_{gi} \cdot \Phi(\varepsilon_i) \cdot \sigma_o A_i \end{cases} \tag{3.14}$$

where x_{gi} and y_{gi} are the distances from the element i to the origin of a local axis located in the precise position of the instantaneous "centre of gravity" (CG), and $\Phi(\varepsilon_i)$ represents the non-dimensional strength of the element, which has an appearance like the examples in fig. 3.4.

The load-shortening curve is controlled by two main parameters, which are the effective plate slenderness and the effective column slenderness. These slendernesses are associated with the geometry of the stiffened element and its mechanical properties like the nominal slendernesses, but they are also related to the average strain state. Thus, with the increase of the compressive strain a loss of effectiveness of the plate may be felt once

the effective slenderness exceeds one. The very stocky plates do not have any loss of rigidity in the pre-collapse region and they may sustain stresses near the yield stress until very large plastic strains. On the other extreme, very slender plates lose structural rigidity at an early stage of the loading process and they show a more pronounced load shedding after collapse than the stocky ones.

The plates of intermediate slenderness exhibit the most marked shedding after collapse because in these plates the variation of effective width with the slenderness has an absolute minimum. These changes in the effective width of the plate during the loading process have a direct repercussion on the column slenderness through the calculation of the effective moment of inertia.

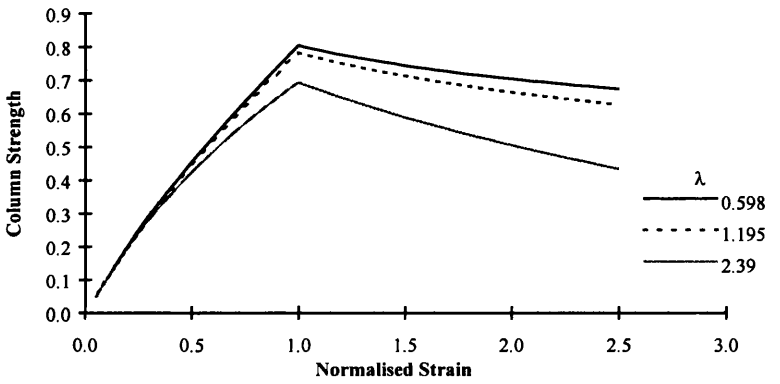

Figure 3.4: Load shortening curves of stiffened plates with plate slenderness of 2.32 and different column slendernesses, λ

The modulus of the total bending moment is:

$$M = \sqrt{M_x^2 + M_y^2} \tag{3.15}$$

This is the bending moment on the cross section if the assumed instantaneous position of the centre of gravity is correct. However, during the stepwise process of increasing the hull's curvature, the location of the centre of gravity is shifting and it becomes necessary to calculate the shift between two imposed curvatures. Rutherford and Caldwell (1990) suggested that the shift could be taken equal to:

$$\Delta NA = \frac{\sum(A_i \cdot \sigma_i)}{C \cdot \sum(A_i \cdot E_i)} \tag{3.16}$$

but it was felt by Gordo and Guedes Soares (1996) that this expression underestimated the shift and may cause problems in convergence.

For this reason a trial-and-error process was implemented, having as stopping criteria one of the two conditions: the total net load in the section, *NL*, or the error in the shift estimation ΔNA should be less than or equal to a sufficiently low value. Equations 3.17 and 3.18 represent analytically these two conditions, where ξ was taken equal to 10^{-6}.

$$NL = \sum(\sigma_i \cdot A_i) \leq \xi \cdot \sigma_o \cdot \sum(A_i) \tag{3.17}$$

$$\Delta NA = k_E \cdot \frac{NL}{C \cdot E \cdot \sum A_i} \leq 0.0001 \tag{3.18}$$

The factor k_E is a function of the curvature and yield strain introduced to allow a better convergence of the method, and it is a result of the variation in the structural tangent modulus of the overall section with curvature.

The plate panels are treated according to Faulkner's method for the flexural buckling of panels and the tripping of the stiffeners is estimated when necessary (Gordo and Guedes Soares, 1993). Different shedding patterns after buckling are available depending whenever flexural buckling or tripping is dominant.

In (Gordo and Guedes Soares, 1996), the predictions of the method just described were compared with various experimental results performed by different authors, showing very good correlation.

Results

The ultimate longitudinal strength of the ships in sagging (deck in compression) and hogging (bottom in compression) are summarised in table 3.3. The same table also presents the moment that corresponds to the first yield when the section is considered to behave elastically, denoted as yield moment, and the fully plastic moment without considering any buckling effects or shedding after yielding, denoted as plastic moment.

In the modelling of the ship's cross section the existence of 'hard-corners' was considered in the intersection of the main framing and the plating and also at the intersection of the sheerstrake and the deck plating. 'Hard-corners' are defined as elements that have an elastic perfectly plastic behaviour and thus are considered to be totally effective both in tension and compression.

Table 3.3
Longitudinal bending moment of the ships

Bending Moment	TK1	TK2	TK3	TK4
Yield (MN.m)	980	8259	8161	19332
Plastic (MN.m)	1161	9768	9716	22618
Sagging (MN.m)	910	6652	7123	16392
Hogging (MN.m)	932	7120	8354	19164
Plastic /Yield	1.18	1.18	1.19	1.17
Sagging / Yield	0.93	0.81	0.87	0.85
Hogging / Yield	0.95	0.86	1.02	0.99
Hogging / Sagging	1.02	1.07	1.17	1.17

Some general conclusions for this type of ship may be readily recognised. The coefficient between plastic and yield moment is approximately 1.18 for single skin and its variability is low. However these ships are old designs and one may expect an increase in this coefficient for double hull tankers due to existence of new material at low level of stresses which is a reserve of strength.

It can also be seen that the strength of tankers under sagging bending moment is always less than the yield moment by about 20%. The main reason for this difference is that the buckling strength of the stiffened plate elements of the deck is somewhat lower than the yield stress due to their slenderness.

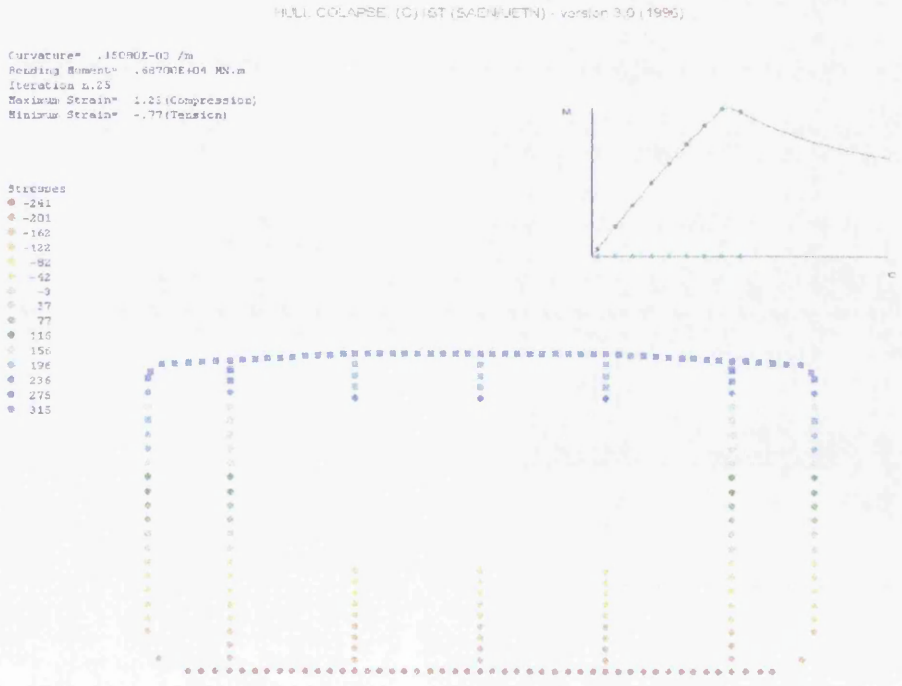

Figure 3.5: Stress distribution at the ultimate bending in sagging (TK3)

Figure 3.5 shows the stress distribution of tanker TK3 near the collapse. Most part of the deck has already collapsed, where the collapse is represented by squares while the elastic behaviour by circles.

It can be seen that the deck stiffened plates and the web of the deck girders have collapsed and its capability of sustaining loading is low which means that these elements should have a greater thickness in order to avoid premature collapse. Figure 3.6 illustrates the stiffener behaviour of the typical deck stiffened plate and the web of the deck girders. These elements loose structural rigidity in the pre-collapse region and they show a pronounced load shedding with the increase of compressive strain leading to a lower value of ultimate bending strength in sagging when compared with the yield bending moment.

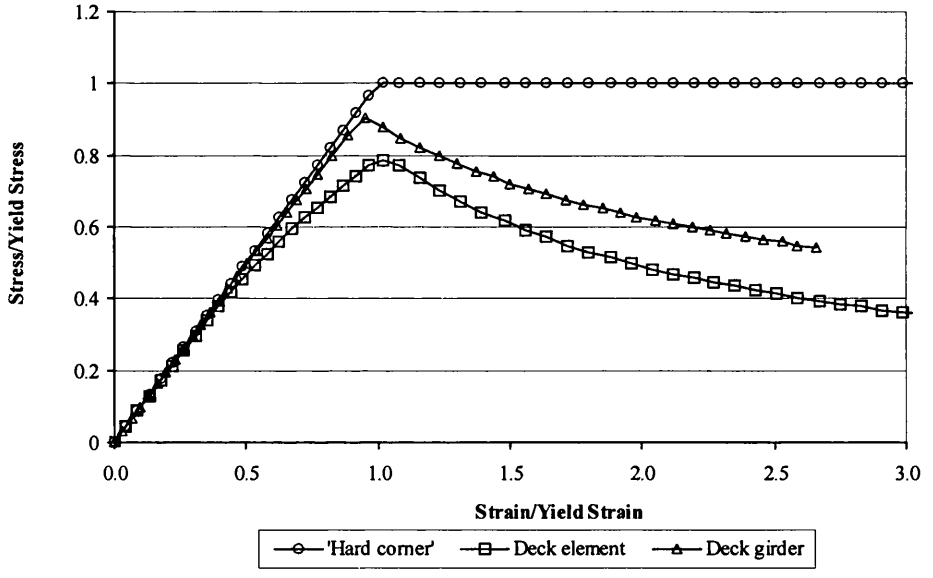

Figure 3.6: Load shortening curves of the stiffened deck elements

Table 3.3 also shows that the ultimate bending moment in hogging is close to the yield moment and higher than the ultimate bending moment in sagging. This fact can be explained by the analysis of the stress distribution of tanker TK3 near the collapse (figure 3.7). The collapse occurs with yielding at the deck followed by buckling at the bottom stiffened plate. However, the ship is still able to sustain more bending moment due to the existence of the bottom girders. Thus, the moment curvature curve continues to increase after the yielding of large part of a the structure. Moreover, the bottom elements are thicker than the deck elements and thus they are able to sustain more load.

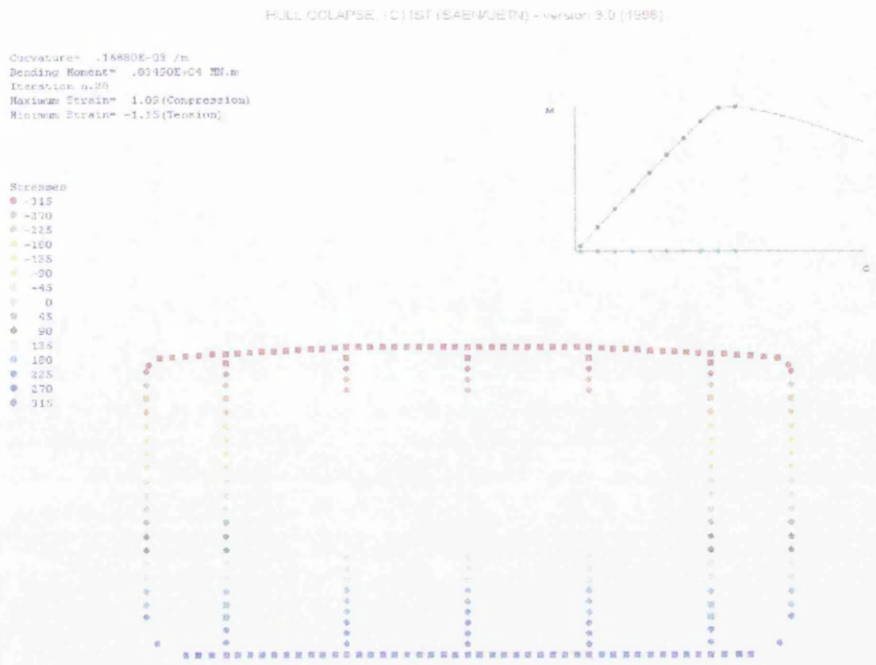

Figure 3.7: Stress distribution at the ultimate bending in hogging (TK3)

1.1.1 Stochastic model of wave induced bending moment

Long-term formulation

Wave loads are forces that result from the wave action. They include vertical and horizontal bending and torsional moments, shear forces, hydrodynamic pressure and transient loads such as springing and slamming. However, as far as the primary ship hull loads are concerned the most important wave load is the vertical wave bending moment.

The main developments of the methods of predicting wave induced motions and associated loads occurred during the late 60's and early 70's, based on linear strip theories, with different degrees of sophistication. For design purposes extreme values of the wave induced load effects during the ship's lifetime are required and therefore long-term formulations were developed based on modelling the succession of sea states in which the ship is sailing.

Due to the random nature of the ocean, wave loads are stochastic processes both in the short-term and long-term. The short-term vertical wave induced bending moment corresponds to a steady (random) sea state, which is considered as stationary with duration of several hours. Within one sea state the amplitudes of the wave induced load effects follow a Rayleigh distribution. The response is modelled as a Gaussian zero mean stationary stochastic process described by its variance R:

$$R = \int_0^\infty S_R(\omega)\, d\omega \tag{3.19}$$

where $S_R(\omega)$ is the response spectrum given by the product of the linear transfer function $H(\omega)$ for a specified relative heading and significant wave height and the seaway spectrum $S_H(\omega)$,

$$S_R(\omega) = S_H(\omega) \cdot H^2(\omega) \tag{3.20}$$

The seaway spectrum used here is the ISSC version of the Pierson-Moskowitz spectrum given by Warnsinck (1964):

$$S_H(\omega) = 0.11\, H_s^2\, T_m \left(\mathrm{T_m}\frac{\omega}{2\pi}\right)^{-5} exp\left(-0.44\left(T_m\frac{\omega}{2\pi}\right)^{-4}\right) \tag{3.21}$$

where T_m is the average wave period and H_S is the significant wave height.

However, the sea waves cannot be adequately described by only a frequency spectrum. In general, the patterns observed in the ocean show the existence of many components travelling in various directions.

The directional spectrum represents the distribution of wave energy both in frequency of the wave components and also in direction θ. The analysis of directional buoy records has shown that the spreading function G is a function of both direction and frequency. Therefore, a directional spectrum $S(\omega,\theta)$ can be represented as,

$$S(\omega,\theta) = S(\omega)G(\omega,\theta) \tag{3.22}$$

The directional spreading function is given by:

$$\begin{aligned} G(\theta) &= \frac{2}{\pi}\cos^2(\theta) \qquad |\theta| \le \pi/2 \\ G(\theta) &= 0 \qquad\qquad\quad |\theta| \ge \pi/2 \end{aligned} \tag{3.23}$$

The amplitudes of the Gaussian zero mean stationary stochastic process (eq. 3.19), with a narrow band assumption, follow a Rayleigh distribution such that the probability of exceeding the amplitude x is given by Longuet-Higgins (1952):

$$Q_s(x \mid R) = exp\left(-\frac{x^2}{2 \cdot R}\right) \tag{3.24}$$

The probability distribution of the wave induced load effects that occur during long-term operation of these ship in the seaway is obtained by weighting the conditional

Rayleigh distribution by the probability of occurrence of the various sea states in the ship route (Fukuda, 1967, Söding, 1971, Guedes Soares and Viana, 1988 and Guedes Soares and Trovão, 1991),

$$Q_L(x) = \int Q_s(x \mid R) \cdot f_R(r)\, dr \tag{3.25}$$

where $f_R(r)$ is the probability density of the response variance in the considered sea states. It depends on several variables such as the wave climate represented by H_s and T_z, the ship heading θ, speed v and loading condition c, i.e.,

$$f_R(r)\, dr = f(h_s, t_Z, \theta, v, c)\, dh_S\, dt_Z\, d\theta\, dv\, dc \tag{3.26}$$

where the joint distribution of the five variables is usually represented by the product of several conditional distributions (Guedes Soares and Viana, 1988 and Guedes Soares and Trovão, 1991).

The resulting long-term distribution $Q_L(x) = P(VBM > x)$, which represents the exceedance probability of the vertical wave bending moment x, can be approximated to the Weibull distribution $F_{VBM}(x)$ given by:

$$F_{VBM}(x) = 1 - \exp\left[-\left(\frac{x}{w}\right)^k\right] \tag{3.27}$$

where w and k are the scale and the shape parameters to be estimated from a Weibull fit of $F_{VBM}(x)$ to $1 - Q_L(x) = P(VBM \le x)$.

In the assessment of wave induced load effects that occur during long-term operation of ships in the seaway, the Global Wave Statistics data are often used (Hogben et al., 1986). In the Global Wave Statistics atlas the ocean areas are divided into 104 regions as shown in figure 3.8.

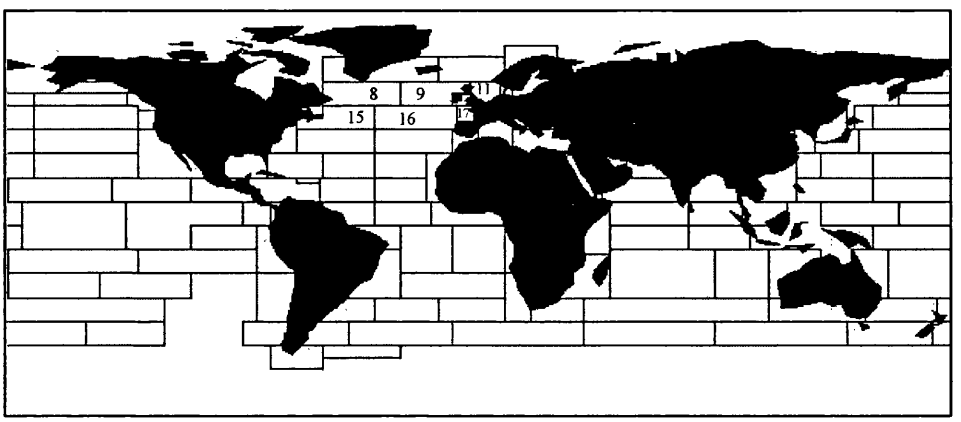

Figure 3.8: Global Wave Statistics ocean areas

Different authors have analysed the effect of using different wave scatter diagrams on the long-term predictions of wave induced loads in ship structures. It was demonstrated that the North Atlantic and the North Sea represent the most severe wave condition. Other ocean areas may yield extreme response values up to 20% less than these areas.

In the present study, the Global Wave Statistics is used to define an average scatter diagram denoted by ATLN (table 3.4). ATLN refers to the wave induced bending moment in the North Atlantic calculated based on the world sea areas 8, 9, 11, 15, 16 and 17.

Table 3.4
Wave Scatter Diagram (ATLN)

H_s / T_z	3.5	4.5	5.5	6.5	7.5	8.5	9.5	10.5	11.5	12.5	13.5
0.5	2.74E-3	1.52E-2	2.72E-2	2.64E-2	1.39E-2	4.07E-3	7.57E-4	1.02E-4	1.10E-5	1.14E-6	0.00E+0
1.5	4.66E-4	7.50E-3	2.94E-2	6.28E-2	7.16E-2	4.24E-2	1.47E-2	3.44E-3	6.02E-4	8.63E-5	1.07E-5
2.5	1.00E-4	2.52E-3	1.32E-2	3.99E-2	7.32E-2	6.90E-2	3.63E-2	1.22E-2	2.94E-3	5.53E-4	8.71E-5
3.5	2.40E-5	8.13E-4	5.04E-3	1.77E-2	4.30E-2	5.56E-2	3.94E-2	1.73E-2	5.31E-3	1.24E-3	2.36E-4
4.5	6.29E-6	2.68E-4	1.89E-3	6.99E-3	1.99E-2	3.21E-2	2.85E-2	1.54E-2	5.71E-3	1.58E-3	3.53E-4
5.5	1.86E-6	9.31E-5	7.28E-4	2.71E-3	8.37E-3	1.59E-2	1.67E-2	1.07E-2	4.61E-3	1.47E-3	3.73E-4
6.5	5.71E-7	3.44E-5	2.94E-4	1.09E-3	3.44E-3	7.31E-3	8.82E-3	6.45E-3	3.17E-3	1.14E-3	3.22E-4
7.5	1.43E-7	1.33E-5	1.25E-4	4.61E-4	1.44E-3	3.31E-3	4.46E-3	3.66E-3	2.00E-3	7.97E-4	2.48E-4
8.5	1.43E-7	5.43E-6	5.56E-5	2.06E-4	6.26E-4	1.52E-3	2.24E-3	2.02E-3	1.21E-3	5.29E-4	1.79E-4
9.5	0.00E+0	2.43E-6	2.60E-5	9.74E-5	2.85E-4	7.13E-4	1.13E-3	1.11E-3	7.26E-4	3.41E-4	1.24E-4
10.5	0.00E+0	1.14E-6	1.26E-5	4.81E-5	1.36E-4	3.46E-4	5.86E-4	6.17E-4	4.33E-4	2.18E-4	8.47E-5
11.5	0.00E+0	5.71E-7	6.29E-6	2.47E-5	6.83E-5	1.74E-4	3.09E-4	3.48E-4	2.60E-4	1.40E-4	5.76E-5
12.5	0.00E+0	2.86E-7	3.29E-6	1.33E-5	3.53E-5	9.03E-5	1.67E-4	1.99E-4	1.58E-4	8.99E-5	3.90E-5
13.5	0.00E+0	1.43E-7	1.71E-6	7.29E-6	1.90E-5	4.81E-5	9.23E-5	1.15E-4	9.66E-5	5.80E-5	2.64E-5
14.5	0.00E+0	1.43E-7	2.29E-6	1.00E-5	2.56E-5	6.19E-5	1.24E-4	1.71E-4	1.61E-4	1.10E-4	5.67E-5

The hydrodynamic calculations were performed based on linear strip theory considering a single ship speed. In figure 3.9, the Response Amplitude Operator (RAO) of the vertical bending moment for tanker TK3 in ballast load condition is illustrated for different headings. Other load conditions can be found in appendix 2.

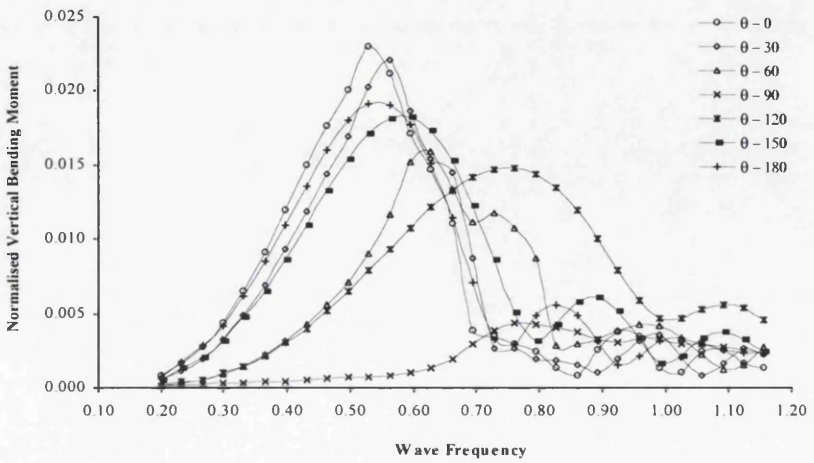

Figure 3.9: RAO of vertical wave induced bending moment

Table 3.5 summarises the scale and shape Weibull parameters estimated from a Weibull fit. It has been found that the shape parameters k are around 0.9, which agrees with earlier results of Guedes Soares and Moan (1991).

Table 3.5
Parameters of Weibull distribution

Ship	Weibull Parameters.	Load Condition		
		FL	*BL*	*PL*
TK1	*w*	19.6	15.0	16.2
	k	0.912	0.868	0.892
TK2	*w*	195.5	148.3	161.8
	k	0.890	0.845	0.871
TK3	*w*	206.4	156.6	170.9
	k	0.89	0.845	0.871
TK4	*w*	456.0	344.6	383.6
	k	0.879	0.834	0.865

In figure 3.10 the long-term distribution and the Weibull fit are illustrated for tanker TK3 in full and ballast load condition. The curves obtained for the others have a similar appearance.

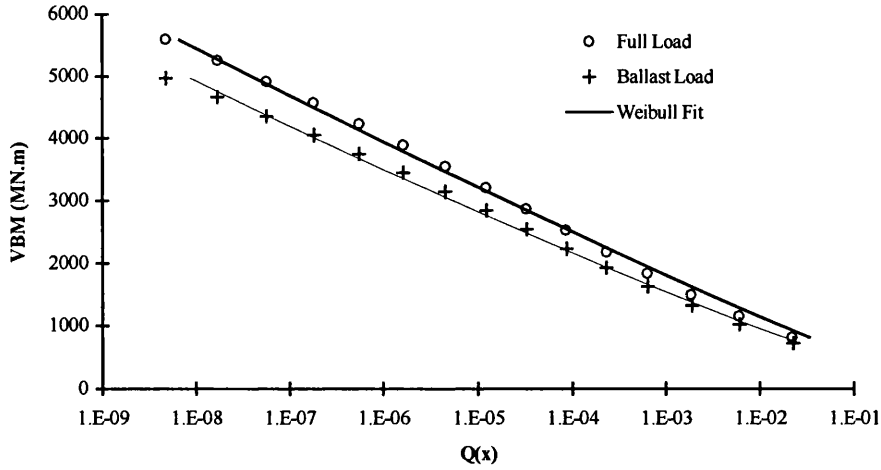

Figure 3.10: Weibull fit for TK3 in full and ballast load condition

Extreme model

The reliability formulation, adopting the Weibull model to describe the wave induced load effects, calculates the probability that at a random point in time the ultimate hull moment is smaller than the applied load effects. However, a more severe formulation of the reliability problem can been considered, by requiring that the structure is safe under the maximum wave induced load effect that occurs in the reference period. This implies

that the model of wave induced load effects must be described by a Gumbel instead of a Weibull distribution.

In this stochastic model the wave induced load effects are represented by the distribution of the maximum value M_{we}, based on the underlying Weibull distribution of the basic model.

The design wave bending moment can thus be represented by a Gumbel distribution given by:

$$F_{we}(x_{we}) = exp\left[-exp\left(-\frac{x_{we} - x_{nw}}{\sigma_{nw}}\right)\right] \tag{3.28}$$

According to Guedes Soares (1985) the Gumbel parameters x_{nw} and σ_{nw} can be estimated from the initial Weibull distribution with parameters w and k using the following equations:

$$x_{nw} = w \cdot [ln(n)]^{\frac{1}{k}} \tag{3.29}$$

$$\sigma_{nw} = \frac{w}{k}[ln(n)]^{\frac{1-k}{k}} \tag{3.30}$$

where n is the number of peaks counted in the time period T_C given by:

$$n = \frac{T_C}{\overline{T}_Z} \tag{3.31}$$

and $\overline{T}_Z$ the average mean zero crossing period of waves. Using equation 3.31 corresponds to assuming that the average load period is equal to the average wave period and the average number of load peaks is one per load cycle (narrow band approximation).

The mean value and the standard deviation of the extreme distribution is given respectively by:

$$\mu_{we} = x_{nw} + \gamma \cdot \sigma_{nw} \tag{3.32}$$

$$\sigma_{we} = \frac{\pi}{\sqrt{6}} \cdot \sigma_{nw} \tag{3.33}$$

where γ is the Euler constant equal to 0.5772.

Figure 3.11 shows the distribution of the maximum value $M_{we} = [F_w(x)]^n$ based on the underlying Weibull distribution and the Gumbel model to describe the extreme model of wave induced load effects.

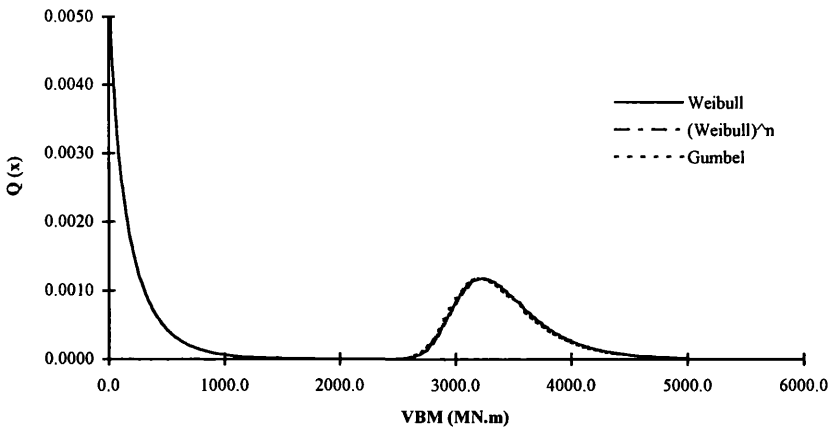

Figure 3.11: Extreme model of wave induced load effects (n=100000)

Table 3.6 shows the stochastic model of extreme wave induced bending moment for the adopted operational profile (see table 3.2). For each loading condition, the distribution of the extreme wave load is calculated over the period of time that the ship spend in this condition T_C. The average of wave period is assumed to be 7s in North Atlantic.

Table 3.6
Stochastic model of the extreme wave induced moment

Ship	Cond.	Weibull Parameters		Moments		Gumbel Moments		
		w	*k*	*Mean V.*	*Std. Dev.*	*n*	*Mean V.*	*Std. Dev.*
TK1	FL	19.6	0.912	20.5	22.5	1.58E+06	377.6	35.6
	BL	15.0	0.868	16.1	18.6	1.58E+06	336.6	33.3
	PL	16.2	0.892	17.1	19.2	6.76E+05	312.6	31.9
TK2	FL	195.5	0.890	206.9	233.1	1.58E+06	4051.6	391.3
	BL	148.3	0.845	161.9	192.5	1.58E+06	3612.7	366.7
	PL	161.8	0.871	173.4	199.7	6.76E+05	3348.6	350.0
TK3	FL	206.4	0.890	218.5	246.1	1.58E+06	4277.8	413.2
	BL	156.6	0.845	171.0	203.3	1.58E+06	3814.3	387.1
	PL	170.9	0.871	183.2	211.0	6.76E+05	3535.9	369.6
TK4	FL	456.0	0.879	486.2	544.6	1.58E+06	9815.4	959.4
	BL	344.6	0.834	379.5	457.5	1.58E+06	8752.7	899.6
	PL	383.6	0.865	412.9	478.9	6.76E+05	8106.3	853.0

3.2.6 Stochastic model of still water bending moment

Still water loads are forces that result from action of ship self-weight, the cargo or deadweight and the buoyancy. They include bending moment, shear force and lateral pressure. Typically, the most important still water load is the vertical still water bending moment.

The variation of still water loads depends on the amount of cargo and its distribution along the ship. The shipmasters have to load their ships in a way not dramatically different from those reference conditions given in a load manual, in the hope that maximum values are not exceeded.

The shipmaster's decision has been idealised in probabilistic terms and the resulting probability density function has indicated a clear decrease in the probability of occurrence of values larger than the design values (Guedes Soares, 1990). The application of modern computerised load distribution procedure gives shipmaster much freedom to load the ship. Unfortunately, this freedom of choice also leads to a larger probability of load exceedance due to human errors.

The analysis of operational data has shown that the variability of the cargo embarked in successive voyages will make the load effects experience values that change in a random manner. Thus, proposals have been put forward to model the still water load effects probabilistically based on statistical analysis.

Statistical analysis of still water bending moment has been addressed since 1970's. Lewis (1975) has drawn attention to the statistical nature of the still water bending moment based on limited data of several cargo ships and one bulk carrier. Ivanov (1975) fitted the normalised maximum still water bending moment by a normal distribution according to full or partial cargo load conditions from eight cargo ships for periods of two to seven years. Mano (1977) studied the nature of still water conditions by surveying log-books of 10 containerships and 13 tankers, and concluded that their distribution is approximately normal.

In the early 1980's, some still water bending stresses were reported by Akita (1982) separately for a group of 10 containerships as well as for a group of 8 tankers. Based on this information, Kaplan (1984) found that the coefficient of variation of the still water bending moment is around 0.99 and 0.52 for tankers in full and ballast load condition, respectively, and 0.29 for containerships.

More recently Guedes Soares and Moan (1988) analysed the still water bending moment resulting from about 2000 voyages of 100 ships belonging to 39 shipowners in 14 countries. The still water load effects were assumed to vary from voyage to voyage for a particular ship, from one ship to another in a class of ships and also from one class of ships to another.

Basic model

The stochastic model of the still water bending moment used in the present reliability assessment of tankers ships is defined on the basis of the statistical analysis performed by Guedes Soares and Moan (1988). The results of the statistical analysis have shown that the maximum value of the vertical still water bending moment is normally distributed. The parameters can be estimated using regression equations as a function of the ship length (L) and the nondimensional mean deadweight (W),

$$X = A_0 + A_1 \cdot W + A_2 \cdot L \tag{3.34}$$

where X is the mean value of the maximum still water bending moment, ($Max\ BM$), or is the mean value of the standard deviation of $Max\ BM$ ($SD[Max\ \mathrm{BM}]$). It can also be the standard deviation of the mean still water bending moment (SD), which accounts for the variations of the mean from one ship to another within a particular class of ships. The regression coefficients are presented in table 3.7.

Table 3.7
Regression coefficients of equation 3.34

Regression Variable X	A_0	A_1	A_2
$Max\ BM$	114.7	-105.6	-0.154
$SD[Max\ BM]$	17.4	-7.0	0.035
SD	11.6	-5.0	0.030

These values are given as a percentage of the maximum allowed value of still water bending moments, which are the nominal code values m_{ns}. Thus, the stochastic model for still water bending moment becomes completely defined by the mean value:

$$\overline{m_s} = \frac{MaxBM \cdot m_{ns}}{100} \tag{3.35}$$

and the standard deviation for one ship:

$$SD_s = \frac{SD[MaxBM] \cdot m_{ns}}{100} \tag{3.36}$$

If the mean value $\overline{m_s}$ is not known and the model is to be applied to any ship of the same type it is necessary to account for the variability of the mean value between sister ships of the same type. This will increase the standard deviation, which is now given by:

$$STD = \frac{\sqrt{SD[MaxBM]^2 + SD^2} \cdot m_{ns}}{100} \tag{3.37}$$

where the second term in the sum accounts for the variability of the mean value among sister ships.

The nominal value of the maximum still water bending moment was calculated according to the current rules of Det norske Veritas (DnV) given by:

$$m_{ns} = f\, C_w\, L^2\, B\,(C_B + 0.7) \quad \text{(KN.m)} \tag{3.38}$$

where C_B is the block coefficient and f is 0.072 for sagging and 0.078 for hogging moments. The coefficient C_w is given by:

$$\begin{aligned} C_w &= 10.75 - \left(\frac{300 - L}{100}\right)^{1.5} && \text{for } 100\,\text{m} < L < 300\,\text{m} \\ C_w &= 10.75 && \text{for } L > 300\,\text{m} \end{aligned} \tag{3.39}$$

Table 3.8 summarises the resulting statistical moments for the considered tankers. The negative values correspond to sagging moments and the positive ones to hogging.

From the results of table 3.8 it can be seen that the full load condition always induces a sagging bending moment. Note that, although the mean value is close to 20% of the design value for a medium tanker in sagging condition, the coefficient of variation is very high, around 1.15.

Table 3.8
Stochastic model of still water bending moment, M_s.

Ship	Load Condition	m_{ns} (MN.m)	W %	*Max BM* %	*STD* %	*Mean Value* (MN.m)	*STD* (MN.m)
TK1	FL	277.7	0.914	-2.4	19.2	-6.6	53.2
	BL	300.8	0.484	43.0	22.9	129.5	68.8
	PL	300.8	0.699	20.3	21.0	61.2	63.2
TK2	FL	2468.2	0.914	-17.2	23.6	-425.5	582.5
	BL	2673.9	0.484	28.2	27.3	753.2	730.0
	PL	2673.9	0.699	5.5	25.5	146.1	680.5
TK3	FL	2595.1	0.914	-18.2	23.9	-471.3	619.6
	BL	2811.4	0.484	27.2	27.6	766.0	775.3
	PL	2811.4	0.699	4.5	25.7	127.7	723.3
TK4	FL	5590.9	0.914	-30.0	27.4	-1678.4	1532.9
	BL	6056.8	0.484	15.4	31.1	932.0	1884.6
	PL	5590.9	0.699	-7.3	29.3	-409.0	1636.3

An alternative stochastic model for the still water bending moment can be defined based on the ship loading manual. The model assumes that the still water loads vary monotonically during a voyage, between a departure and an arrival value. This implies that the distribution of the still water values at a random point in time is considered to be

a uniform distribution conditional on the departure and arrival values. The marginal distribution is obtained by unconditioning on the arrival and departure values, as proposed by Guedes Soares and Dogliani (1995):

$$f_{sw}(x_p) = \iint \frac{1}{|b-a|} f_{SW\,Dep}(a) f_{SW\,Arr}(b)\, da\, db \tag{3.40}$$

where the distribution of the still water bending moment on departure $f_{SW\,Dep}(x)$ and on arrival $f_{SW\,Arr}(x)$ are assumed to be Gaussian.

From numerical simulation results it was observed that the resulting distribution is no longer uniform and for the purpose of reliability analysis, it may be assumed to be a Gaussian distribution having the following parameters,

$$\mu = \frac{|\mu_{Dep} + \mu_{Arr}|}{2} \tag{3.41}$$

$$\sigma = \frac{|\sigma_{Dep} + \sigma_{Arr}|}{2} \tag{3.42}$$

For each load condition (Full, Ballast and Partial load) the mean and standard deviation of the still water load both in departure and arrival condition can be derived based on the available data from the loading manual.

The statistical parameters were calculated based on the available data from the ship loading manual for tanker TK3. Table 3.9 presents the stochastic model for still water bending moment in full and ballast load condition based on both general ship statistics and loading manual.

Table 3.9
Comparison of different stochastic models for still water bending moment

Ship	Load Condition.	Ship Statistics		Loading Manual	
		Mean	*STD*	*Mean*	*STD*
TK3	FL	-471.3	619.6	-599.0	294.2
	BL	766.0	775.3	1325.5	707.1

It is clear that in this specific case the loading manual leads to significantly higher values for the mean value of still water bending moment. However, the coefficient of variation is around 0.5 while based on ship statistics this value is equal to 1.3 and 1.0 in full and ballast load condition, respectively.

Extreme model

The intensity of the still water load effect is modelled as a normally distributed random variable that refers to a single voyage. The extreme distribution of the still water load over the fraction of time T_c that the ship spends in load condition "c" can be obtained by assuming independence of the maxima between different voyages,

$$F_{se}(x_e;T_c)=[F_s(x)]^{n_C} \tag{3.43}$$

where n_c is the number of voyages in the period T_c which is calculated according to the operational profile adopted (see table 3.2).

Since the distribution function $F_{se}(x_e;T_c)$ cannot be expressed in algebraic form, an approximation has to be used in the reliability assessment. When the values μ_s and σ_s of the normal distribution are known the distribution of the extreme values over the time period T_c can be approximated as a Gumbel law with the following parameters:

$$\mu_{ns}=u_n=F_s^{-1}\left(1-\frac{1}{n_c}\right) \tag{3.44}$$

$$\sigma_{ns}=[h(u_n)]^{-1} \tag{3.45}$$

with,

$$h(u_n)=\frac{f_s(u_n)}{1-F_s(u_n)} \tag{3.46}$$

where h is the hazard function and the characteristic largest value u_n is the value of x that, on average, is exceeded once in a sample of size n_c.

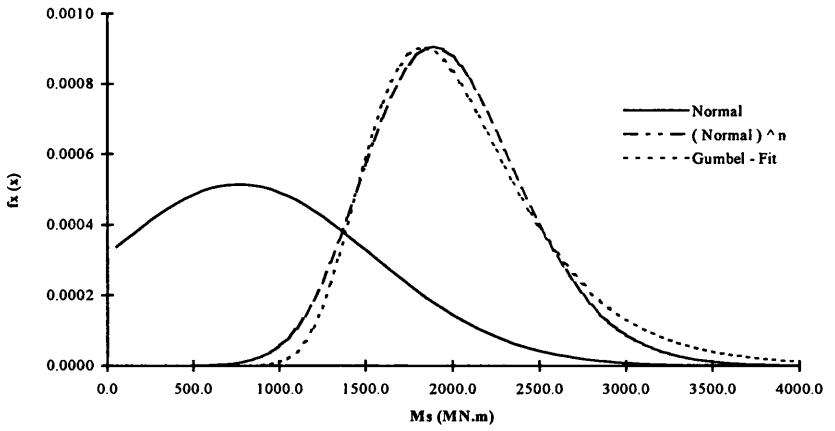

Figure 3.12: Extreme model for still water bending moment (n=10 voyages)

Figure 3.12 illustrates the distribution of the maximum value $[F_s(x)]^{n_C}$ based on the underlying normal distribution and the approximated Gumbel model to describe the extreme model of still water loads effects.

Table 3.10 presents the parameters of the stochastic model for the extreme still water bending moment according to the operational profile adopted ($n_{C\,FL} = n_{C\,BL} = 5.4$ voyages and $n_{C\,PL} = 27.4$ voyages).

Table 3.10
Stochastic model of the extreme still water bending moment

Ship	Condition	Normal Moments		Gumbel Moments	
		μ_s	σ_s	μ_{se}	σ_{se}
TK1	FL	-6.6	53.2	-75.7	47.2
	BL	129.5	68.8	218.9	61.0
	PL	61.2	63.2	191.1	37.0
TK2	FL	-425.5	582.5	-1182.5	516.7
	BL	753.2	730.0	1701.9	647.5
	PL	146.1	680.5	1545.3	398.4
TK3	FL	-471.3	619.6	-1276.6	549.6
	BL	766.0	775.3	1773.5	687.6
	PL	127.7	723.3	1614.7	423.4
TK4	FL	-1678.4	1532.9	-3670.5	1359.6
	BL	932.0	1884.6	3381.2	1671.6
	PL	-409.0	1636.3	-3773.1	957.9

3.2.7 Load combination between still water and wave bending moment

Having defined the probabilistic models for still water and wave induced bending moment the prediction of combined loads should be assessed due to the random nature of the loads.

In the reliability assessment of the primary ship structure it is required to know the maximum value of the two most important load effects. However, the maximum value of the sum of two loads is usually less than the sum of the two maxima that can occur in any time,

$$M_{te} = M_{se} + \Psi M_{we} \tag{3.47}$$

where Ψ is the load combination factor normally ranged from 0.8 to 0.95 depending on the assumptions.

The combination between the still water and wave induced bending moment can be done using stochastic methods, which combine the stochastic processes directly, or by deterministic methods that combine the characteristic values of the stochastic processes.

Ferry-Borges method (Ferry Borges, 1971), load coincident method (Wen, 1977), and point-crossing method (Larrabee, 1981) are examples of stochastic methods while deterministic methods include the peak coincidence method, Turkstra's rule (Turkstra, 1970) and the square root of the sum of squares (SRSS) rule (Goodman, 1954).

These methods have been applied to combine the still water and wave induced vertical bending moment and the different load combination solutions have been compared as done by Guedes Soares (1992) and Wang and Moan (1996).

It was concluded that the peak coincident method is very conservative. However, other deterministic methods as the Turkstra's rule and the SRSS rule underestimate the combined bending moment. Using stochastic methods it was found that all lead to identical predictions. Since, of these, the point-crossing method provides the exact solution, this indicates that these models are very precise for further applications.

In the present study the Ferry-Borges method is used to estimate the load combination factors. However, reliability results using Turkstra's rule are presented since this method may be considered a lower bound solution to load combination.

Turkastra's rule

Turkstra's rule assumes that, for the sum of two independent random processes, the total maximum moment occurs when either moment of the individual processes has its maximum value,

$$M_{te} = max\left\{\left(M_{se} + M_{w}\right), \left(M_{s} + M_{we}\right)\right\} \tag{3.48}$$

where M_{se} and M_{we} are the extreme value distributions of still water and wave induced bending moment, respectively, and M_s and M_w are the arbitrary-point-in-time values of the random variables.

Ferry-Borges method

The method assumes that the loads change intensity after prescribed deterministic, equal time intervals, during which they remain constant. The intensity of the loads in the different elementary time intervals are outcomes of identically distributed and mutually independent random variables.

The probabilistic distribution F_{te} of the maximum value during n repetitions of the load i or equivalently during the time $T=n\tau$, where τ is the pulse duration, is given by:

$$F_{te}(x)=[F_x(x)]^n \tag{3.49}$$

where $F_x(x)$ is the probability distribution function of the load intensity.

In the application of this method to the combination of still water and wave induced bending moment, two load processes with durations τ_s and τ_w have to be considered (Figure 3.13).

The probability distribution of the maximum of the combined process during time T can be determined exactly provided that the two process are in phase, and that the ratios $\tau_s/\tau_w=n_w$ and $T/\tau_s=n_s$. In this case one has:

$$F_{te}(x)=\left\{\int_{-\infty}^{x} f_s(z)[F_w(x-z)]^{n_w}\,dz\right\}^{n_s} \tag{3.50}$$

The density distribution function f_s is the still water bending moment in one voyage which is a normal distribution with parameters given in table 3.8. $[F_w]^{n_w}$ is the Gumbel distribution of the extreme wave induced bending moment in one voyage derived from the Weibull distribution assuming n_w wave loads in one voyage.

The distribution of extreme combined vertical bending moment can be calculated for the different load conditions according to the operational profile that indicates the number of voyages n_s in each load condition.

Figures 3.14 and 3.15 illustrate the resultant density distributions for the medium size tanker TK3 in full and partial load condition, respectively.

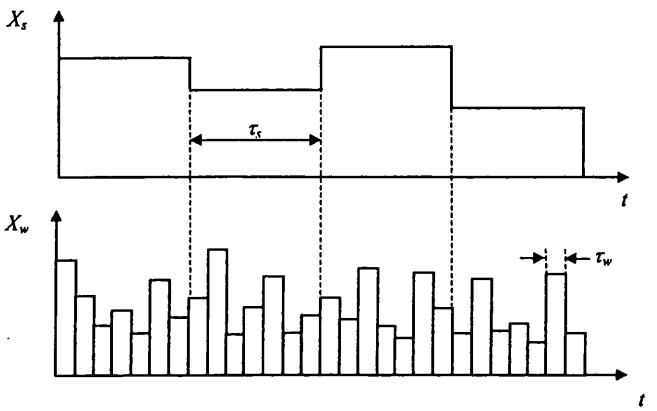

Fig 3.1.3 : Illustration of the Ferry-Borges model

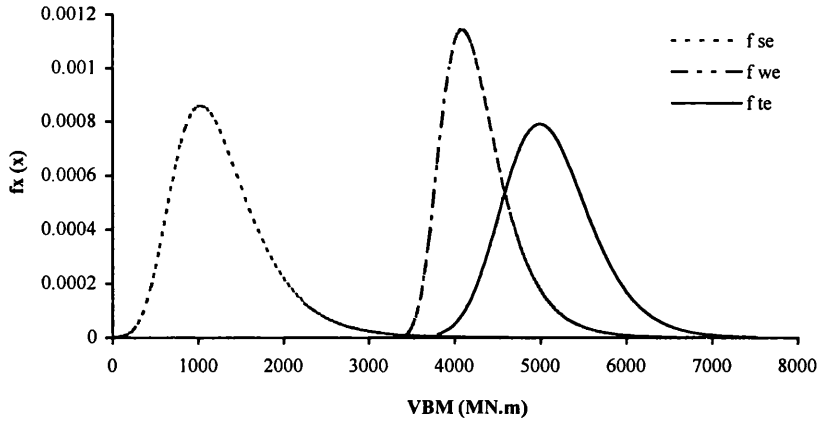

Figure 3.14: Density function of the combined load in full load condition

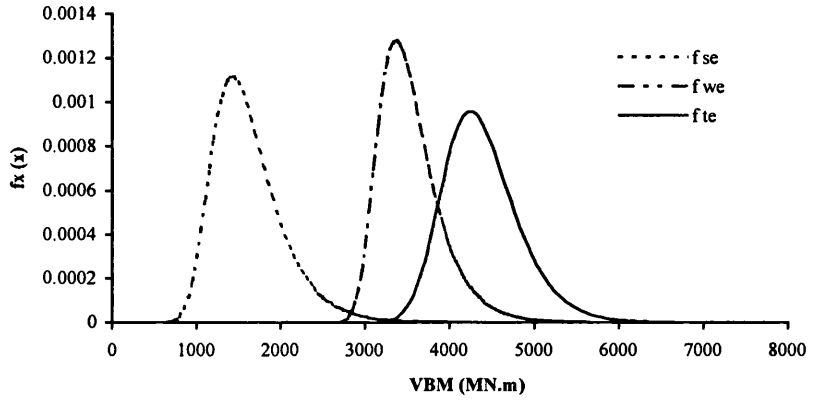

Figure 3.15: Density function of the combined load in partial load condition

The load coefficient parameter Ψ is now introduced by solving the following relationship,

$$F_{te}(x) = F_{se}(x) + \Psi F_{we}(x) \tag{3.51}$$

where extreme distributions are considered at 0.5 exceedance level. Thus, the combination factor is evaluated by:

$$\Psi = \frac{F_{te}^{-1}(x = 0.5) - F_{se}^{-1}(x = 0.5)}{F_{we}^{-1}(x = 0.5)} \tag{3.52}$$

Figures 3.16 and 3.17 illustrate the difference between the distribution functions of the individual loads and the combined effect for tanker TK3 in full and partial load condition.

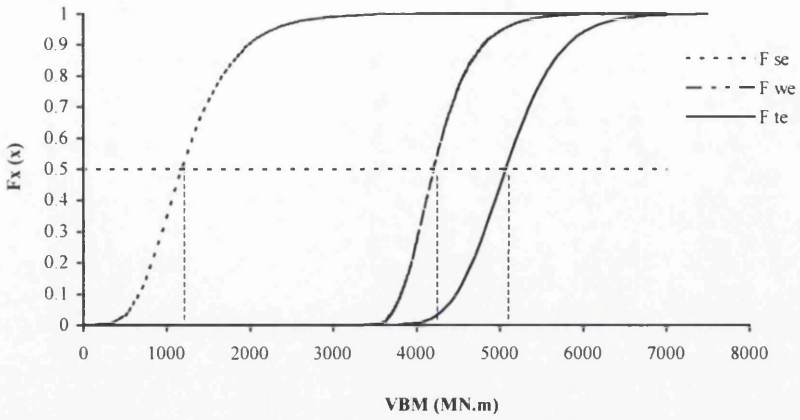

Figure 3.16: Distribution function of the combined load in full load condition

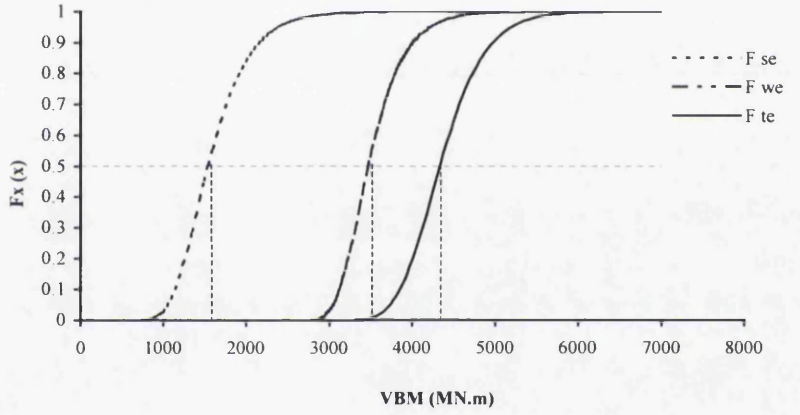

Figure 3.17: Distribution function of the combined load in partial load condition

Table 3.11 shows the resulting values of the load combination factor for tanker TK3 in full, ballast and partial load condition.

Table 3.11
Values of the load combination factors for tankers

Load Condition	$F_{se}^{-1}(x=0.5)$	$F_{we}^{-1}(x=0.5)$	$F_{te}^{-1}(x=0.5)$	Ψ
FL	1186	4210	5074	0.923
BL	1661	3751	5085	0.913
PL	1545	3475	4337	0.803

The values for the load combination presented in table 3.11 lie within the range calculated by Guedes Soares (1992) and Casella, Dogliani M. and Guedes Soares (1996), and hence were adopted for the present reliability assessment of tankers.

3.2.8 Model uncertainties

Uncertainty on ultimate capacity χ_U

This random variable takes into account both the uncertainty in the yield strength and the model uncertainty on the ultimate capacity of the ship. Its stochastic model adopts a log-normal distribution function with mean value equal to one and a coefficient of variation equal to 0.15.

The ultimate collapse moment results from the contribution of the different plate elements, which are in principle all made from the same material, having thus a high correlation. It is well known that the sum of a number of independent and identically distributed normal random variable has a variance that decreases as the square root of the number of variables. However in this case in which there is strong correlation between them, the effect can be basically neglected and the COV to be adopted should be the one of the yield stress.

If the steel comes all from the same mill and the same batch, a value of a COV=0.08 could be used, which combined with a small model uncertainty would lead to the optimistic value of 0.10 for the ultimate moment.

If the steel plates result from different batches and different mills or are of different types such as mild steel and high strength steel or if the steel of the plates is different from the one of the stiffeners, then a COV between 0.11 and 0.13 may result. This type of value with a small model uncertainty will lead to a value around 0.15 and with a large model uncertainty it can go up 0.20. Thus, the value of COV=0.1 can be considered an optimistic one, 0.15 will be a realistic one and 0.20 is a conservative value.

Non-linear effects χ_{NL}

The effect of the non-linearity of the response is particularly significant for ships with a low block coefficient, leading to differences between sagging and hogging bending moments. This effect was identified by Guedes Soares (1991) who proposed an expression to improve the linear predictions,

$$\frac{M_S}{M_L} = 1.74 - 0.93\, C_b \tag{3.53}$$

$$\frac{M_H}{M_L} = 0.26 + 0.93\,C_b \tag{3.54}$$

where, C_b is block coefficient and M_L, M_S *and* M_L are respectively the linear, sagging and hogging vertical wave induced bending moment.

Equations 3.53 and 3.54 were used to define the mean value of a normally distributed random variable that takes in to account the non-linear effects in the reliability formulation. The results are given in table 3.12, in which a COV of 0.15 was adopted.

Table 3.12
Corrections for non-linear effects

Ship	Condition	*Mean Value*	*STD.*
TK1	Sag.	0.911	0.137
	Hog.	1.089	0.163
TK2	Sag.	1.021	0.153
	Hog.	0.979	0.147
TK3	Sag.	1.009	0.151
	Hog.	0.991	0.149
TK4	Sag.	1.032	0.155
	Hog.	0.968	0.145

Uncertainty on wave load evaluation χ_W

The calculations of wave induced load effects are normally made with programs based on the linear strip theory that differ in the detailed way in which the hydrodynamic coefficients are calculated. The long-term distributions calculated based on transfer functions obtained by the different methods have demonstrated that a large degree of uncertainty is associated with the predicted midship wave induced loads (Shellin et al., 1996).

The uncertainty on the transfer function can be assessed by calculating the corresponding long-term distributions and quantifying the uncertainty on the characteristic value, as proposed by Guedes Soares and Trovão (1991).

Figure 3.18 shows the long-term distribution for a containership calculated with methods of Instituto Superior Técnico (IST), Registro Italiano Navale (RINA), and Germanischer Lloyd based on both strip theory (GL2D) and diffraction theory (GL3D) (Guedes Soares, 1996).

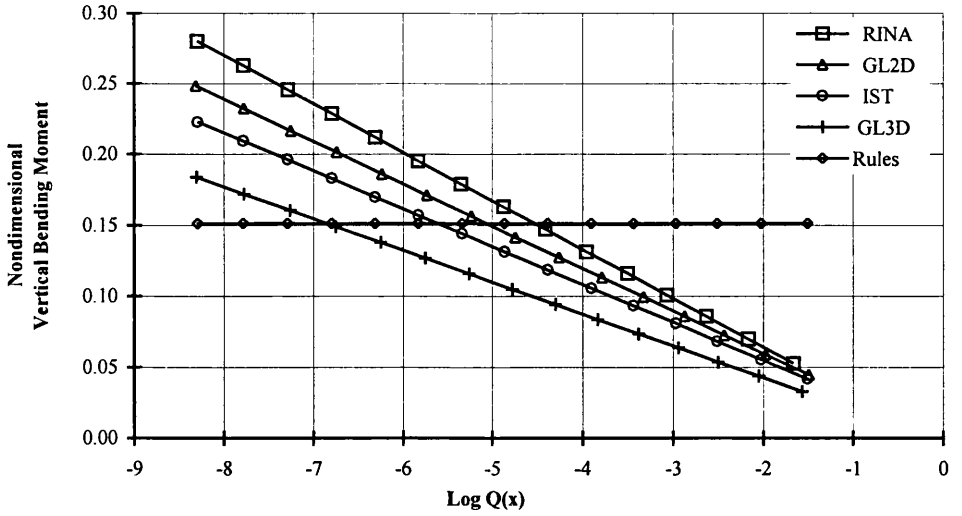

Figure 3.18: Long-term distribution of wave induced bending moments calculated for a North Atlantic scatter diagram from Global Wave Statistics

From inspection of the benchmarking results, summarised in table 3.13, a random variable χ_w was defined to introduce the uncertainty of the wave induced load calculations in the reliability formulation. It was assumed a normal distribution function with mean value equal to 0.70 obtained as the ratio of the IST (Instituto Superior Técnico) to actual IACS (International Association of Classification Societies requirement (IACS, 1993) and a coefficient of variation equal to 0.15.

Table 3.13
Characteristic value of the wave induced load effects calculated for a containership

	10^{-8} reference value	
	Vert. Bend. Moment	VBM_i / VBM_{RULES}
RINA	0.270	0.56
GL2D	0.239	0.63
IST	0.215	0.70
GL3D	0.177	0.85
Average Global Wave	0.225	0.67
Average IACS	0.285	0.53
Rules	0.151	1.00

3.2.9 Results of the reliability analysis

The reliability calculations were carried out using the computer program COMREL (Gollwitzer, Abdo and Rackwitz, 1988). Table 3.14 summarises the stochastic model used in the reliability analysis considering the distribution of the extreme values of the load effects in the three load conditions.

Table 3.14
Stochastic models for reliability assessment of tankers

Ship	LC	M_u	M_{se} – Gumbel		M_{we} - Gumbel		Ψ	χ_{nl} - Normal		χ_w - Normal		χ_u – LogNorm.	
		Const	*Mean*	*STD*	*Mean*	*STD*	*Const*	*Mean*	*STD*	*Mean*	*STD*	*Mean*	*STD*
	FL	910	-76	47	378	36	0.923	0.911	0.137				
TK1	BL	932	219	61	337	33	0.913	1.089	0.163				
	PL	932	191	37	313	32	0.803	1.089	0.163				
	FL	6652	-1183	517	4052	391	0.923	1.021	0.153				
TK2	BL	7120	1702	647	3613	367	0.913	0.979	0.147				
	PL	7120	1545	398	3349	350	0.803	0.979	0.147	0.700	0.105	1.0	0.15
	FL	7123	-1277	550	4278	413	0.923	1.009	0.151				
TK3	BL	8354	1773	688	3814	387	0.913	0.991	0.149				
	PL	8354	1615	423	3536	370	0.803	0.991	0.149				
	FL	16392	-3670	1360	9815	959	0.923	1.032	0.155				
TK4	BL	19164	3381	1672	8753	900	0.913	0.968	0.145				
	PL	16392	-3773	958	8106	853	0.803	1.032	0.155				

The reliability indices for tankers in the different load condition are presented in table 3.15. The table also shows the global annual reliability index in sagging and hogging obtained by:

$$\beta = \Phi^{-1}(P_{f\,BL} + P_{f\,FL} + P_{f\,PL}) \tag{3.55}$$

Table 3.15
Reliability index for tankers in sagging and hogging condition

Ship	Cond.	β_{FL}	β_{BL}	β_{PL}	P_{ft}	β_t
TK1	Sag.	4.28	6.65	7.00	9.27E-06	4.28
	Hog.	5.03	3.14	4.20	8.70E-04	3.13
TK2	Sag.	2.28	4.75	5.47	1.13E-02	2.28
	Hog.	4.72	2.70	3.66	3.65E-03	2.68
TK3	Sag.	2.35	4.82	5.55	9.51E-03	2.34
	Hog.	4.77	2.77	3.75	2.86E-03	2.76
TK4	Sag.	2.03	4.53	2.99	2.25E-02	2.00
	Hog.	4.99	2.91	6.33	1.81E-03	2.91

As one can see the full load case is dominant in the sagging condition. However, in hogging condition the ballast load case is the dominating one.

In the following, the results of a sensitivity analysis are presented for the two dominating load conditions, full load for sagging and ballast load for hogging.

The importance of the contribution of each variable to the uncertainty of the limit state function $g(x)$ can be assessed by the sensitivity factors which are determined by:

$$\alpha_i = -\frac{1}{\sqrt{\sum_{i=1}^{\infty}\left(\frac{\partial g(\underline{x})}{\partial x_i}\right)^2}}\frac{\partial g(\underline{x})}{\partial x_i} \tag{3.56}$$

Table 3.16 shows the sensitivities of the failure function with respect to changes in the variables. A positive sensitivity indicates that an increase in a variable results in an increase in the failure function and positively contributes to reliability.

Table 3.16
Sensitivities of the variables

Load Cond.	M_s	X_w	X_{nl}	M_w	X_u
FL – Sag.	-0.572	-0.346	-0.345	-0.270	0.601
BL – Hog.	-0.744	-0.232	-0.232	-0.179	0.554

From table 3.16 it can be seen that the importance of the uncertainty on the ultimate strength remains constant in the two load conditions. However, the overall importance of the wave induced loads variables (M_w, X_{nl} *and* X_w) decreases from full to ballast load condition, as illustrated in figure 3.19.

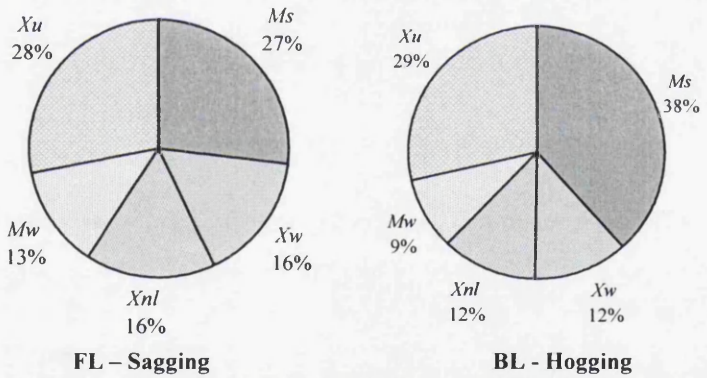

Figure 3.19: Sensitivities of the variables in different load conditions

Interpretation of the reliability results

The reliability results obtained are presented in figure 3.20 (table 3.17) as a function of the ship length for tankers in sagging and hogging condition.

Table 3.17
Reliability index for tankers in sagging and hogging condition

Ship	L (m)	B (m)	C_b	$\beta_{Sagging}$	$\beta_{Hogging}$
TK1	133.4	18.0	0.700	4.28	3.13
TK2	230.0	42.0	0.818	2.28	2.68
TK3	236.0	42.0	0.805	2.34	2.76
TK4	313.0	48.2	0.830	2.00	2.91

As can be seen the β-values in sagging tend to decrease as the length of the ship increase. However, the reliability index in hogging condition does not follow this tendency.

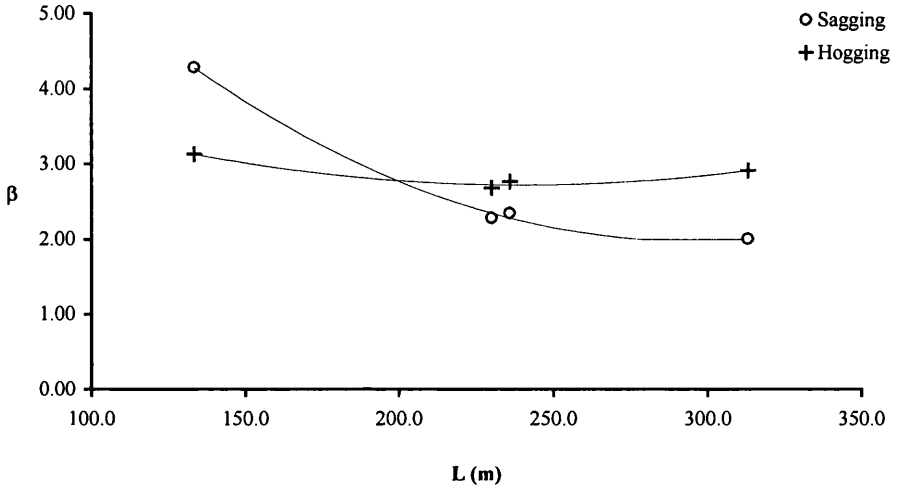

Figure 3.20: β-values as function of the ship length

The interpretation of the reliability results can be made comparing the mean value of the stochastic variables with the minimum requirement values defined in Rules.

According to the IACS (1993) unified requirements, the vertical wave bending moment amidships are required to be not less than:

$$\begin{aligned} m_{nw} &= 0.11 C_W L^2 B(C_B + 0.7) \quad \text{kNm in sagging} \\ &= 0.19 C_W L^2 B C_B \qquad\quad \text{kNm in hogging} \end{aligned} \tag{3.57}$$

where C_W is the wave load coefficient which can be taken as:

$$\begin{aligned} C_W &= 0.0792L && \text{for } L \le 100 \\ &= 10.75 - [(300 - L)/100]^{3/2} && \text{for } 100 < L < 300 \\ &= 10.75 && \text{for } 300 \le L \le 350 \\ &= 10.75 - [(L - 350)/150]^{3/2} && \text{for } L > 350 \end{aligned} \tag{3.58}$$

The still water bending moment amidships are not to be taken less than:

$$\begin{aligned} m_{ns} &= -0.065\, C_W L^2 B(C_B + 0.7) \quad \text{kNm in sagging} \\ &= C_W L^2 B(0.1225 - 0.015\, C_B) \quad \text{kNm in hogging} \end{aligned} \tag{3.59}$$

The total longitudinal bending moment can be estimated as:

$$m_t = m_{nw} + m_{ns} \tag{3.60}$$

In table 3.18 the IACS reference values for wave loads at the $10^{-6.5}$ probability level are presented. This value corresponds to the return period of one year, which is in correspondence with the annual reliability indices. The same table also presents the difference in percentage determined by the equation 3.61 that shows the overloading of the wave induced bending moment (M_w) in relation to the minimum Rules requirement (m_{nw}):

$$\Delta M_w(\%) = \frac{M_w - M_{w,r}}{M_{w,r}}(100) \tag{3.61}$$

Table 3.18
Wave induced bending moments compared with the rules values

Ship	L (m)	Weibull Parameters		M_w (MN.m)	Rules (MN.m)	ΔM_w
		w	k	$Q_x=10^{-6.5}$	m_{mw}	(%)
TK1	133.4	19.6	0.912	-381	-424	-10
TK2	230.0	195.5	0.890	-4088	-3771	8
TK3	236.0	206.4	0.890	-4317	-3965	9
TK4	313.0	456.0	0.879	-9906	-8542	16

As one can see the wave induced loads in sagging condition increase with the ship length. In fact the wave induced bending moment in the shorter ship is about 10% less than the rules value while the longer one exhibits a larger value when compared with the rules.

Identical results are obtained for tankers in hogging condition. However, in this case the still water bending moment has to be analysed since it has a large effect on the reliability results as shown by the sensitivity analysis.

Table 3.19 shows a comparison of the nominal values defined in IACS rules with the still water bending moment in ballast load condition used in the reliability analysis.

Table 3.19
Still water bending moments compared with the rules values

Ship	L (m)	Gumbel Parameters			Rules (MN.m)	ΔM_s
		Mean V.	*STD*	*COV*	m_{ns}	(%)
TK1	133.4	219	61	0.28	309	-29
TK2	230.0	1702	647	0.38	2489	-32
TK3	236.0	1773	688	0.39	2645	-33
TK4	313.0	3381	1672	0.49	5585	-39

It can be seen that the still water bending moment in hogging varies between 29% and 39% from the rules nominal value. Table 3.19 also shows that the still water load effects

tend to decrease with the length of the ship. However, the uncertainty on the values of the bending moment increases for longer ships. This combined effect explains the small variability between the reliability indices obtained for tankers in hogging condition.

From figure 3.20 it can be seen that the failure in sagging has a higher probability for longer ships. This fact can not be explained based only on the comparison of the load effects. Therefore, the ultimate bending moment in sagging and hogging conditions should be analysed.

Table 3.20 shows a comparison between the ultimate bending moment used in the reliability calculations and the nominal value defined in the IACS rules. The values of ΔM_u were defined according to equation 3.61. They can be interpreted as a reserve of strength of the ship when compared with the rules requirement.

Table 3.20
Ultimate bending moments compared with the rules values

Ship	L (m)	Sagging (MN.m)	Hogging (MN.m)	Rules m_{nu}	ΔM_u (%) Sagging	ΔM_u (%) Hogging
TK1	133.4	910	932	675	35	38
TK2	230.0	6652	7120	5999	11	19
TK3	236.0	7123	8354	6308	13	32
TK4	313.0	16392	19164	13589	21	41

Figure 3.21 shows that the midship section of the ships have a lower reserve of strength in sagging bending moment. Additionally, the difference between the reserve of strength in sagging and hogging tend to increase as the length of the ship increases.

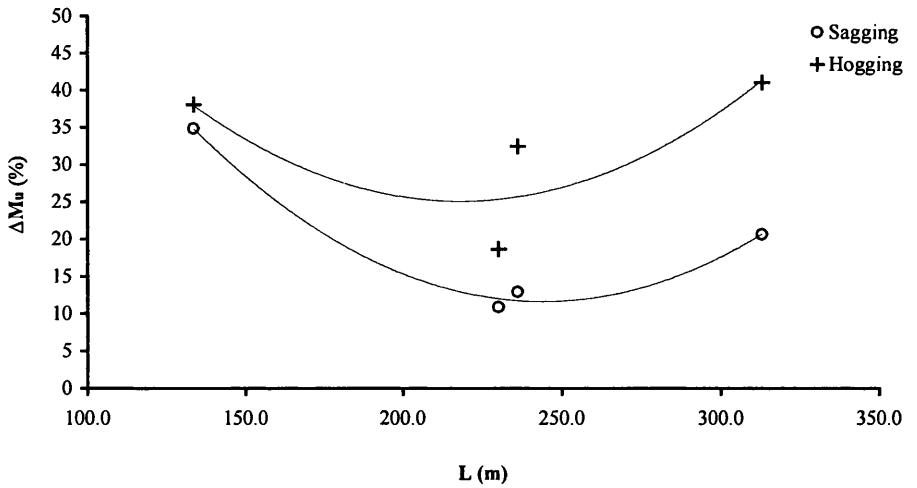

Figure 3.21: Ultimate bending moments compared with the rules values

The combined analysis of the load effect and the ultimate strength of the ships explain the variability between the reliability indices obtained. This variability clearly illustrates the different reserves of safety in relation to the practice prescribed in rules.

3.2.10 Relation between the reliability formulations

In section 3.2.5 and 3.2.6 different formulations for the still water and wave induced load effects were defined. The model that has been traditionally used in this field uses the random point in time formulation in which M_s is a normal distribution and M_w a Weibull. However, if one wants to calculate the reliability during a certain period of operation, the extreme loads during that period should be considered i.e M_{se} and M_{we}, which are then Gumbel distributions. Combination of extreme and random point in time distributions could also be considered in the spirit of the Turkstra rule.

Table 3.21 summarises the reliability results for tanker TK3 in the full load condition using different reliability formulations.

Table 3.21
β- values for the different reliability models

Ship	$M_{se}+M_{we}$	M_s+M_{we}	$M_{se}+M_w$	M_s+M_w
TK3	2.35	2.85	4.26	5.75

The main objective of presenting these results is to emphasise the fact that depending in the way the reliability problem is formulated the reliability index can change dramatically (in this case from 2.35 to 5.75). However, the formulations represent different statements about the same reality and they are acceptable since one can relate them to each other.

Relation between β-values using basic and extreme value model

The relationship between the model of the long-term distribution of individual waves and the extreme model is obtained by the most likely maximum wave to occur in the reference period.

If the reference period is described in number of waves n, then the probability that the most likely maximum occurs during the reference period is $P_e=1/n$, if one assumes independence between successive waves. In fact the existence of correlation will imply that within the same time frame the number of independent waves is smaller, but this effect is not considered here.

The probability of failure calculated with the extreme formulation can be considered as conditional ($P_{f|e}$) on that maximum (P_e). Thus, the total probability of failure is obtained by unconditioning:

$$P_f = P_{f|e} \cdot P_e \tag{3.62}$$

with $P_{f|e} = \Phi(-\beta_e)$ being the probability of failure considering the extreme wave model, and P_e is the probability of the occurrence of the extreme wave, i.e. $P_e = 1/n$.

Since the safety is measured in terms of the reliability index, the unconditional probability of failure obtained in equation3.62 can be expressed in terms of β by using the inverse normal distribution:

$$\beta = \Phi^{-1}[P_{f|e} \cdot P_e] \tag{3.63}$$

Table 3.22 shows the results of these calculations. The values indicate that the two formulations can in fact be related as described. Dealing with such small levels of probability and performing calculations with single precision, one must expect some numerical deviations, of the type shown in table3.22.

Table 3.22
Relation between β-values using the Weibull and extreme value models

M_{we} - Gumbel (n = 1.58E+06)				M_w - Weibull
β_e	$P_{f\|e}$	$P_{f\|e} \cdot P_e$	β	β_w
2.85	2.19E-03	1.39E-09	5.94	5.75

It is also possible to estimate the reliability in the reference time period, considering a sequence of n wave peaks for each of which the reliability R_i is calculated with the Weibull model.

$$\beta'_e = \Phi^{-1}\left[1 - (R_i)^n\right] \tag{3.64}$$

The results in table 3.23 show that β obtained in both cases are similar.

Table 3.23
Relation between β-values using the extreme value and Weibull models

M_w - Weibull			M_{we} - Gumbel (n = 1.58E+06)		
β_w	P_f^b	$R_e = R_i^n$	P_f^e	β'_e	β_e
5.75	4.42E-09	9.93E-01	6.95E-03	2.46	2.85

Relation between β-values using two extreme value models

A different analysis can be made by comparing the results of using the extreme model for different reference times. For the sake of illustration, if one considers two halves of the reference time, the extreme distributions must be referred to a shorter duration but the overall result must be the same.

If one defines the probability of failure in the duration of n cycles as $P_f(n)$, it can be related with the probability of failure in any of the two disjoint intervals of half duration by:

$$P_f(n) = 1 - \left[1 - P_f\left(\frac{n}{2}\right)\right]\left[1 - P_f\left(\frac{n}{2}\right)\right] \tag{3.65}$$

The same argument can be generalised to any number of intervals into which a reference period can be divided. This can be applied for example to relate the lifetime probability of failure with the yearly probability of failure and this one with the probability of failure in a voyage.

Table 3.24 shows the relation between the results of two extreme models assuming one voyage and one year of operation in which 5 voyages were considered for tanker TK3 in full load condition.

Table 3.24
Relation between β-values using two extreme value models

One voyage (n = 0.32E+06)			k = 5		One Year
$M_s+M_{we\ 1\ voy.}$	P_f	1-P_f	1-(1- P_f) ^{k}	$\beta_{e\ 5\ voy.}$	β_e
3.28	5.19E-04	9.995E-01	2.59E-03	2.80	2.85

It can be observed that the reliability indices obtained by the two formulations are very similar demonstrating that it is possible to relate one formulation to the other.

In table 3.25 a similar calculation is performed to estimate the 20-years probability of failure based on the one-year reliability index.

Table 3.25
Relation between one-year and 20-years reliability index

One Year			k = 20		20 Years
$M_s+M_{we\ 1\ year.}$	P_f	1-P_f	1-(1- P_f) ^{k}	$\beta_{e\ 20\ years.}$	β_e
2.85	2.18E-03	9.98E-01	4.269E-02	1.72	2.10

3.3 PARTIAL SAFETY FACTORS

During the last decades there have been considerable developments of methods and tools for probabilistic computation purposes that are capable of representing in a rational manner the uncertainties in the design of structures. However, there exists currently a gap between existing design practice based on partial safety factor format design codes and the potential usage of probabilistic methods.

In fact, the results of reliability analyses have shown that the semi-empirical design rules have not been calibrated against a uniform reliability level. Therefore, partial safety factors calibrated on the basis of a probabilistic reliability analysis have been derived in order to achieve pre-defined target safety levels.

This section presents the calculation of the partial safety to be used for a probability based design rule for tankers. The results are obtained on the basis of reliability analysis using the FORM algorithm as described in section 3.2.

It was shown that different reliability formulations for the load variables can be used. The choice of one or the other would lead to different values but they could be related to each other. Therefore, only one formulation needs further consideration and then it was decided to adopt here the extreme model of still water and wave induced bending moment.

3.3.1 Safety format with partial safety factors

The partial safety factors are already used in a number of structural design codes. Its formulation, for ultimate structural failure of the hull girder, might be expressed in a code or design format as,

$$\gamma_s m_{ns} + \gamma_w m_{nw} \leq \frac{m_{nu}}{\gamma_u} \tag{3.66}$$

where γ_u is the partial safety factor applied to the nominal ultimate vertical bending moment as obtained from direct analysis of midship cross section of the ship (m_{nu}=m_u); γ_s and γ_w are the partial safety factors applied to the nominal values of the still water and wave induced bending moment, respectively, defined according to the IACS (1993) unified requirements (equations 3.59 and 3.57).

For reliability analysis based on a FORM algorithm, a stochastic safety margin g was defined as,

$$g = \chi_u M_u - \left(M_s + \Psi\, \chi_{nl}\, \chi_W M_W\right) \tag{3.67}$$

where M_u is the stochastic description of the ultimate longitudinal bending strength of the ship, M_s and M_w are the stochastic still water and wave induced bending moments, respectively. The definition of partial safety factors for ship structures under specified stochastic actions implies the determination of the design values of the variables (m_u^*, m_s^*, m_w^*, χ_u^*, χ_w^* and χ_{nl}^*) defined as those points on the limit state function that have the maximum conditional probability when failure occurs.

For the formulation of a design code it is necessary to specify the nominal values for the loads m_{ns} and m_{nw}. Then meaningful partial safety factors can be calculated as

$$\gamma_s = \frac{m_s^*}{m_{ns}} \qquad \gamma_w = \frac{\Psi^* \chi_w^*\, \chi_{nl}^*\, m_w^*}{m_{nw}} \qquad \gamma_u = \frac{1}{\chi_u^*} \tag{3.68}$$

With these definitions, the value of ultimate vertical bending strength (m_{ul}) for a given reliability target can be estimated as follows,

$$m_{ul} = \gamma_u \gamma_s m_{ns} + \gamma_u \gamma_w m_{nw} \tag{3.69}$$

In this formulation the still water bending moment is considered the input from the designer, the wave bending moment is calculated from rules and the partial safety factors are input from this study.

The nominal value of the ultimate strength under vertical bending is taken to be the result of an advanced collapse analysis, as was done in section 3.2.4. Such values can be influenced by structural design parameters, thus giving designers a rather efficient means of optimising structures with respect to weight or other objectives.

3.3.2 Nominal partial safety factors

From table 3.17 (and figure 3.20) presented in section 3.2.9, it can be seen that the reliability indices for tankers of different size deviate significantly from a unique value. It is also apparent that the β-values have a tendency to decrease as the ship length increases. However, the main objective of this study is the formulation of a code that provides structural designs with an uniform safety level.

The assessment of the target safety levels is a very complicated problem that involves not only results from reliability analysis but also considerations of social preferences.

Based on the results of the reliability analysis and on engineering judgement, it was decided to use the target β-value of 2.5 as an average risk level for tankers. This value will be used to derive the partial safety factors using the extreme model for still water and wave induced bending moment. It should be noted that the partial safety factors could also be derived from the basic model of the load effects. In this case, different target safety levels would be applicable.

Figure 3.22 illustrates the target reliability level compared with the β-values that were obtained for tankers.

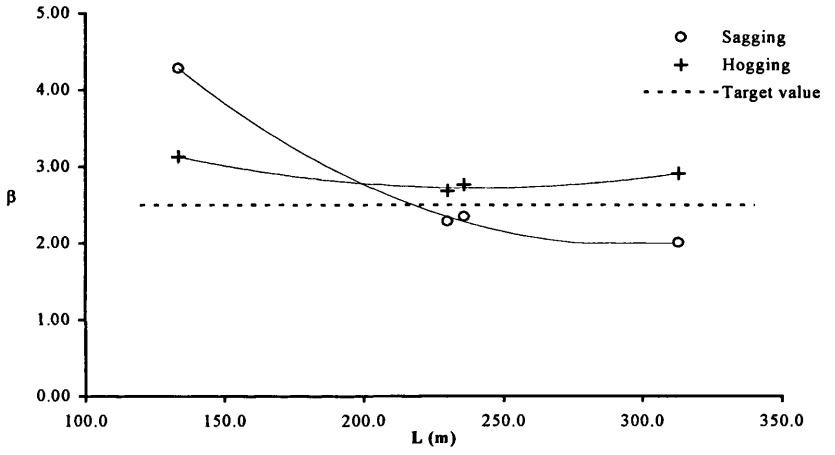

Figure 3.22: Target reliability index

The safety levels will be established by iteratively adapting the ultimate strength until the target β-value is achieved. In the same procedure, the design values m_s^*, m_w^*, χ_u^*, χ_w^* and χ_{nl}^* of the basic variables are also estimated. The partial safety factors γ_u, γ_s and γ_w can be defined according to equation 3.68 using the nominal values of still water and wave bending moment given by the IACS-rules (table 3.26).

Table 3.26
Nominal values m_{ns} and m_{nw}

Ship	L	B	C_b	Sagging		Hogging	
				m_{ns}	m_{nw}	m_{ns}	m_{nw}
TK1	133.4	18.0	0.700	251	424	309	366
TK2	230	42.0	0.818	2228	3771	2489	3510
TK3	236	42.0	0.805	2343	3965	2645	3663
TK4	313	48.2	0.830	5047	8542	5585	8004

Tables 3.27 and 3.28 summarise the results of the partial safety factors for tankers, respectively in sagging and hogging condition. The calculations were performed for the dominating load condition that is the full load for sagging and ballast load for hogging.

Table 3.27
Partial safety factors for tankers in sagging

	Ship	TK1	TK2	TK3	TK4
"as built"	M_u	910	6652	7123	16392
	β	4.28	2.28	2.34	2.00
Target	M_u	565	7025	7405	18375
	β_T	2.50	2.50	2.50	2.50
Design Values	m^*_s	161	1968	2133	5868
	Ψ^*	0.923	0.923	0.923	0.923
	χ^*_w	0.786	0.791	0.789	0.785
	χ^*_{nl}	1.023	1.153	1.137	1.158
	m^*_w	394	4261	4493	10277
	χ^*_u	0.801	0.791	0.791	0.789
Partial Safety Factors	γ_s	0.64	0.88	0.91	1.16
	γ_w	0.69	0.95	0.94	1.01
	γ_u	1.25	1.26	1.26	1.27

Table 3.28
Partial safety factors for tankers in hogging

	Ship	TK1	TK2	TK3	TK4
"as built"	M_u	932	7720	8354	19164
	β	3.13	2.68	2.76	2.91
Target	M_u	797	7330	7765	17035
	β_T	2.50	2.50	2.50	2.50
Design Values	m^*_s	335	3108	3264	7315
	Ψ^*	0.913	0.913	0.913	0.913
	χ^*_w	0.769	0.764	0.765	0.760
	χ^*_{nl}	1.196	1.069	1.083	1.051
	m^*_w	347	3718	3927	8983
	χ^*_u	0.786	0.802	0.803	0.814
Partial Safety Factors	γ_s	1.09	1.25	1.23	1.31
	γ_w	0.80	0.79	0.81	0.82
	γ_u	1.27	1.25	1.25	1.23

Figures 3.23 and 3.24 illustrate the partial safety factors as a function of the ship length, respectively in sagging and hogging condition. The partial safety factors should be interpreted as a factor that should be applied on the nominal values of the loads effects to obtain a uniform safety level.

It can be seen that the partial safety factors applied to the ultimate strength remains almost constant with the ship length for both conditions. However, the partial safety factors on the still water and the wave induced bending moment exhibit a large variation as function of the ship length as well as for the different load conditions.

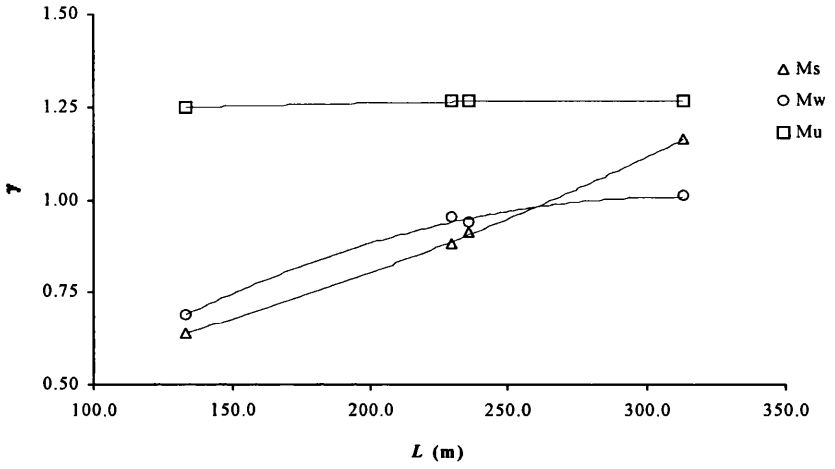

Figure 3.23: Partial safety factors for tankers in sagging condition

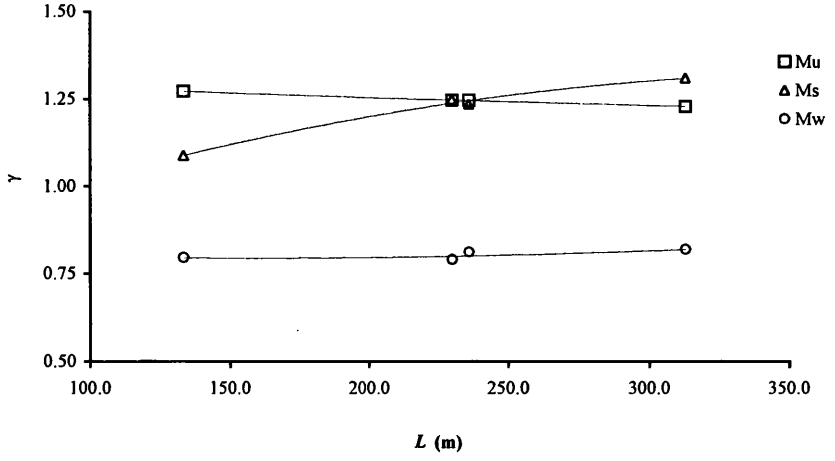

Figure 3.24: Partial safety factors for tankers in hogging condition

From figure 3.23 it can be seen that the ship TK1 in sagging condition requires a partial safety factor lower than 1.0 to be applied on the nominal values of both still water and wave induced bending moment. However, as the ship length increases larger values of the partial safety factors should be used to obtain a required larger value of ultimate strength.

Figure 3.24 shows the variation of the partial safety factors in hogging condition. It is clear that the most important variable in this load condition is the still water bending moment. In fact, the tankers seem to be overdesigned with respect with the wave induced

bending moment (γ^*_w<0) and underdesigned with respect to the still water bending moment (γ^*_s>0).

3.3.3 Ship re-design

Using the partial safety together with the nominal value of the load effects the designer can estimate the required value of ultimate vertical bending strength m_{ul} for the pre-defined reliability target as follows:

$$m_{ul} = \gamma^*_s m_{ns} + \gamma^*_w m_{nw} \tag{3.70}$$

with,

$$\gamma^*_s = \gamma_u \gamma_s \quad \text{and} \quad \gamma^*_w = \gamma_u \gamma_w \tag{3.71}$$

Table 3.29 shows the ultimate bending moment calculated with equation 3.70 compared with the limiting (operational) bending moment given by IACS-rules.

Table 3.29
Ultimate strength based on nominal rules values of load effects

Ship	Cond.	m_{ns}	m_{nw}	$m_{nt}=m_{ns}+m_{nw}$	γ^*_s	γ^*_w	m_{ul}	m_{ul}/m_{nt}
TK1	Sag	251	424	675	0.80	0.86	565	0.84
	Hog	309	366	675	1.38	1.01	797	1.18
TK2	Sag	2228	3771	5999	1.12	1.20	7025	1.17
	Hog	2489	3510	5999	1.56	0.99	7330	1.22
TK3	Sag	2343	3965	6308	1.15	1.19	7405	1.17
	Hog	2645	3663	6308	1.54	1.01	7765	1.23
TK4	Sag	5047	8542	13589	1.47	1.28	18375	1.35
	Hog	5585	8004	13589	1.61	1.01	17035	1.25

The design of a midship section to achieve a target reliability level is relatively easy using the computer program HullColl to calculate the ultimate hull collapse moment. This will be illustrated with the tanker TK3.

Having the value of 2.5 as the target reliability, it was decided to increase the thickness of the deck. One can also reduce thickness of the bottom since the reliability in hogging is 2.76.

The thickness of the deck plating was increased by 1.5 mm, which corresponds to about 8% and in the bottom the plating thickness was reduced by 2 mm, which represents about 6%. The thickness of the longitudinal stiffeners in the bottom was also decreased

by 1 mm. The ultimate capacity in sagging and hogging obtained for the re-designed ship is presented in table 3.30.

Table 3.30
Ultimate bending moments for the re-designed ship TK3

	"as built"		Target safety level			
Cond.	M_u	β	Deck Plating	Bottom Plating	Stiffeners	M_u
Sag	7123	2 .34	+1.5 mm	-2 mm	-1 mm	7430
Hog	8354	2.76				7780

From table 3.30 it can be seen that the sagging bending moment increased by 4.3% and hogging collapse bending moment decreased by about 7%. These values were used in the reliability analysis of the re-designed ship. The results are presented in table 3.31.

Table 3.31
Reliability index for re-designed tanker

Ship	Cond.	β_{FL}	β_{BL}	β_{PL}	P_{fi}	β_i
TK3	Sag.	2.35	4.82	5.55	9.51E-03	2.34
"as built"	Hog.	4.77	2.77	3.75	2.86E-03	2.76
TK3	Sag.	2.51	4.94	5.69	5.97E-03	2.51
Target safety level	Hog.	4.54	2.51	3.45	6.32E-03	2.49

It is clear that the reliability indices obtained for the re-designed ship are closest to the target reliability level of 2.50 for both sagging and hogging condition. It should be noted that the partial safety factors were derived for the dominating load condition that is the full load for sagging and ballast load for hogging.

In sagging, the full load condition is by far the dominant case. However, the β-value in hogging is lower than the target due to the importance of the partial load. Thus, this load condition should also be included in the evaluation of partial safety factors for tankers in hogging.

3.4 RELIABILITY ASSESSMENT OF DIFFERENT SHIP TYPES

In this section the reliability formulation is applied to different ship types with the objective of achieving indications of the safety levels of the different designs.

A 233.4 m long containership and two different structural designs (single and double hull) of a 279 m long bulk carrier, are used in the reliability assessment. The results are compared with the ones obtained for tankers.

The ultimate longitudinal moment of the ships as well as their main dimensions are presented in table 3.32. Sketches of the midship sections can be found in appendix 1.

Table 3.32
Ultimate strength of the ships

Ship	Ship Type	L (m)	B (m)	C_b	*Ultimate Moment* M_u	
					Hogging	*Sagging*
CT	Containership	233.4	32.2	0.66	5455	4132
BSH	Bulk Carrier Single Hull	279.0	45.0	0.86	12518	12716
BDH	Bulk Carrier Double Hull	279.0	45.0	0.86	12931	13890

The one-year reliability index is also used in the present reliability calculations. The operational profile defined in section 3.2.3, in which three different load conditions are defined, is also applied for the reliability analysis of bulk carriers (see table 3.2).

However, a different operational profile is required for containerships since the still water loads always cause a hogging bending moment. Therefore, only one hogging condition is considered in the reliability assessment of containerships. Table 3.33 resumes the operational profile adopted.

Table 3.33
Operational profile adopted for containership CT

Load Condition	N. Voyages	Voyage Duration
Hogging	20	7 days

Still Water Loads

The still water loads for both ship types are defined on the basis of the statistical analysis as described in section 3.2.6 for tankers. However, equation 3.34 can be rewritten to account for the ship type,

$$X = A_0 + A_1 \cdot W + A_2 \cdot L + \sum_i B_i D_i \tag{3.72}$$

where X is the mean value of the maximum still water bending moment, (*Max BM*), or is the mean value of the standard deviation of *Max BM* ($SD[Max\ \mathrm{BM}]$). It can also be the standard deviation of the mean still water bending moment (*SD*), which accounts for the variations of the mean from one ship to another within a particular class of ships. The regression coefficients are presented in table 3.7. The dummy variable D_i is equal to one for the ships type i and is zero otherwise. Table 3.34 shows the values of the variable B_i, which quantifies the difference of load effects between different ship types.

Table 3.34
B_i regression coefficient of equation 3.72

Regression Variable X	Containership (D_2=1)	Bulk Carrier (D_3=1)
	B_2	B_3
Max BM	66.6	2.3
$SD[Max\ BM]$	-1.9	10.0
SD	-1.5	7.2

For each load condition, the nondimensional mean deadweight W was defined according to the statistical study reported by Guedes Soares and Moan (1988). Table 3.35 summarises the resultant stochastic model for the still water vertical bending moment for one voyage and for one year of operation.

Table 3.35
Statistical moments of still water loads for bulk carriers and containerships

Ship	Load Condition	One Voyage (Normal Distribution)			One Year (Gumbel Distribution)		
		W %	*Mean Value* (MN.m)	*STD* (MN.m)	number of voyages	*Mean Value* (MN.m)	*STD* (MN.m)
CT	Hog	0.796	1405.8	395.8	20.0	2167.6	246.1
BSH BDH	FL	0.893	-849.5	1607.7	5.4	-2938.9	1426.0
	BL	0.565	652.5	1869.8	5.5	3082.5	1658.5
	PL	0.729	-123.6	1666.9	27.4	-3550.6	975.9

Wave induced bending moment

For both ship types the evaluation of the wave induced load effects that occur during long-term operation of the ships in the seaway was carried out. Figures 3.25 and 3.26 illustrate the resultant probability distribution fitted to the Weibull model.

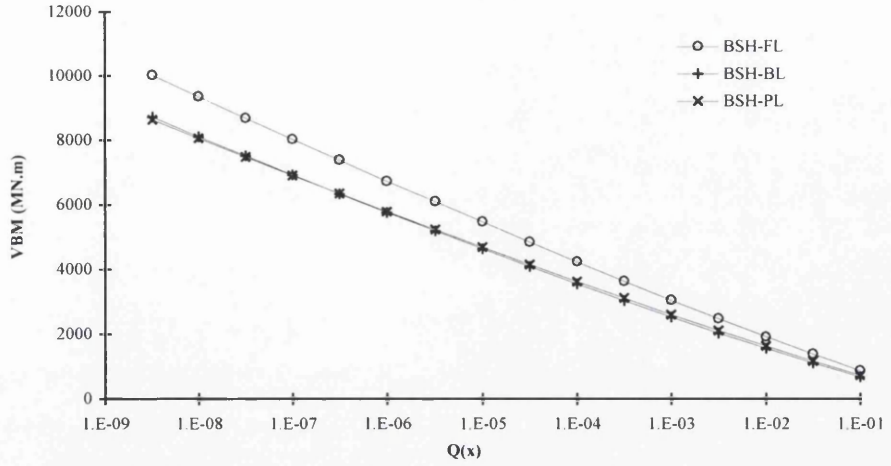

Figure 3.25: Long-term distribution for bulk carrier BSH

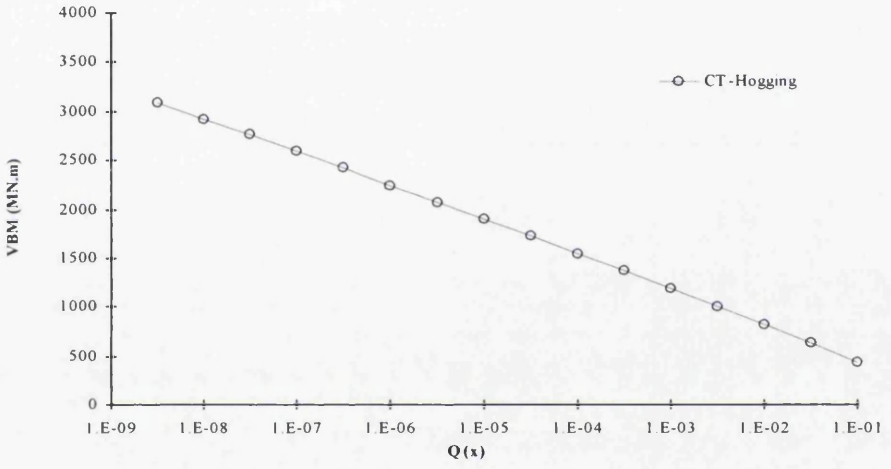

Figure 3.26: Long-term distribution for containership CT

Table 3.36 shows the stochastic model of the wave induced bending moment for the bulk carriers and containership.

Table 3.36
Stochastic model of wave induced bending moment

Ship	Condition	Weibull Parameters		Gumbel Moments (one year)		
		w	*K*	*n*	*Mean Value*	*STD*
CT	FL	202	1.090	1.73E+06	2414.1	190.7
BSH BDH	FL	335	0.875	1.58E+06	7312.1	717.8
	BL	253	0.840	1.58E+06	6279.0	640.9
	PL	281	0.868	6.76E+05	5876.2	616.3

Load combination between still water and wave bending moment

The load combination factors derived for TK3 in section 3.2.7 are used for the reliability analysis of bulk carriers. In fact, it was noted that the values of the load

combination do not change significantly for different amplitudes of the load variables within the same operational profile.

For containerships a different operational profile was defined and thus new values of load combination should be derived. Figure 3.27 illustrates the density distribution function f_{te} of the combined vertical bending moment for the containership in hogging condition.

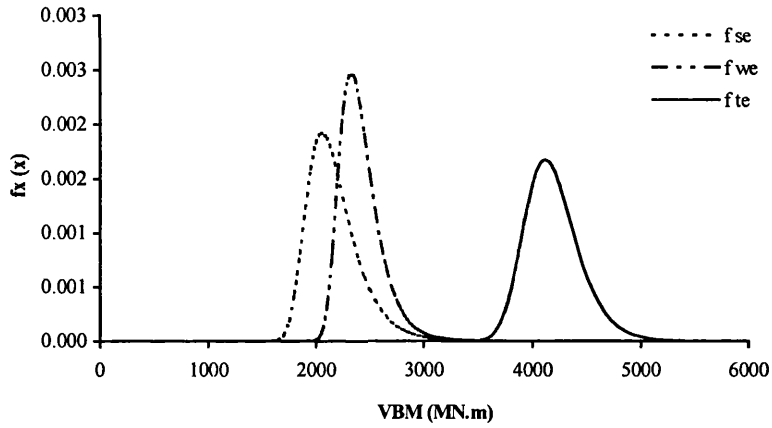

Figure 3.27: Combined bending moment for containership CT in hogging condition

Table 3.37 resumes the values of load combination used in the reliability calculations.

Table 3.37
Values of the load combination factors for containerships and bulk carriers

Ship	Load Condition	Ψ - Factor of load Comb.
CT	Hogging	0.866
BSH BDH	Full Load	0.923
	Ballast Load	0.913
	Partial Load	0.803

Results of the reliability analysis

The results of the annual reliability index for the bulk carriers in sagging and hogging condition are presented in table 3.38. It can be seen that the failure has a higher probability in sagging than in hogging. However, the difference between these two failure modes is not so large when compared with the results obtained for tankers. In fact, the ballast load case is also an important mode of failure in hogging condition due to the importance of the still water loads.

Table 3.38
Reliability index for bulk carriers in sagging and hogging condition

Ship	Cond.	β_{FL}	β_{BL}	β_{PL}	P_{fi}	β_i
BSH	Sag.	1.86	4.73	2.59	3.64E-02	1.79
	Hog.	4.62	2.09	6.17	1.85E-02	2.09
BDH	Sag.	2.18	5.00	2.95	1.62E-02	2.14
	Hog.	4.72	2.19	6.26	1.43E-02	2.19

Table 3.39 shows the reliability results for containership CT in hogging. The β-value of 4.69 was obtained in sagging indicating that the hogging condition is in fact the dominating mode of failure for containerships

Table 3.39
Reliability index for containership CT in sagging and hogging condition

Ship	Cond.	β_i	P_{fi}
CT	Hog.	2.24	1.25E-02
	Sag.	4.69	1.38E-06

Figure 3.28 illustrates the reliability results for containership CT and bulk carriers compared with the ones that were obtained for tankers.

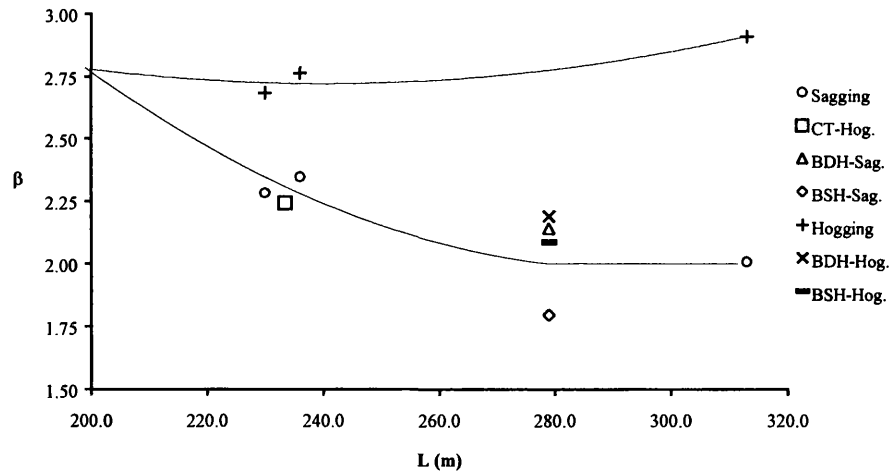

Figure 3.28: β-values for different ship types

As one can see the reliability level for containership in hogging is almost the same of the tankers TK2 and TK3 in sagging. The single hull bulk carrier exhibits a reliability index which is lower than the trend with the ship length obtained for tankers in sagging condition. However, this value increases for the double hull bulk carrier. It is clear that the new alternative design of a traditional bulk carrier has a reliability level larger than the trend obtained based on the analysis of tankers. Additionally, the bulk carrier BDH has almost the same safety level for both hogging and sagging conditions.

An attempt to explain the reliability results obtained for different ship types can be made by comparing the mean value of the stochastic variables with the minimum requirement values given by the IACS rules as done in section 3.2.9.

Figure 3.29 presents the difference in percentage between the ultimate strength and the total bending moment defined by the rules.

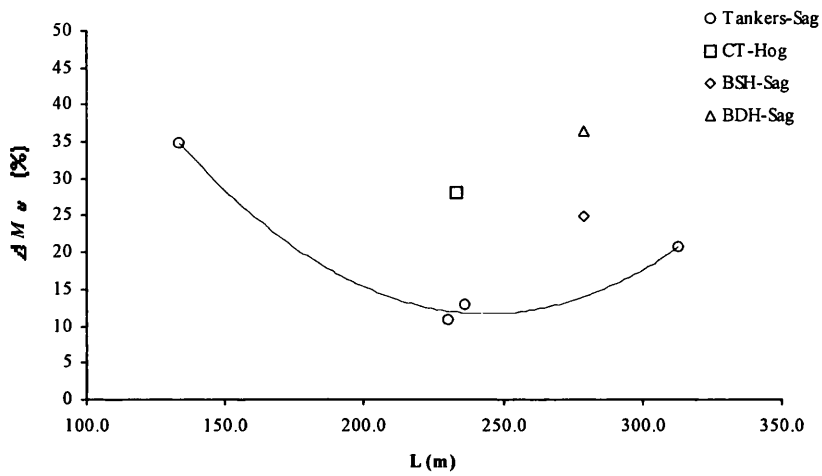

Figure 3.29: Comparison of the ultimate strength with the rules values

As seen from figure 3.29, both the single and the double hull bulk carrier and the containership have a large reserve of strength when compared with the tankers. Thus, the lower reliability index obtained for these ships can only be explained by analysing the particularities of the load effects in containerships and bulk carriers.

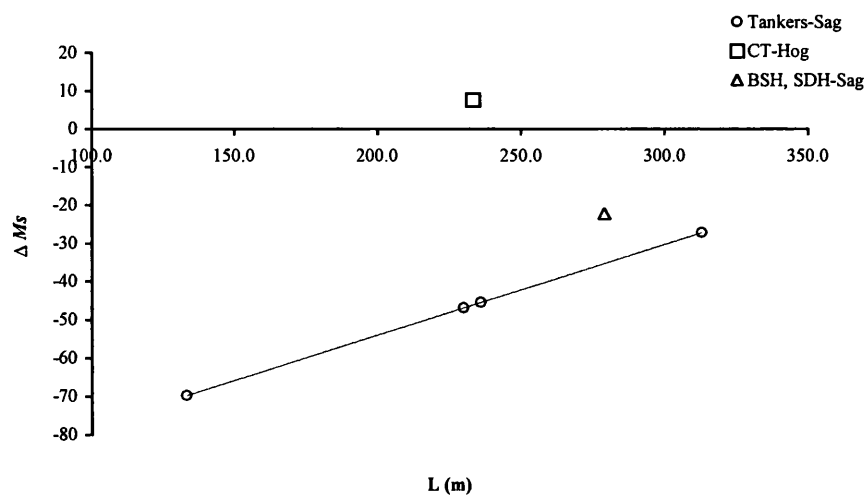

Figure 3.30: Comparison of the still water loads with the rules values

In figure 3.30 the still water loads used in the reliability calculations are compared with the nominal Rules values. Inspection of this figure indicates that the still water load in the containerships is 8% larger than the rules value and lower by about 40% for a

tanker with the same length. It should be also noted that the bulk carriers have typically larger values of still water bending moment in sagging condition when compared with tankers.

The wave induced bending moment for containership CT in hogging condition is very close to the tanker values, as shown in figure 3.30, indicating that the still water load is in fact the variable that makes the difference on the safety levels of containerships and tankers.

As concerns the reliability of bulk carriers no clear variable that influence their safety level is identified. In this case, it seems that the reserve of strength is in some cases not sufficient to compensate the higher values of still water and wave induced bending moment when compared with those to which tankers are subjected.

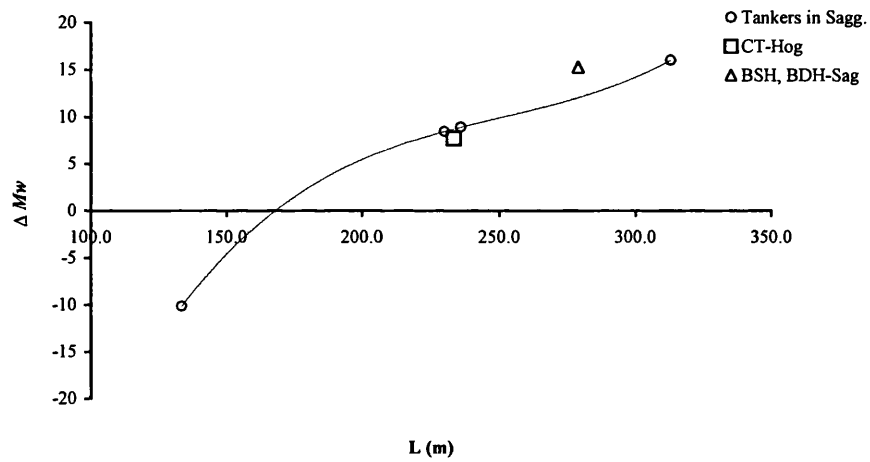

Figure 3.31: Comparison of the wave induced loads with the rules values

The wave induced load effects in containerships are normally low compared to the influence of the still water loads. However, this is not necessarily so for other ship types like bulk carriers and tankers as was shown in figures 3.30 and 3.31. Thus, the present analysis indirectly underlines that modern rules must be developed separately for different ship types.

It is clear that there are clear differences between the levels of the basic governing variables as defined in the rules and as they occur in the different ship types. The main conclusion is that having general rule requirements applicable to all types of ships will force different reliability levels. The second important conclusion is that individual ships have different reserves of safety in relation to the practice prescribed in rules.

3.5 OPTIONS OF OPERATIONAL SCENARIOS

The risk of shipping in coastal waters results from the contributions of different hazards such as collision, grounding, fire, explosion, structural failure and others. An overall risk model must account for the different sources of accident as well as their geographical variability.

Since the ships are designed for global and unrestricted services, the effect of different wave climate induces a significant variability on the probability of failure of the primary ship structure.

The North Atlantic has been used as a reference wave climate for calculation of the wave induced load effects. However, the wave environment regarded as the most severe may generally overestimate the design loads for ships sailing in other ocean areas.

Several studies have been reported to quantify the effect of using different of wave climate on the long-term predictions of wave induced loads. Guedes Soares and Viana (1988) showed that the 10^{-8} characteristic value of wave induced bending moment can differ as much as 100% when applying different sources of wave data. Recently, Chen and Thayambali (1991) based on the US Navy Fleet Central hindcast data and Guedes Soares and Moan (1991) using the Global Wave Statistics data (Hogben, Da Cuna and Ollivier, 1986) have indicated the variation in the shape factor of a two-parameters Weibull distribution for the stress range and wave induced bending moments.

Bitner-Gregersen and Loset (1994) have studied the variability of the long-term distribution of the ship wave induced bending moment that arises from use of the GWS data and compares it to the variation in loads and fatigue between ocean areas.

The present study aims at quantifying the changes in the notional reliability levels that result from the ships being subjected to different wave environments in European coastal waters. The evaluation of the wave induced load effects that occur during long-term operation of the ship in the seaway is carried out for different areas in the North of Europe given in Global Wave Statistics (GWS).

The 236 m long tanker (TK3) is considered for the reliability assessment. The stochastic model of wave induced bending moment is defined for different areas in Northern Europe according to Global Wave Statistics (Figure 3.32)

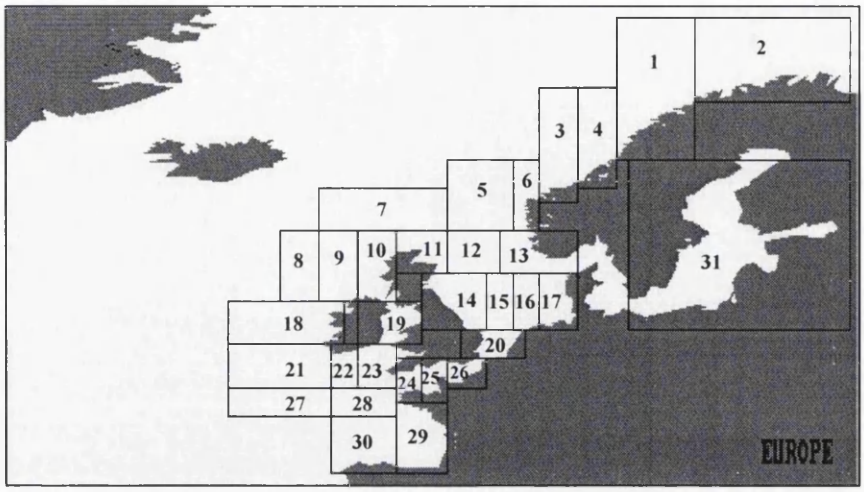

Figure 3.32: Sea areas in Europe

In figure 3.33 the long term distribution in full load condition is illustrated for different sea areas showing a significant variability in the calculated wave induced loads. The figure also shows the long-term distribution based on the average scatter diagram used in the previous reliability assessment.

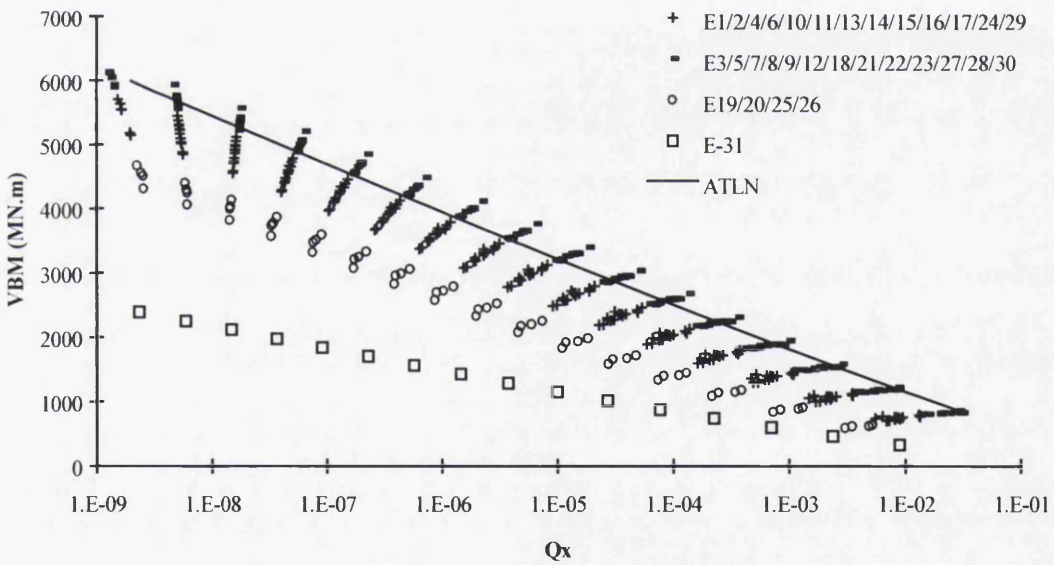

Figure 3.33: Long-term distribution for different sea areas

Table 3.40 shows Weibull parameters and the resultant values of the vertical bending moment calculated at the $10^{-6.5}$ probability level compared with the rules requirement for the different areas. The deviation from the rules value m_{nw} is calculated by:

$$\Delta M_{Rule} = \frac{VBM\left(Q_x = 10^{-6.5}\right) - m_{nw}}{m_{nw}} \tag{3.73}$$

Table 3.40
Weibull parameters for the different sea areas

Sea Area	Weibull Parameters		VBM (MN.m)	ΔM_{Rule}	Sea Area	Weibull Parameters		VBM (MNm)	ΔM_{Rule}
	w	k	(Q_x=$10^{-6.5}$)	(%)		w	k	(Q_x=$10^{-6.5}$)	(%)
ATLN	206.4	0.890	4317	8.9	E16	75.0	0.703	3515	-11.3
E1	93.8	0.726	3904	-1.5	E17	80.0	0.713	3552	-10.4
E2	85.2	0.717	3700	-6.7	E18	208.3	0.883	4454	12.3
E3	150.2	0.807	4297	8.4	E19	63.7	0.700	3041	-23.3
E4	126.1	0.782	4004	1.0	E20	59.4	0.700	2834	-28.5
E5	164.6	0.833	4234	6.8	E21	197.5	0.874	4374	10.3
E6	134.2	0.795	4038	1.9	E22	168.7	0.835	4319	8.9
E7	240.9	0.913	4668	17.7	E23	154.2	0.817	4238	6.9
E8	232.5	0.916	4464	12.6	E24	103.7	0.748	3872	-2.3
E9	217.6	0.896	4462	12.5	E25	66.0	0.700	3148	-20.6
E10	132.5	0.786	4140	4.4	E26	62.4	0.700	2976	-24.9
E11	110.6	0.760	3886	-2.0	E27	212.6	0.886	4501	13.5
E12	151.7	0.809	4302	8.5	E28	199.4	0.872	4434	11.8
E13	90.0	0.727	3727	-6.0	E29	92.6	0.723	3914	-1.3
E14	78.6	0.700	3751	-5.4	E30	184.0	0.855	4355	9.9
E15	98.0	0.737	3860	-2.6	E31	40.2	0.730	1637	-58.7

It can be seen that the values of the vertical bending moment range from 4668 MN.m to 1637 MN.m calculated at the $10^{-6.5}$-probability level for the areas 7 and 31, respectively. The correspondent deviation from the rules requirement is 18 and –59%, respectively.

The larger values correspond to ocean areas located in the North Sea, while in the Baltic Sea the lower value of wave induced bending moment is obtained. Additionally, should be noted that values of vertical bending moment around 2950 MN.m are obtained for the sea areas in the English Channel (E20, E25 and E26), which correspond to 25% less than the rules requirement.

The probability of failure in a given area was calculated using the extreme reliability formulation, with the model for the wave induced bending moment corresponding to the area.

Table 3.41 gives the reliability indices and the related probability of failure in full load situation. It should be noted that there is significant variability between the probability of failure obtained for the different areas as shown in the last column of table 3.41 which gives the probability of failure in each area normalized by the maximum value that occurs in sea area 7. Knowing the probability of failure in each area (P_f^A) and the probability that a ship is on that area (P_A), one can estimate the total probability of failure for a particular route.

Table 3.41
β-values for the different sea areas

Sea Area	β	P_{fi}	P_{fi}/P_{fmax}	Sea Area	β	P_{fi}	P_{fi}/P_{fmax}
ATLN	2.345	9.51E-03	0.59	E16	2.800	2.56E-03	0.16
E1	2.571	5.07E-03	0.31	E17	2.779	2.73E-03	0.17
E2	2.692	3.55E-03	0.22	E18	2.262	1.18E-02	0.73
E3	2.348	9.44E-03	0.58	E19	3.070	1.07E-03	0.07
E4	2.520	5.87E-03	0.36	E20	3.181	7.34E-04	0.05
E5	2.389	8.45E-03	0.52	E21	2.309	1.05E-02	0.64
E6	2.501	6.19E-03	0.38	E22	2.338	9.69E-03	0.60
E7	2.138	1.63E-02	1.00	E23	2.384	8.56E-03	0.53
E8	2.259	1.19E-02	0.73	E24	2.594	4.74E-03	0.29
E9	2.259	1.19E-02	0.73	E25	3.011	1.30E-03	0.08
E10	2.439	7.36E-03	0.45	E26	3.105	9.51E-04	0.06
E11	2.588	4.83E-03	0.30	E27	2.234	1.27E-02	0.78
E12	2.345	9.51E-03	0.59	E28	2.273	1.15E-02	0.71
E13	2.678	3.70E-03	0.23	E29	2.565	5.16E-03	0.32
E14	2.658	3.93E-03	0.24	E30	2.318	1.02E-02	0.63
E15	2.600	4.66E-03	0.29	E31	3.745	9.02E-05	0.01

Figure 3.34 clearly shows the variability in the notional probability of structural failure along the sea areas in which the ship is. As can be seen the information given by this figure is meaningless outside of the defined sea areas.

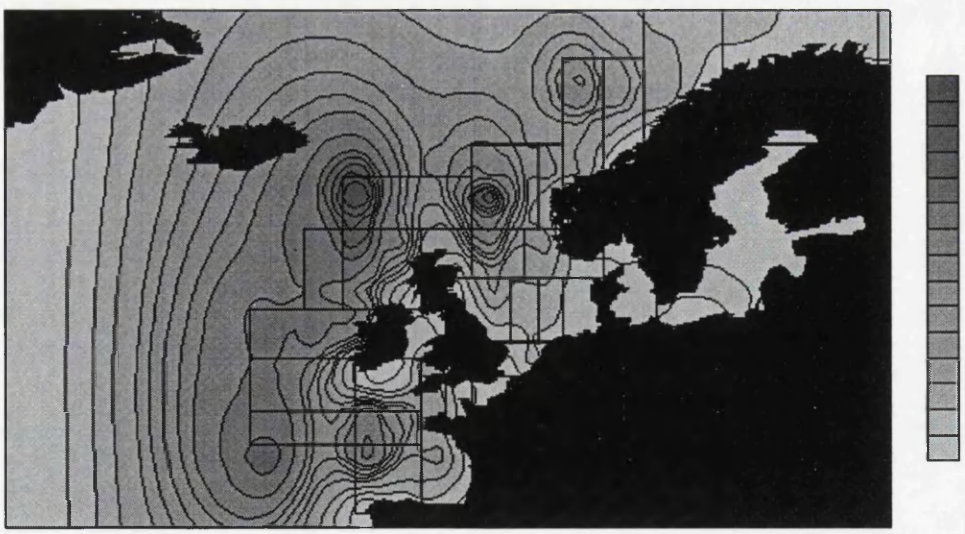

Figure 3.34: $P_{fi}/P_{f\max}$ for different sea areas

CHAPTER 4
RELIABILITY OF TOPSIDE COMPONENTS UNDER FIRE CONDITIONS

In this chapter a reliability formulation is presented for thermally insulated steel plates subjected to a pool fire.

The methodology is developed by integrating the structural reliability analysis with the non-linear structural analysis of plate elements subjected to thermal load as well as fire and heat transfer modelling.

The basic mechanisms that influence the shape of the flame of a pool fire are described and a first order second moment approach is presented to quantify the uncertainty of the heat loads and to describe the importance of the governing variables. Having modelled the thermal radiation due to a pool fire, the temperature of the insulated plate is calculated using a heat transfer model.

The reliability problem is then formulated in terms of plate temperature using the results of a systematic study on plate collapse under increasing heat loads.

When the heat load is not applied to the whole plate surface, but instead is localised, the plates are able to sustain additional in-plane compressive loads before collapse. Therefore, in this situation it is appropriate to formulate the reliability problem in terms of stresses because this is the condition that will govern collapse.

4.1 STRENGTH OF PLATE ELEMENTS SUBJECTED TO HEAT LOADS

The behaviour of plate elements under compressive loads has been studied for many years. Major developments have occurred during the early 70's with the development of numerical procedures based on finite differences and on finite-elements. It became then possible to study realistic cases of elasto-plastic collapse of plates with large deflections. Several parametric studies have been performed to indicate the effect of different parameters on the collapse strength, including the initial distortions and residual stresses (Frieze et al., 1977, Harding et al., 1977, Little, 1980, Crisfield, 1975, Dow and Smith, 1983, Ueda and Yao, 1985 and Guedes Soares, 1993).

Although most of the studies dealt with uniaxial loads some have considered the collapse resistance under biaxial loads as reviewed in (Guedes Soares and Gordo, 1996). However no studies have been identified on the collapse strength of plate elements subjected to elevated temperatures.

In fact, much research has been done related with the effect of fires on the components in building structures and here the concern has been the behaviour of columns (Janss and Minne, 1981, Witteveen and Twilt, 1975), Stanzak and Lie, 1973 and Wang, 1997) as well as frames (Saab and Nethercot, 1991 and Najjar and Burgess, 1996).

This study has determined the load-shortening behaviour of plates with different aspect ratios, slenderness and initial distortions by using a non-linear finite element code. The loading is a heat source that leads to a monotonically increasing temperature with uniform distribution in the plate, which varies from ambient temperature to values up to 800 °C.

Since plate elements are part of a structure subjected to thermal loads due to a localised fire, its boundary conditions are far from being fixed. However, the structural interaction between the plate element and other steel elements can be studied, using elastic supports to restrain the in-plane displacement as well as localised heat loads.

4.1.1 Steel properties at high temperatures

For a thermal and structural analysis, the knowledge of the thermal and mechanical properties of the structural material is required. Steel does not provide any significant resistance to heat transfer and, furthermore, the thermal properties of steel that are of interest do not vary significantly with the temperature, as opposed to the mechanical properties.

To calculate the strength of steel structures and components under the induced fire load temperatures it is essential to have knowledge of the stress-strain properties of steel at elevated temperatures.

Different experimental programmes have been conducted in the past, providing stress-strain curves for different kinds of steels and a synthesis of the results together with proposals of analytical models were presented (Anderberg, 1983, Kirby and Preston, 1988 and Twilt, 1991).

The data presently available about the strength of steel at high temperatures are experimental results that have been used as a basis to develop design curves. Important work has been performed in Europe related to the development of design curves for steel structures under fire loads based on data from different sources. The experimental programmes conducted so far have shown that the effect of temperature on the stress-strain curves of steel is the same for all types of steel. This is very important in that only one theoretical model is enough to describe the mechanical behaviour of all steels.

In the present study, the European Recommendation (Commission for the European Communities, 1990) was used. Five different curves were defined to describe the steel properties, respectively for temperatures of 0°, 200°, 400°, 600° and 800°C, as indicated in figure 4.1. For intermediate temperatures, a linear interpolation between the two nearest curves must be made.

It can be seen that at 200°C there is a decrease of the yield and ultimate stresses but the difference between the yield stress and the ultimate stress is not very large. For 400°C, the yield stress is much lower and, although the ultimate stress is very similar to the one of 200°C, it is only reached at a much larger strain. For 600°C and 800°C there is a very significant decrease in the ultimate stress but the difference between the yield stress and ultimate stress is small again i.e. the overall behaviour becomes again similar to the one at 200°C.

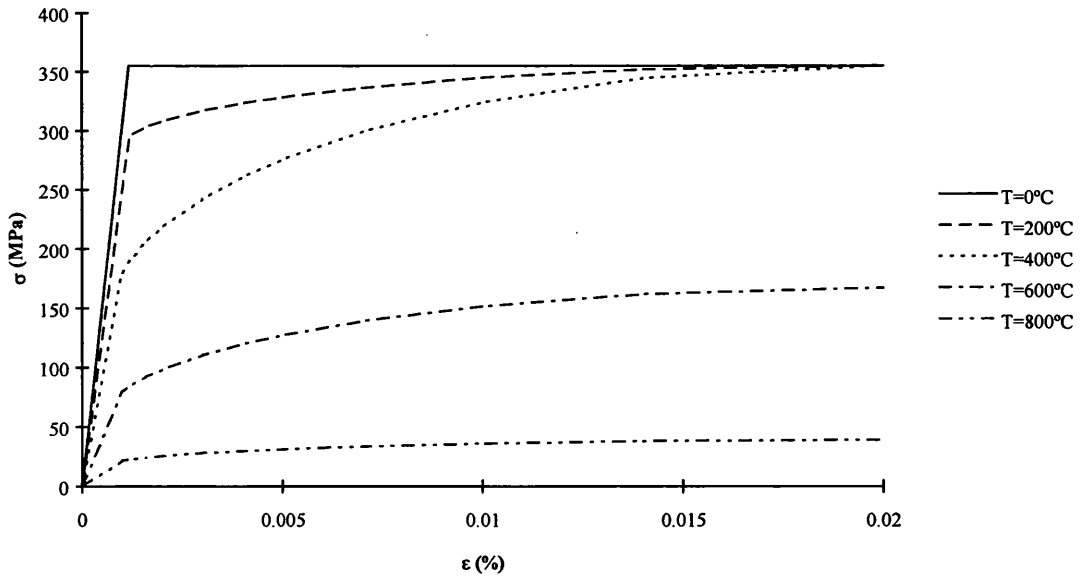

Figure 4.1: Stress-strain curves for different temperatures of high tensile steel, Fe360

The stress-strain curves for different temperatures of steels of different yield stress are similar to those presented in figure 4.1 only scaled by the yield stress at ambient temperature. The main change in the maximum stress occurs at 400°C corresponding to a sudden drop in this stress. However, for temperatures lower than that one, the ratio between the proportional limit and the maximum stress increases with temperature.

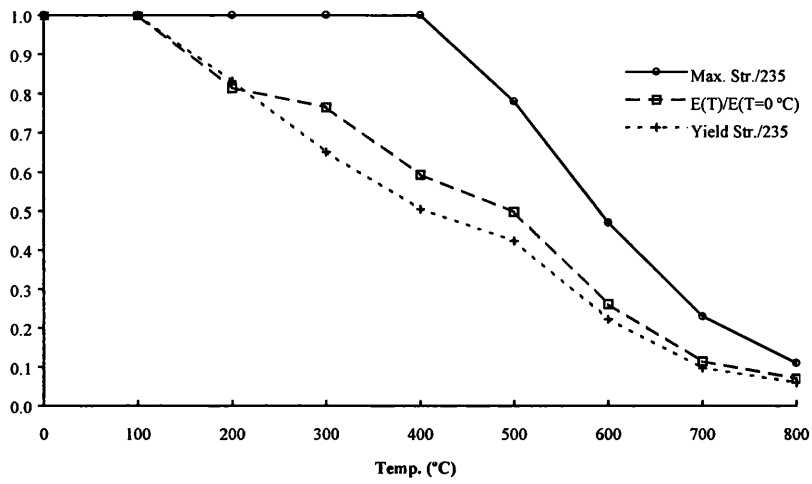

Figure 4.2: Material properties of mild steel

Figure 4.2 shows the dependence on temperature of the yield stress (Yield Str.), maximum stress (Max, Str.) and Young modulus (E), normalised by their values at ambient temperature. It is clear that while the yield stress and the Young modulus start decreasing at temperatures of 100°C, the maximum stress only starts being degraded at 400°C.

4.1.2 Thermo-elasto-plastic analysis

The numerical calculations were performed using the ASAS-NL software (ASASNL, 1990) which takes thermal loads into account. This is a general-purpose non-linear finite element code in which large displacement effects are handled using an updated Lagrangian formulation with inclusion of geometric stiffness terms for plate elements.

The plasticity is modelled by the Von-Mises or Tresca yield criteria. The material behaviour can be non-linear and is defined by a piecewise linear stress-strain curve for various temperatures. Properties at intermediate temperatures are obtained by linear interpolation.

The non-linear solution of a thermo-elastic-plastic analysis is approached in an incremental-iterative manner using Newton's method to solve the non-linear equilibrium equation,

$$\Delta\{\delta\} = -|K_t|_i^{-1}\{\varphi\}_i \tag{4.1}$$

where $|K_t|_i^{-1}$ is the incremental stiffness matrix evaluated for displacement at iteration i $\{\delta\}_i$ and the improved set of nodal displacements is given by,

$$\{\delta\}_{i+1} = \{\delta\}_i + \Delta\{\delta\} \tag{4.2}$$

This procedure is carried out iteratively until the unbalanced load vector $\{\varphi\}$ has converged to zero. The incremental load vector consists of the mechanical and thermal components:

$$\Delta\varepsilon = \Delta\varepsilon_e + \Delta\varepsilon_p + \Delta\varepsilon_{th} \tag{4.3}$$

where $\Delta\varepsilon_e$, $\Delta\varepsilon_P$ and $\Delta\varepsilon_{th}$ are the incremental elastic, plastic and thermal strains, respectively. The temperature is increased incrementally according to what has been specified as input and the thermal load vector is computed from the thermal strain increment by:

$$\Delta\varepsilon_{th} = \alpha\Delta T + \Delta_\alpha T \tag{4.4}$$

where α is the coefficient of thermal expansion, ΔT is the temperature increment, Δ_α is the change in α due to temperature change ΔT and T is the temperature at the beginning of the step with respect to the reference temperature state.

To compute the element stiffness the material properties are updated according to the actual thermal load. The material stiffness can be either elastic or elasto-plastic depending whether plasticity has occurred at an integration point.

After the calculation of the nodal displacements, the plastic strain increment is calculated from the plastic and state information. Hence, stresses are then obtained using the constitutive law.

4.1.3 Strength of plates subjected to uniform heat loads

When trying to understand the behaviour of a plate under heat loads, the first problem that arises is the one concerned with the difference of temperature at that particular region compared with the temperature of the rest of the structure.

If one considers an unloaded structure subjected to a temperature increase and if the whole structure has the same temperature increase there will be no restraining boundary conditions to a substructure and thermal stresses will not be present, i.e., the whole structure will simply expand.

When there is a temperature differential within a structure, this will generate thermal stresses which increase with temperature until they reach a level that induces the collapse of the plate. After that level the plate sustains a lower level of load.

Calculations were conducted for several simply supported plates starting from an initial temperature, subjected to a temperature increase up to collapse and continuing in the post-collapse range. The increase of temperature, uniform over the whole plate, will induce a tendency for the plates to expand. The restrictions provided by the boundary conditions induce biaxial compression on the plates of such a magnitude as to induce plate collapse. Figure 4.3 illustrates the boundary conditions used in the finite element model.

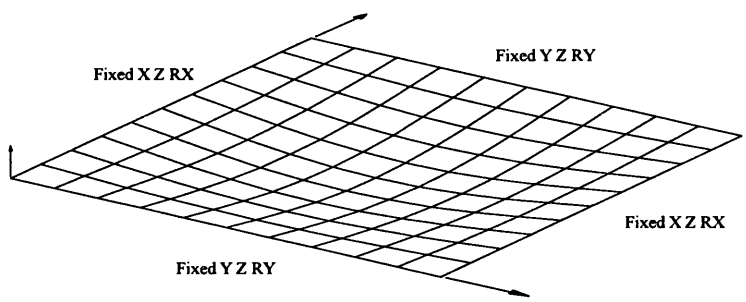

Figure 4.3: Boundary conditions for the plate model

The aspect ratio of the plates are 1 and 3 and the slenderness covered range from a *b/t* of 20 to 100. The nominal plate slenderness is defined at ambient temperature as:

$$\beta = \frac{b}{t}\sqrt{\frac{\sigma_o}{E}} \tag{4.5}$$

where σ_o and E are the yield stress and Young's modulus, respectively. However, when dealing with changing temperature, the definition of the plate slenderness presents a

difficulty since the material properties of the plate are changing with temperature. Thus, it is less meaningful to identify a plate with its slenderness at ambient temperature. In order to avoid this problem the plates were identified by their b/t ratio.

The initial geometric imperfections were also investigated. An average level of distortions, was considered in the present study

$$w_{max} / t = 0.10 \beta^2 \tag{4.6}$$

where β is the plate slenderness at ambient temperature.

Table 4.1 describes the finite element model used to derive the strength curves for thermal loaded plates.

Table 4.1
Finite element model

	N° of elements	*a* (mm)	*b* (mm)	*t* (mm)	*b/t*	High strength steel		Mild steel	
						β	w_{max} (mm)	β	w_{max} (mm)
Square Plates	8 × 8 = 64	1000	1000	50.0	20	0.84	3.6	0.69	2.4
				25.0	40	1.69	7.1	1.37	4.7
Rectang. Plates	8 × 24 = 192	3000		16.7	60	2.53	10.7	2.06	7.1
				12.5	80	3.37	14.2	2.74	9.4
				10.0	100	4.21	17.8	3.43	11.8

The shape of the initial imperfections may be represented by a Fourier series as:

$$w = \sum_m \sum_n \delta_{mn} \sin\frac{m\pi x}{a} \sin\frac{n\pi y}{b} \tag{4.7}$$

where a and b are the plate dimensions and δ_{mn} are the amplitude of the components.

In each calculation the initial distortion of the plate was represented by a shape with only one component of this series. However each type of plate was considered twice with a different initial distortion described by the order (m, n) of the Fourier component of the initial distortions in order to quantify the sensitivity to this parameter. Thus all plates were run with the pair ($m = 1; n = 1$) and some of them with the pair ($m = a/b; n = 1$). The last ones proved to have the same response of the square plates and thus their behaviour may be represented by the behaviour of these plates.

Figure 4.4 and 4.5 show the shape of the initial imperfections for square and rectangular plates, respectively.

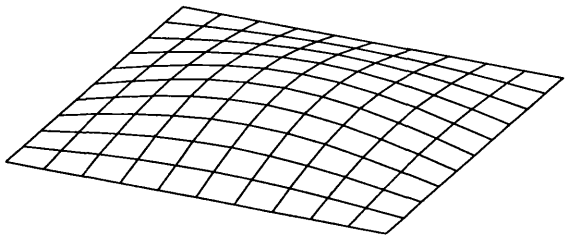

Figure 4.4 Shape of the initial imperfections for square plates (a/b=3)

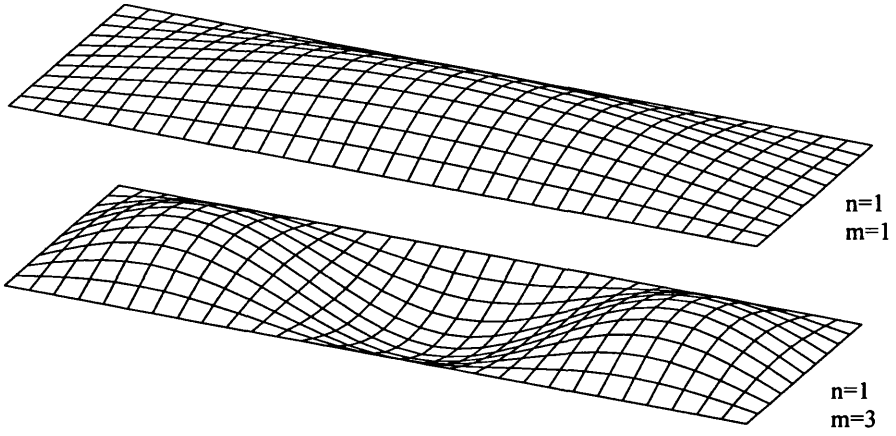

Figure 4.5: Shape of the initial imperfections for rectangular plates (a/b=3)

Restrained boundary conditions

Figure 4.6 shows the load-temperature curves for plates of high strength steel (figure 4.1) with a/b=1 but with different slenderness (b/t = 20, 40, 60, 80 and 100). Each curve indicates the relationship between the stress and the temperature. Note that temperatures values correspond to a differential with respect to the initial temperature and not to an absolute temperature.

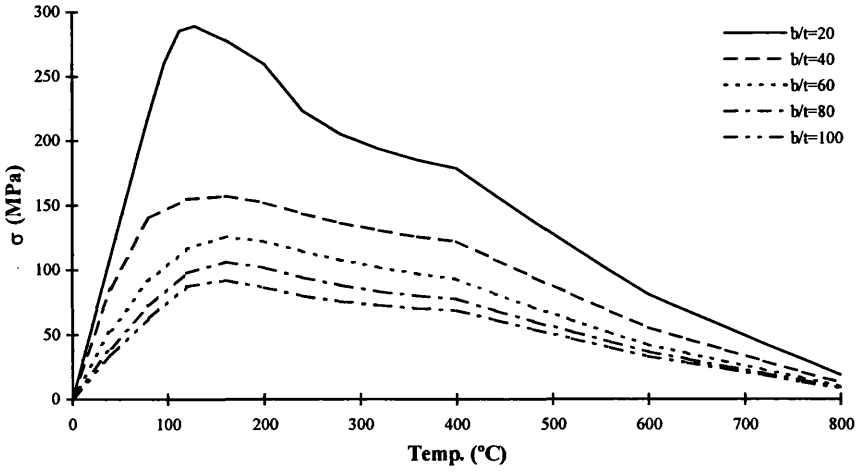

Figure 4.6: Stress-temperature curves of square plates of high strength steel

The stresses indicated in figure 4.6 may be understood as the longitudinal or the transverse stresses since they are the same for square plates due to symmetry. This means that the strength of the plates under thermal loads has to be understood as the biaxial strength instead of the uniaxial strength.

Figure 4.7 illustrates the results for plates of a/b=3 with a mode of imperfections equal to the length of the plate (X denotes the stresses in the longitudinal direction while Y denotes those in the transverse one). The influence of biaxial stresses is important in all plates, especially in the elastic range (T<100ºC). Collapse in the transverse direction is reached at a lower temperature and at lower stress levels; after the collapse in the transverse direction, the stresses in this direction fall quickly to very low levels while the longitudinal stresses keep increasing until the longitudinal collapse is achieved.

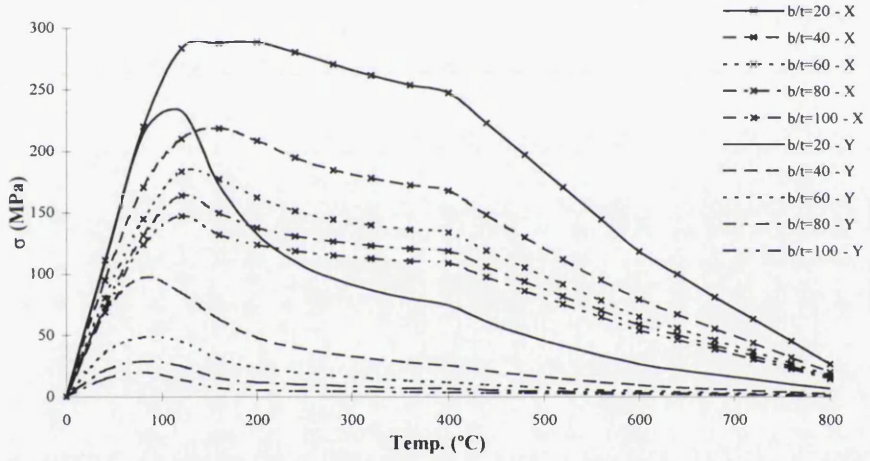

Figure 4.7: Stress-temperature curves of rectangular plates (a/b = 3) of high strength steel with average distortion

The first main conclusion for plates with aspect ratio greater than one is that the collapse in the transverse direction is achieved at lower temperatures (T≈75ºC) than the collapse in longitudinal direction or the collapse of square plates (T≈120ºC) in which failure occurs simultaneously in both directions.

The effect of initial geometric imperfections was also investigated considering another level of imperfection. A plate "almost" perfect was considered having a maximum lateral displacement of 1 mm. The main conclusion that one may draw is the insensitivity of the post buckling collapse strength with respect to the initial imperfection in square plates. Furthermore the effect of imperfections on the ultimate load is negligible for plates with b/t>60 (see appendix 3).

For rectangular plates, the influence of the initial imperfections is confirmed to be negligible. However, the "almost" perfect rectangular plates with b/t=100 change their shape of deformations in the elastic range to a mode $m=\alpha$ which makes the collapse similar to the one of a square plate (figure 4.8). After collapse, the transverse stress tends to be lower than the longitudinal stress due to the effect of the mode of the initial imperfections, m=1, which is still present.

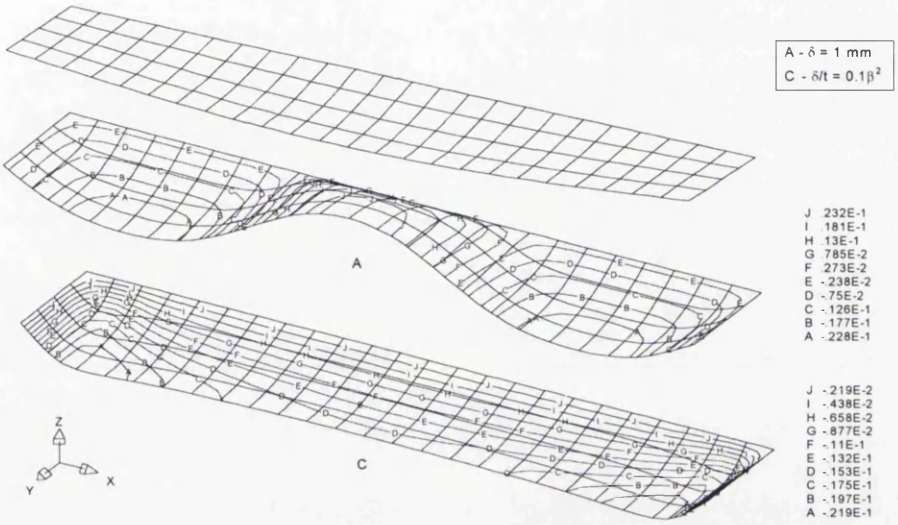

Figure 4.8: Deflections of plates α=3 and b/t=100 for small (A) and large (C) imperfections at initial collapse

Figure 4.9 has results of a plate of b/t=60 and it is a typical example of the lack of sensitivity to the level of imperfections when dealing with temperature load. In the elastic range some differences in the behaviour of the plate due to initial imperfections may be detected, but after collapse of the plate, the curves of the stresses in each direction tend to be independent of distortions.

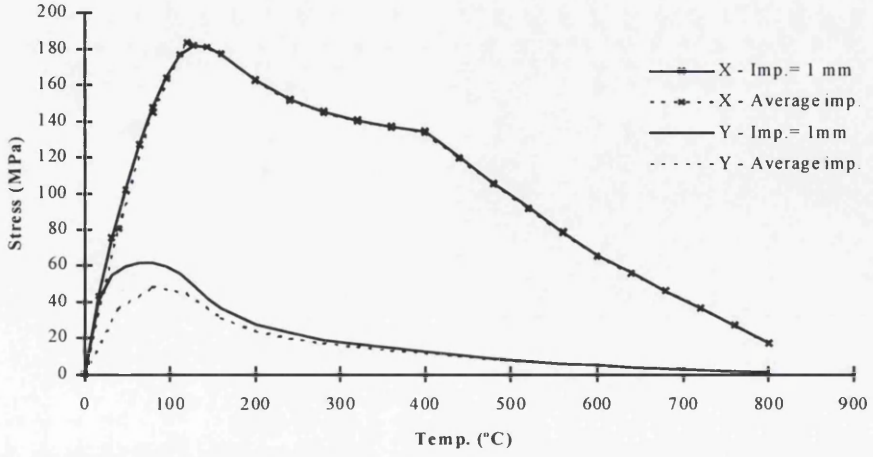

Figure 4.9: Stress-temperature curves of rectangular plates (a/b=3) of high strength steel and b/t=60 for two levels of imperfections

It can be seen that the transverse stresses are more sensitive to imperfections because for a plate with this aspect ratio and mode of imperfection the first collapse is in that direction. However, far beyond the collapse, the influence of distortions tends to disappear even in the transverse direction.

A detailed analysis of figures 4.6 and 4.7 shows discontinuities of the derivative of $\sigma(T)$ at 400 and 600°C, which may be consequence of a too crude definition of the material properties, i.e., a large step in the difference of temperature that defines the material behaviour. Because of that a second series of analysis was carried out using the properties of mild steel, and a step half of the one used earlier, (i.e., a step of 100°C). This analysis also allows to study the influence of the different material properties.

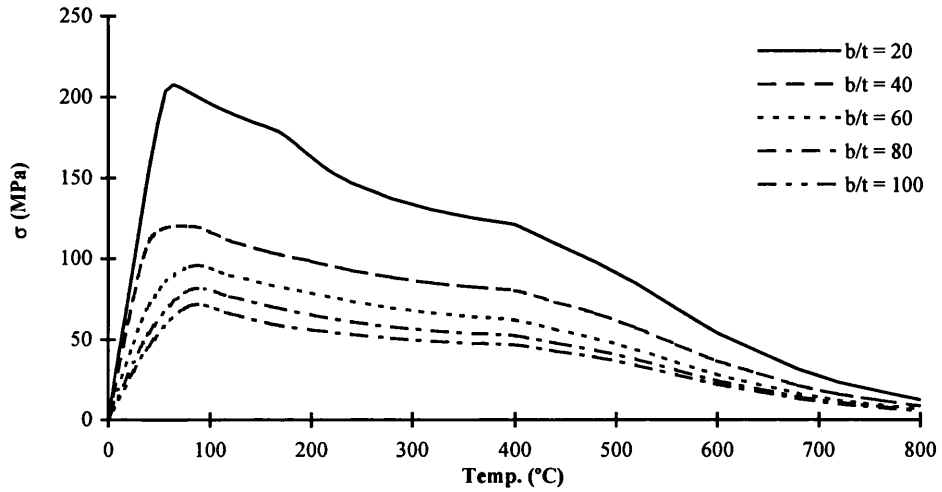

Figure 4.10: Longitudinal stress-temperature curves of square plates (a/b=1) with different slenderness for mild steel

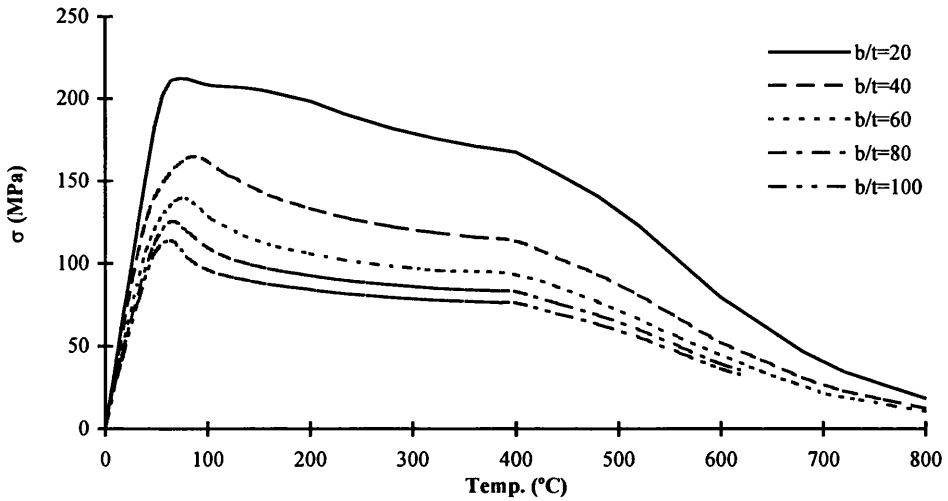

Figure 4.11: Longitudinal stress-temperature curves of rectangular plates (a/b=3) with different slenderness for mild steel

Figures 4.10 and 4.11 plot the results for plates with an aspect ratio of 1 and 3. These figures shall be checked against figures 4.6 and 4.7.

Figure 4.12 illustrates the out-of-plane deflection against temperature of a square plate, showing that a large level of deflection is attained for high temperatures.

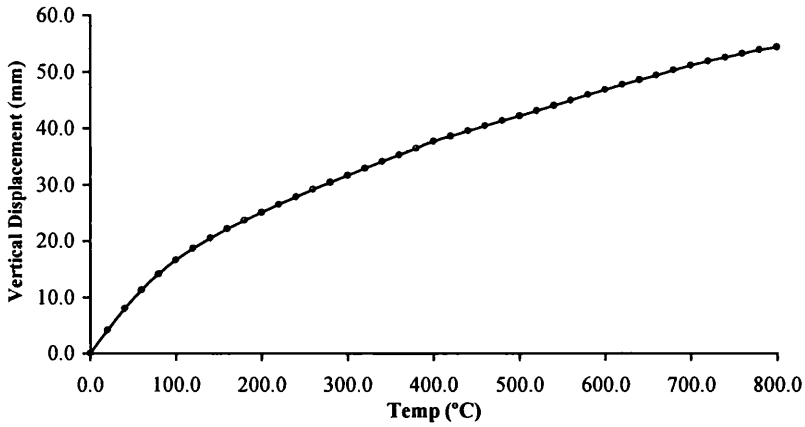

Figure 4.12: Vertical displacement-temperature curve of a square plate for mild steel (b/t=60)

Figure 4.13 compares the behaviour of the plates with average imperfections using different step on the definition of material properties and with different yield stress.

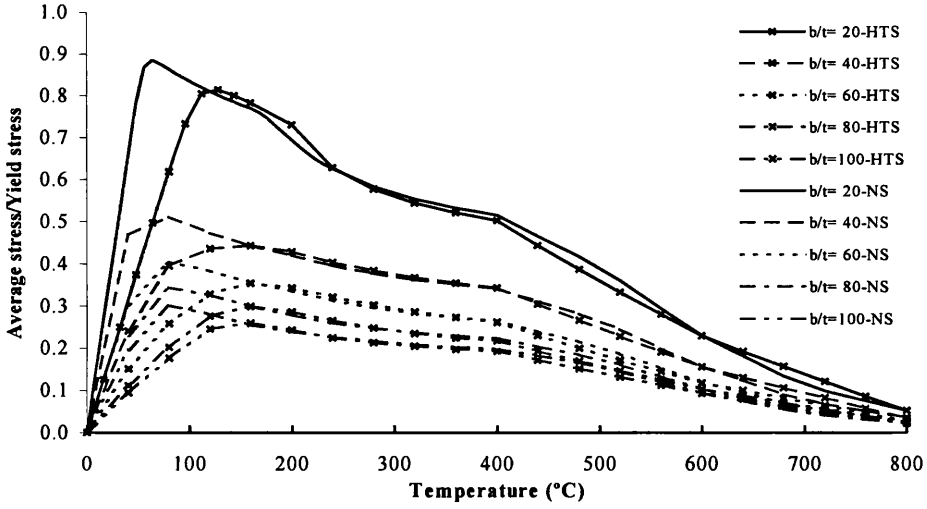

Figure 4.13: Comparison of the normalised stress-temperature curves of square plates with higher strength steel (HSS) and with mild steel (NS)

Two main conclusions may be inferred from the analysis of figure 4.13. First, the behaviour is only scaled by the yield stress. If the curves of material properties in the range of temperatures have the same shape for two materials with different yield stress, then the behaviour at high temperatures, i.e., in the post-collapse regime, is only scaled

by the yield stress. Second, the normalized collapse load is greater for plates of normal steel than for those of high tensile steel.

The fact that one may associate an average strain to the temperature scale instead of an average normalised strain is the main cause of the different derivative of the curves of material with the same *b/t* ratio and of the different temperature of collapse. The difference in the collapse load for the same *b/t* ratio is due to the different nominal slenderness consequence of the yield stress in the two cases, i.e., plates with a higher yield stress than the ones of normal steel have a higher nominal slenderness and thus a lower normalised ultimate stress, usually denoted as ultimate strength (Gordo and Guedes Soares, 1993).

At the temperature of collapse of a plate of normal yield stress it has the same effective slenderness of the high tensile steel plate, thus the stress at that temperature should be similar for the two plates. The differences may be a result of the actual state of imperfections in the two plates but this parameter has little effect when dealing with temperature as pointed out before.

Some differences between the curves of the same *b/t* ratio are observed at temperatures around 500 and 700°C, which are a direct consequence of the improvement in the resolution of the material properties with temperature for the case of normal steel, where the properties were defined at 500 and 700°C while for the HTS they were estimated by interpolation.

Elastic supports

In real structures the supports of the plate elements are the stiffeners and the surrounding structure. The formers provide support mainly for out of plane displacements, while the latter restrain the in-plane displacements. Thus, the boundary conditions of the plate elements are far from being fixed when they are thermally loaded.

In a first approach the elastic support to in-plane displacements may be taken proportional to the area of the edge and the modulus of elasticity. This assumes that the stiffeners do not support any load in these directions and the surrounding plating has a similar thickness to the loaded plate. The constant of proportionality depends mainly on the geometry and dimensions of the frames that are oriented in the same directions of the

displacements, on the ratio between the thickness of the plate and of the surrounding structure and, eventually, on the particular position of plate on the panel.

Using these considerations, springs were connected to the nodes perpendicularly to the edges with a rigidity proportional to $K_o=EA/L$, where $L=a$ is the length of the plate in the direction perpendicular to the edge and A is the cross section area ($A = bt$). Two levels were used: K_o and 0.5 K_o.

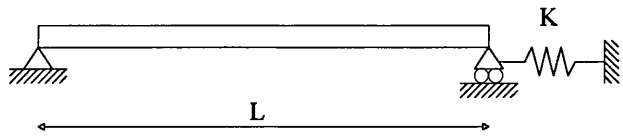

Figure 4.14: Illustration of the elastic support

Figures 4.15 to 4.19 compare the stress-temperature curves varying the degree of restraint to in-plane displacements for five *b/t* ratios. The shape of each curve is similar to the others apart a magnification of the scale due to the slenderness. However the curves of plates with *b/t*=20 have a slight difference from the others. For other slenderness the plates with low rigidity at the boundary have always lower strength at the same temperature than those with high rigidity. However in stocky plates the amount of plastic strain seems to be very important at low temperatures, T<400°C. A large plastic strain tends to magnify the out-of-plane imperfections and this reduces very much the strength comparatively to plates where the plastic strain, and consequently the imperfections, are low.

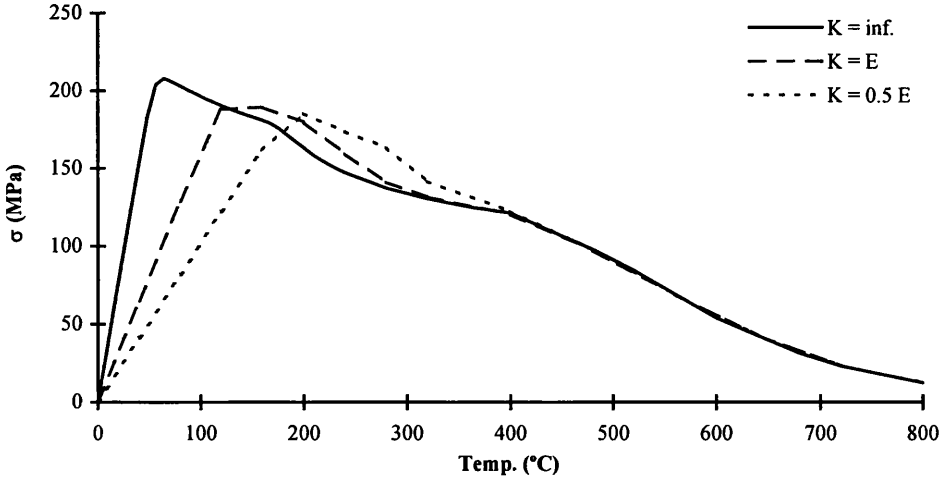

Figure 4.15: Comparison of the stress-temperature curves of plates with different rigidity at the edges and *b/t*=20, for mild steel

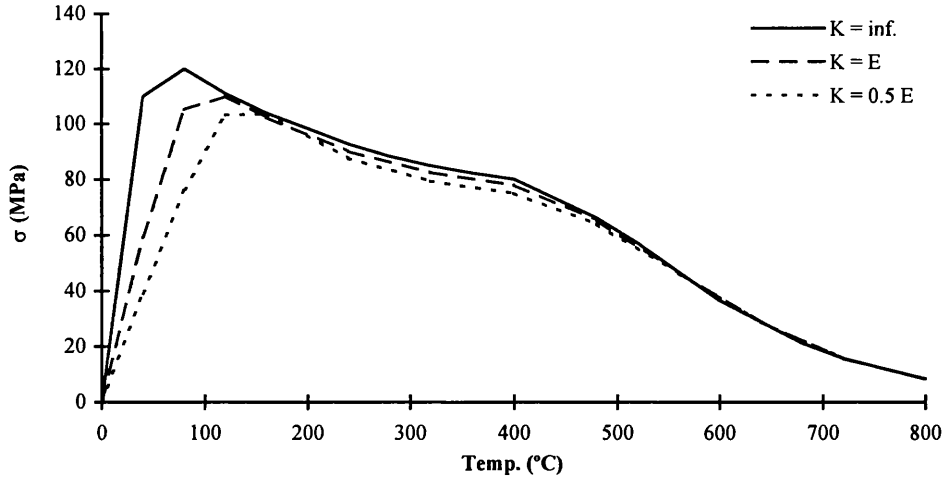

Figure 4.16: Comparison of the stress-temperature curves of square plates with different rigidity at the edges and *b/t*=40, for mild steel

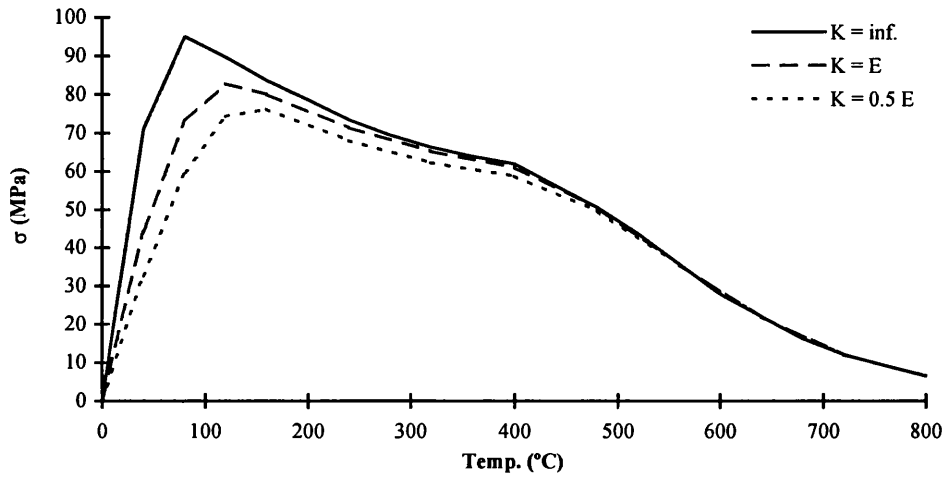

Figure 4.17: Comparison of the stress-temperature curves of square plates with different rigidity at the edges and *b/t*=60, for mild steel

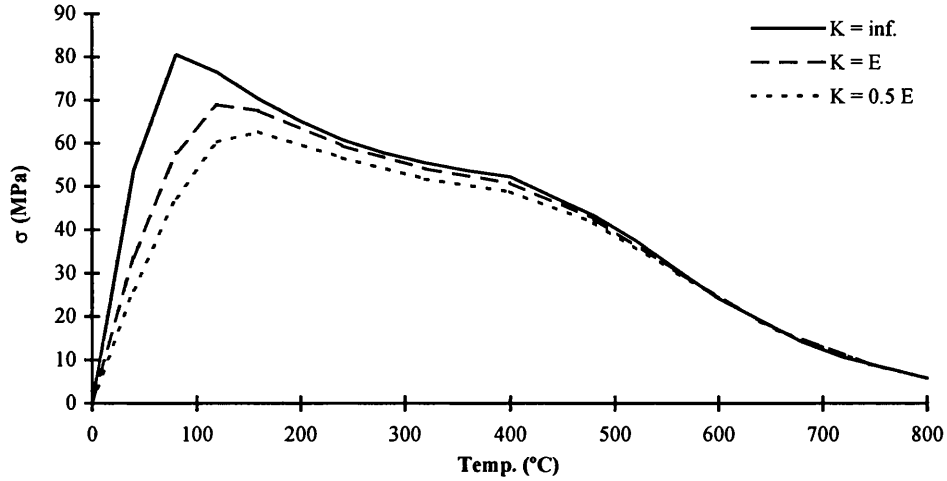

Figure 4.18: Comparison of the stress-temperature curves of square plates with different rigidity at the edges and *b/t*=80, for mild steel

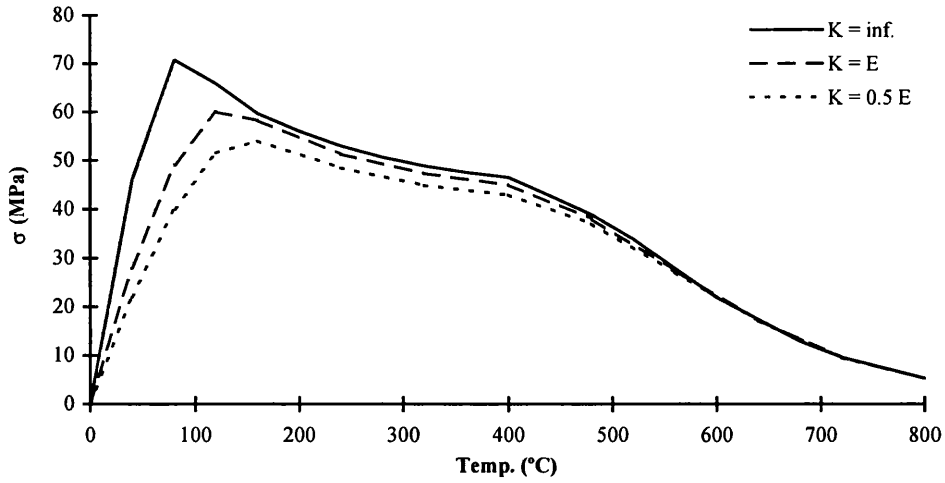

Figure 4.19: Comparison of the stress-temperature curves of square plates with different rigidity at the edges and b/t=100, for mild steel

This analysis is general but in stocky plates with average imperfections the ratio between the maximum initial distortions and the thickness is very low, thus the magnification of imperfections at collapse changes the shape of the plate from an almost perfect plate before buckling to a plate with a marked mode of collapse. When comparing the plate already buckled due to high constraint with the one in a pre-buckling state due to reduced constraint, the level of imperfections at the same temperature is very different and much lower in the latter case, which makes it have a higher strength than the former plate.

The other significant consequence of reducing the rigidity at the edges is the increase of the collapse temperature from around 100°C to 180°C. This is an expected result which may be very important in the design of the structures.

4.1.4 Strength of plates under a localised heat load

In section 4.1.3 the effect of heat loads over the whole plate has been studied. The present study has a different approach. The heat load is applied in a localised area and if the temperature difference is lower than a specified level then the thermal stresses will rise but the collapse of the plate does not occur. In this case, collapse is reached by imposing a proportional displacement to the edges of the plate.

The non-linear calculations were performed for a square plate and breadth to thickness ratio (b/t) from 20 to 100. For the initial geometric imperfections an average value was

used given by Eq. 4.6. The shape of the initial imperfections is represented by a Fourier series (Eq. 4.7) with only one component.

The thermal loads are applied in a localised area keeping the boundary conditions of the plate restrained to displacements in the plane. Heated areas varying between 6 % and 77% of the total area and five temperature levels are analysed in this study.

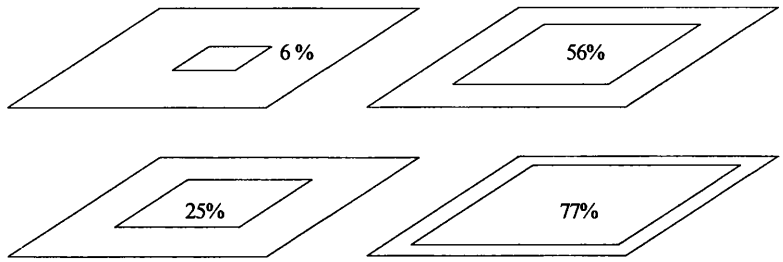

Figure 4.20: Heated areas

After the thermal loads have been applied, the load deflection curve of the plate is obtained by imposing a biaxial compression in its plane (figure 4.21).

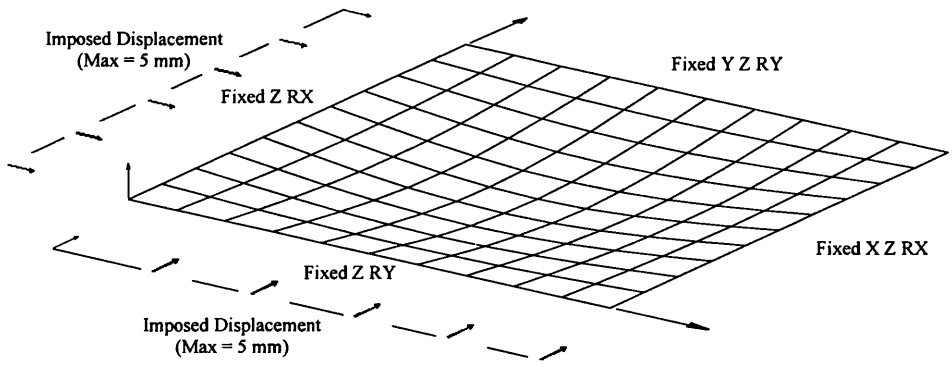

Figure 4.21: Imposed displacements and boundary conditions for the plate model

In order to assess the effects of localised heat loads on the collapse strength of plate elements, the stress-displacement curves obtained by biaxial compression without temperature loads should be first analysed. Figure 4.22 shows the behaviour of square plates of different slendernesses under these conditions.

One may note that the plate of b/t=20 shows a very high strength when compared with the other curves which have a small spread. This is be due to the different mode of collapse of the b/t=20 plate induced by the two orthogonal compressive stresses of the same magnitude (σ_x=σ_y). The first has a plastic collapse while the others have high out-of-plane deformations at the collapse.

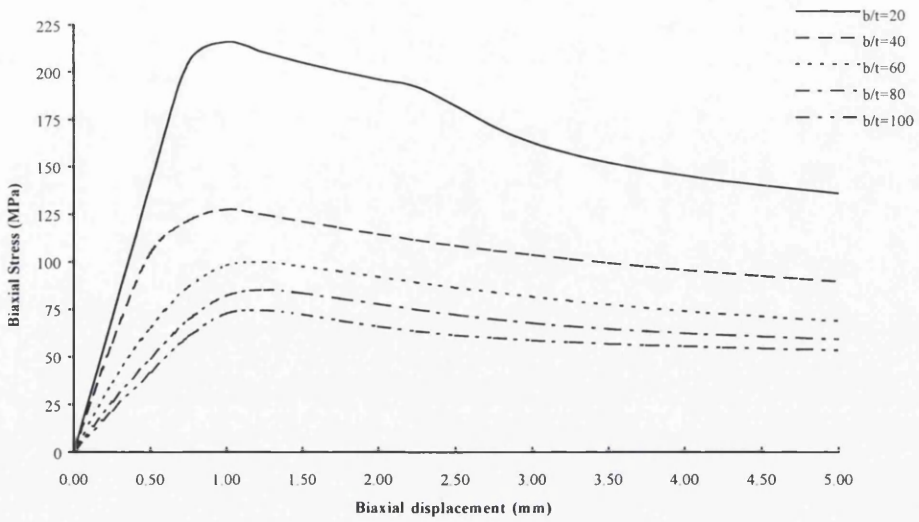

Figure 4.22: Stress-displacement curves without temperature loads

The influence of biaxial stresses is described by interaction curves in terms of the individual strength ratios for each load acting alone:

$$R_x = \frac{\sigma_x}{\sigma_{ux}}; \qquad R_y = \frac{\sigma_y}{\sigma_{uy}} \tag{4.8}$$

where σ_{ux} and σ_{uy} are the ultimate longitudinal and transverse stress, respectively. In the present case of square plates, the ultimate stress is equal for both directions.

Several expressions have been proposed to predict the longitudinal and transversal collapse strength of plate elements subjected to predominantly compressive in-plane loads. In the present case of square plates, the ultimate stress is equal for both directions and it can be estimated using the Faulkner expression (Faulkner, 1975):

$$\phi_F = \frac{\sigma_o}{\sigma_{ux}} = \frac{2}{\beta} - \frac{1}{\beta^2} \tag{4.9}$$

The nature of the interaction depends mainly on the plate slenderness. Different proposals exist in the literature but possibly the most commonly used is the circular interaction:

$$R_x^2 + R_y^2 = R_c^{\,2} \tag{4.10}$$

For thick plates the collapse is due to plasticity of the material and so the interaction curve for the σ_x and σ_y, and hence for R_x and R_y, would tend toward to the Von Mises interaction given by:

$$R_x^2 + R_y^2 - R_x R_y = R_{VM}^{\,2} \tag{4.11}$$

Table 4.2 shows the interaction ratios obtained for square plates using the circular and the Von Mises interactions. As would be expected the Von Mises formula approaches one for the plate of b/t=20 while the circular interaction gives better predictions for slender plates.

Table 4.2
Interaction ratio for the circular and Von Mises formulas

b/t	t (mm)	β	ϕ_F	$\sigma_u=\phi_F\,\sigma_o$	$\sigma_x=\sigma_y$	$R_x=R_y$	$R_c=\sqrt{R_x^2+R_y^2}$	$R_{VM}=\sqrt{R_x^2+R_y^2-R_xR_y}$
20	50.0	0.69	1.00	235.0	216.1	0.92	1.30	0.92
40	25.0	1.37	0.93	217.8	127.5	0.59	0.83	0.59
60	16.7	2.06	0.74	173.0	100.0	0.58	0.82	0.58
80	12.5	2.74	0.60	140.1	85.3	0.61	0.86	0.61
100	10.0	3.43	0.50	117.1	74.6	0.64	0.90	0.64

It can be also seen that the interaction formulas are optimistic for all b/t ratios. This fact may be due to the influence of the initial imperfections on the ultimate load, which is especially important for plates of b/t<60. Figure 4.23 illustrates this effect for a square plate of b/t=20. Furthermore the Faulkner expression was derived to predict the ultimate strength of simply supported plates under longitudinal compression; thus its applicability to biaxial loads is limited.

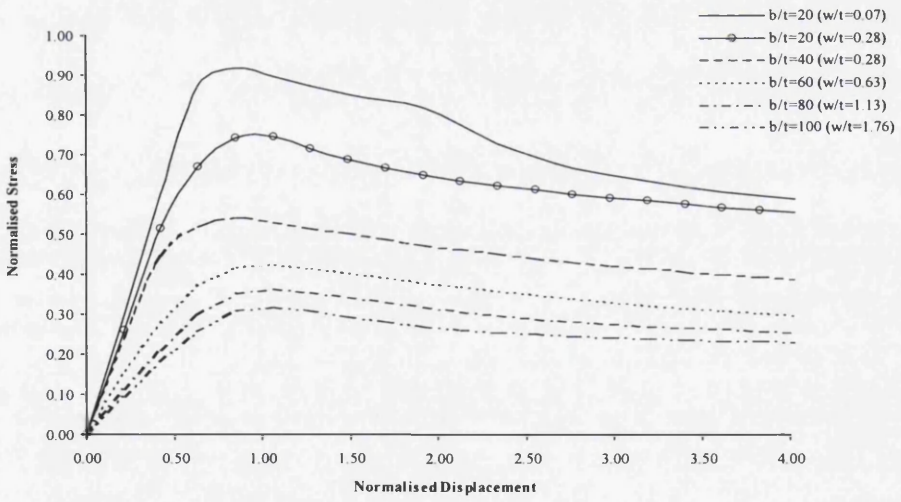

Figure 4.23: Normalised stress-displacement curves without temperature loads

Having briefly analysed the influence of biaxial compression on the strength of square plates, a series of calculations was conducted considering an initial heat load applied in a localised area. The models differ in the dimension of the heated area and in the maximum value of the temperature applied. The curves with stresses as a function of the imposed in-plane displacement are presented in the following figures. These curves are compared with the ones obtained without temperature loads (figure 4.22).

Figures 4.24 to 4.27 show the load-deflection curves for a square plate with a breadth to thickness ratio of 60 heated to temperatures between 0 and 800°C. The areas subjected to thermal loads are 6, 25, 56% and 77% of the plate, respectively.

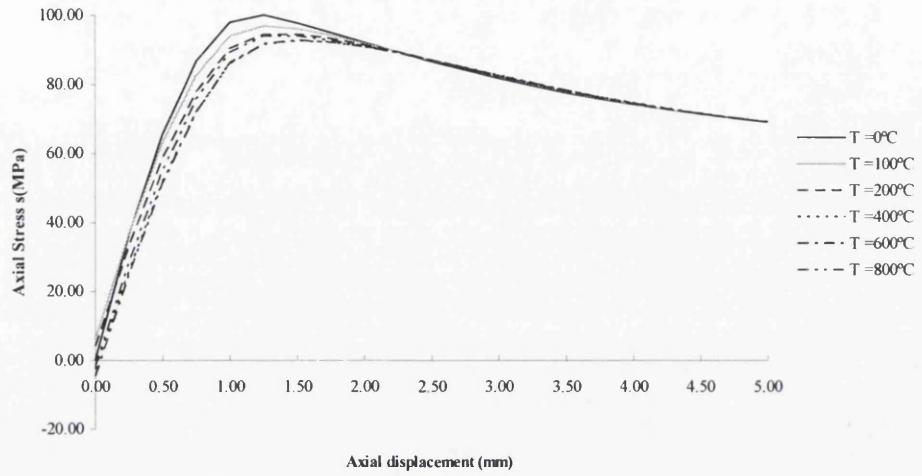

Figure 4.24: Axial stress for 6% of heated area (*b/t*=60)

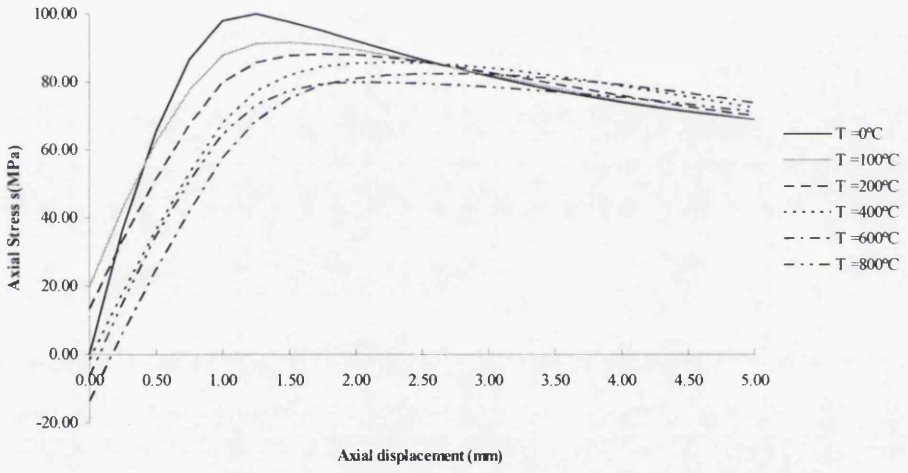

Figure 4.25: Axial stress for 25% of heated area (*b/t*=60)

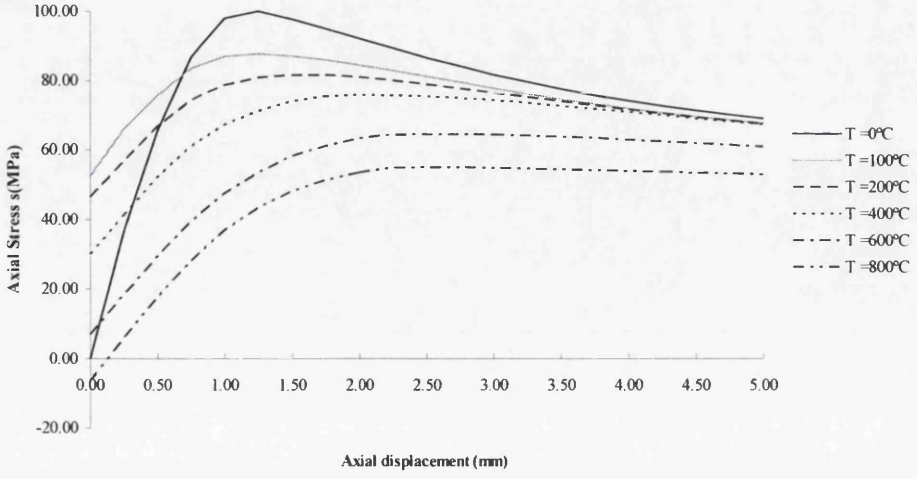

Figure 4.26: Axial stress for 56% of heated area (*b/t*=60)

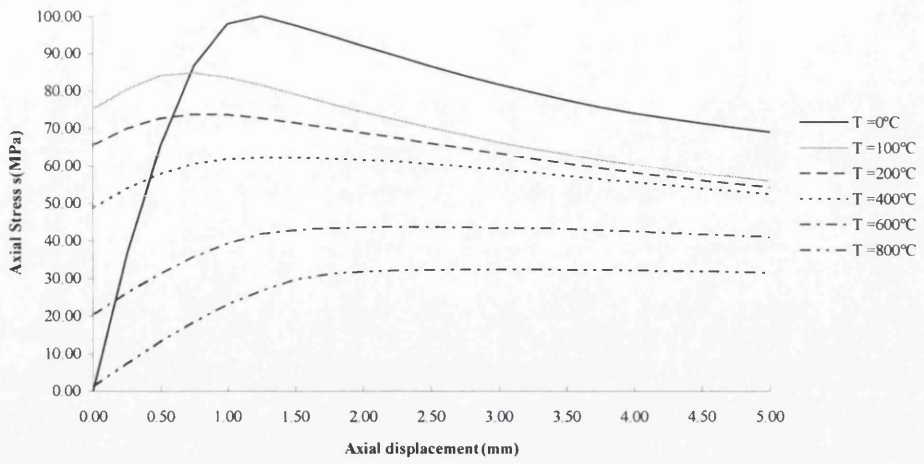

Figure 4.27: Axial stress for 77% of heated area (*b/t*=60)

One can see that, for the plate with 6% heated area an increase in temperature leads to small decrease of the plate strength, but the post buckling behaviour is insensitive to increases in temperature.

For larger heated areas, the thermal stresses developed with the increase in temperature will induce a biaxial state of stress and a degradation of material properties. These two effects will cause a decrease in the collapse load of the plates.

In figure 4.28 it can be observed that for a plate with the whole surface heated, the thermal stresses induce the collapse and the plate does not have additional strength.

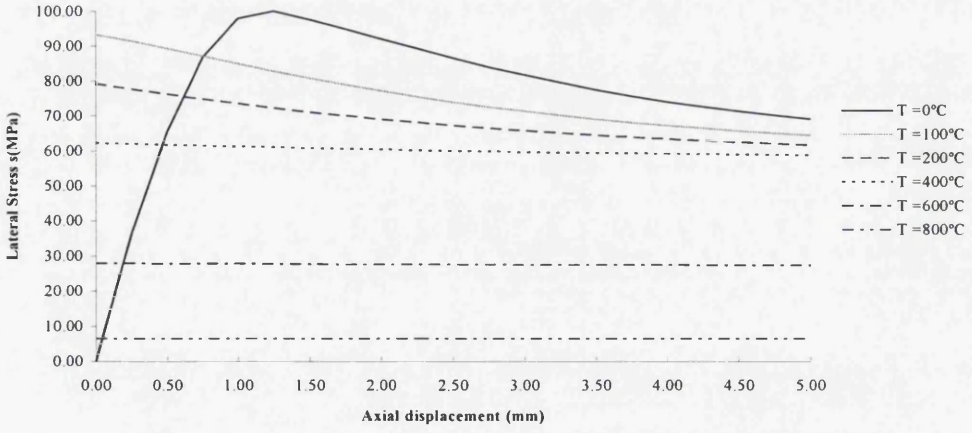

Figure 4.28: Axial stress for 100% of heated area (*b/t*=60)

Figure 4.29 shows that the collapse load decreases as the heated area increases, which is directly related to the reduction of material properties with the increasing temperature. It can also be seen that the maximum load is associated with a larger axial displacement when the heated area is increased.

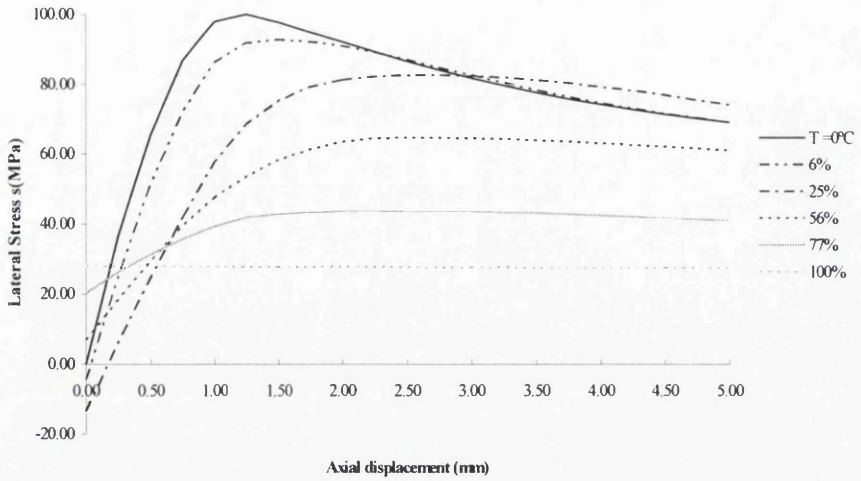

Figure 4.29: Axial stress with T=600°C for different heated areas (*b/t*=60)

Table 4.3 and figure 4.30 summarise the collapse loads for plates of *b/t*=60 with different levels of temperature differentials applied in five different areas.

Table 4.3
Collapse loads for *b/t*=60

ΔT(°C)	6%	25%	56%	77%
0		100.0		
100	96.9	91.6	87.6	84.8
200	94.4	88.2	81.6	73.7
400	92.6	85.8	76.8	62.2
600	92.7	82.5	64.5	43.6
800	94.0	79.8	55.1	32.4

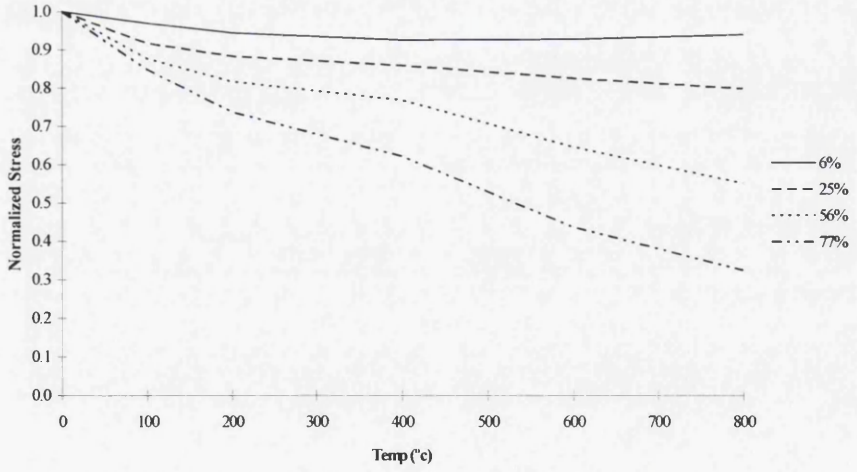

Figure 4.30: Normalised collapse loads for plates with *b/t*=60

It can be seen that the plate collapse load decreases rapidly when the heated area increases beyond 50% of the total area of the plate. A complete compilation of the results obtained from the numerical calculations can be found in appendix 4.

4.2 PROBABILISTIC MODELLING OF OFFSHORE FIRES

To describe the heat load associated with fires, eventually as a function of time, different deterministic models are available both for jet and pool fires which are the main types of fires considered in offshore platforms. This study deals with the probabilistic modelling in order to quantify the uncertainty of the predictions of those models.

The approach presented is limited to pool fires but the methodology is applicable also to jet fires. The model uncertainty, which can have a significant value, is not considered in this study. The probabilistic modelling quantifies the uncertainty of the predictions that result from the variability or the uncertainty of the physical variables. Even without accounting for the model uncertainty, the study of the sensitivity of the results allows the identification of the critical variables from the uncertainty point of view.

4.2.1 Fire models

In recent years, increasing attention has been given to the development and use of computer fire models. In this section, a brief review of the fire modelling approaches available is provided.

Ignited releases are typically categorised into three types; jet fires, pool fires and flashfires. Jet fires occur through ignition of a high/pressure release of flammable gas or liquid, mass discharge rates and release velocities can be high, producing flames tens of metres in extent. Pool fires occur when liquid or flashed vapour spills onto a surface and ignites and are characterised by smoky flames, lower flame temperatures and may flow from their point of origin. Flash fires result from the delayed ignition of gas/vapour releases and in confined spaces they will generally be accompanied by a significant overpressure generated by a rapidly accelerating flame front. The thermal effects on a structure are not considered as the heat load is transitory, although the effect on unprotected personnel is severe.

The primary mechanism for injury or damage from large open hydrocarbon fires is thermal radiation. The different types of fire behave differently and exhibit markedly different radiation characteristics. Radiation and convection are the principal mechanisms for transferring heat from a fire to a structure. The radiation is usually the dominant mode of heat transfer, although convective heat transfer becomes an important mode for structures which are directly impinged, or engulfed, by the fire.

Two basic radiation models for calculating the amount of radiation received from a flame are available. While one assumes that the flame radiates from a single point, or a number of points along the centre of the flame, in the other, the radiation level depends on the flame surface. Except for simple flame geometries, and for large distances from the flame, this method is not accurate and the surface emitter model is preferred.

Two main types of fires are considered in offshore structures, the pool and the jet fire, both of which can be modelled by methods of computational fluid dynamics or by approaches based on empirical formulation, as was reviewed in (Guedes Soares, 1993).

Most of these calculation methods became generally available to the industry through computer codes that incorporate them. For example, FLOW 3D is capable of modelling jet and pool fires (Askadi and Sinai, 1992) utilising computational fluid dynamics (CFD) techniques. Less sophisticated codes are available, which are based on empirical relations to predict pool and jet fires, for example POOL (Rew and Deaves, 1992) and TORCH (McCaffrey and Evans, 1986). Another system is the KAMALEON which is a 3D field model that predicts fires in open air and in enclosures (Opstad et al., 1991).

There are some tools available for deterministic predictions of the effect of fires. The degree of sophistication and the required computing time differ greatly between them and this is reflected in their accuracy. In (Opstad, Wighus, Holen, Hekkelstrand and Stensaas, 1991) some comparisons are made between model and experimental data, but this could be extended in order to derive objective measures of model uncertainty.

4.2.2 Physical pool fire model

In the reliability formulation for offshore structures under heat loads, the incident thermal radiation due to hydrocarbon pool fires is the main variable of interest. The thermal radiation depends on a number of parameters including the composition of hydrocarbon, the size, shape and duration of the fire and its proximity to the object at risk.

The pool fire models are based on the assumption that the pool can be described by an effective equivalent diameter D that does not vary with time. The characteristic quantity that describes the pool fire is the mean height of the visible flame H, usually defined as the distance above the fire source where a flame is present for 50% of the time.

The pool fire is modelled as a flame surface represented by a tilted cylinder shape with an elliptical horizontal base. The thermal radiation intensity at any point outside the flame surface can be estimated using the following expression,

$$\dot{q}'' = \tau E_f VF \tag{4.12}$$

where τ is the atmospheric transmissivity, E_f is the emissive power of the flame and VF is the view factor.

In addition to these factors, to determine the total radiation from one fire, the geometry of the flame should be known, which in turn depends on several factors as discussed in (Guedes Soares, 1993) and summarised here.

Pool Fire Geometry

The flame geometry is generally determined by assuming that the flame is a solid, grey emitter, having a regular well defined shape such as a tilted cylinder. The geometry of the flame for the pool fire model is characterised by the flame base diameter, visible flame height, flame tilt and flame dragged diameter.

The flame diameter is dependent on the spill size and the rate of burning. The visible flame height is predicted by the Thomas correlation (Thomas, 1963) as a function of the circular pool size and mass burning rate in the absence of wind,

$$\frac{H}{D} = 42\left(\frac{\dot{m}''}{\rho_a\sqrt{gD}}\right)^{0.61} \tag{4.13}$$

where H is the flame height, (m), D is the pool diameter, (m), $\dot{m}''$ is the mass burning rate, ($kgm^{-2}s^{-1}$), ρ_a ambient air density, (kgm^{-3}) and g is the acceleration of gravity, (ms^{-2}).

The estimation of the burning rate for hydrocarbon liquids is given by following correlation,

$$\dot{m}''_{\infty} = 1.27\times 10^{-6}\,\rho_L\left(\frac{\Delta H_c}{\Delta H_v - \Delta TC_p}\right) \tag{4.14}$$

where C_p is the specific heat of the liquid, ΔT is the temperature difference between the liquid at its boiling point and its initial condition, ΔH_c and ΔH_v are respectively the net heat of combustion and the vaporisation at the boiling point of the liquid fuel. If the

burning rate of the fuel is known, it is corrected for use in small fires by the equation given by Babrauskas (1983).

To characterise the geometrical properties of the flame in the wind blow situation two additional parameters are required, i.e. the flame drag and the flame tilt angle. The American Gas Association (1974) proposed the following expression for estimation of tilt angle of the flame from the vertical,

$$\cos\theta = \begin{cases} 1 & for \ \dfrac{u_w}{u_c} < 1 \\ \left[\dfrac{u_w}{u_c}\right]^{0.5} & for \ \dfrac{u_w}{u_c} \geq 1 \end{cases} \tag{4.15}$$

where u_w is the wind speed and u_c is given by,

$$u_c = \left[\frac{g\dot{m}'' D}{\rho_o}\right]^{\frac{1}{3}} \tag{4.16}$$

The wind causes the base of the flame to be dragged downwind of the pool, increasing its size. Mudan and Croce (1988) have proposed the following expression for the extended flame base D' which depends on the Froude number and on the vapour fuel density at the normal boiling point ρ,

$$\frac{D'}{D} = 1.25\left[\frac{u_w^2}{gD}\right]^{0.069}\left(\frac{\rho}{\rho_o}\right)^{0.48} \tag{4.17}$$

Atmospheric Transmissivity

The atmospheric transmissivity is given by the following relationship:

$$\tau = 1.389 - 0.135 log_{10}(P_{wv} d) \tag{4.18}$$

where P_{wv} is the partial water vapour pressure (N/m^2) and d is the distance from receiver point to flame centre (m). The partial water vapour pressure is given by:

$$P_{wv} = \frac{RH}{100} exp\left(14.4114 - \frac{5328}{T_a}\right), atm \tag{4.19}$$

where RH is the ambient relative humidity (%) and T_a is the ambient temperature (°K)

Emissivity Power

The emissivity power of a large turbulent fire can be approximated by:

$$E_f = E_b \varepsilon \tag{4.20}$$

where ε is the emissivity and E_b is the black body emissive power in KW/m^2 given by:

$$E_b = \sigma\left(T_f^4 - T_a^4\right) \tag{4.21}$$

where T_f and T_a are the radiation and ambient temperatures of the flame in °K and σ is the Stefan-Boltzmann constant (in KW/m^{4}K^4). The emissivity accounts for the fact that the flame is a grey emitter. It has a component due to soot and another from carbon monoxide and water vapour. It is difficult to estimate these values and an empirical relation for the average emissive power is given by:

$$E_f = 140e^{-0.12d} + 20\left(1 - e^{-0.12d}\right) \tag{4.22}$$

View Factor

The view factor depends on the location of the flame relative to the receiving target. It is calculated by a two-dimensional integral over the flame surface:

$$VF = \int_S \frac{\cos\beta_1 \cos\beta_2}{\pi d^2} dS \tag{4.23}$$

where β_1 and β_2 are the angles made by the normals on the fire and the receiving element and d is the distance from receiver point to the flame center. The integration is carried out numerically over the flame surface.

4.2.3 Probabilistic model of pool fires

The probabilistic model of the fire will be constructed from the physical model just summarised by adopting a first order second moment approach. This formulation is based on describing the random variables by their mean value and standard deviation without specifying the type of probability distribution that governs them.

As in the present case the number of variables that influence the fire model is relatively large and there is not much data for a detailed statistical analysis of the variability of each one to be conducted, this probabilistic model is compatible with that type of information.

Whenever one has a function $f(\underline{x})$ of several random variables, its first two statistical moments can be approximated by:

$$E[f(\underline{x}^*)] = f(\underline{x}^*)$$
$$V[f(\underline{x}^*)] = \sum_{i=1}^{\infty}\sum_{j=i}^{\infty}\left(\frac{\partial f}{\partial x_i}\right)\left(\frac{\partial f}{\partial x_j}\right)\sigma_i \sigma_j \rho_{ij} \tag{4.24}$$

where $E[f(\underline{x}^*)]$ and $V[f(\underline{x}^*)]$ stands for the expected value and variance, respectively, $\underline{x}^*$ is the vector with the linearization point, σ_i is the standard deviation of the variables x_i and ρ_{ij} is the correlation coefficient between the two variables. This formulation implies linearization about the value $\underline{x}^*$ of the variables and therefore it is valid only in its vicinity.

The importance of the contribution of each variable to the uncertainty of $f(\underline{x})$ can be assessed by the sensitivity factors which are determined by:

$$\alpha_i = -\frac{1}{\sqrt{\sum_{i=1}^{\infty}\left(\frac{\partial f(\underline{x})}{\partial x_i}\right)^2}}\frac{\partial f(\underline{x})}{\partial x_i} \tag{4.25}$$

Since the pool fire model is not represented by an analytical expression, which could be handled easily to calculate its derivatives, the partial derivatives indicated in the above expression have to be calculated numerically.

The example chosen for the application of the probabilistic model is a representative one for the effect of a pool fire on an offshore platform, i.e., the radiation heat on a tubular component. The offshore pool fire will be described by the model presented in the previous section, which has been coded in the POOL program (Rew and Deaves, 1992) and was incorporated in the RASOS system (Hulbert, 1993).

For a pool fire model, the incident radiation is calculated at a number of points defined by their location on a particular structural member. The member used in the fire loading calculations can be divided into a number of thermal mesh elements and the incident radiative flux is calculated in the centre of each thermal mesh.

A 5.0 m long tubular member of diameter 0.5 m divided into 30 sub-elements was considered for this study. The fire origin was defined in coordinates X = 15.0 m,

Y = 25.0 m and Z = 7.5 m. Figure 4.31 shows the location of the tube element and of the fire origin.

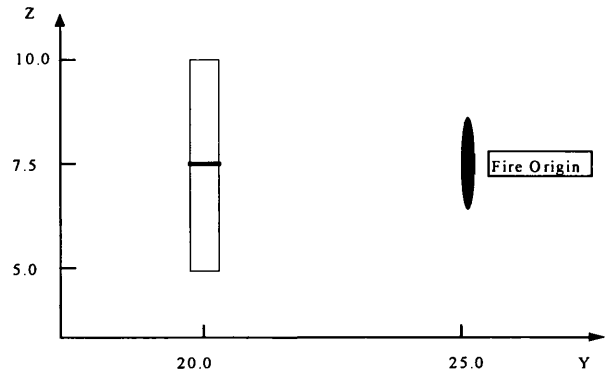

Figure 4.31: System coordinates location of the tube element

The most relevant variables for the pool fire model and their statistical description are shown in table 4.4.

Table 4.4
Statistical description of the variables for probabilistic modelling

	Variables	μ	σ	Unit
m	Mass flow rate of spill	10.0	1.0	Kg/s
m_w	Molecular weight of the fuel	44.0	4.4	Kg/mol
$\dot{m}''$	Maximum burning rate of the fuel	0.1	0.01	Kg/m^2s
K_β	Burning rate coefficient	1.4	0.14	m^{-1}
H_v	Heat of vaporisation of the fuel	430.0	43.0	KJ/Kg
H_c	Heat of combustion of the fuel	46000.0	4600.0	KJ/Kg
C_p	Specific heat capacity	2.4	0.24	$KJ\ Kg^{-1}\ K^{-1}$
E_α	Max. Emissive power of the fuel	220.0	22.0	KW/m^2
k	Extinction coefficient of the fuel	0.4	0.04	m^{-1}
u_w	Ambient wind speed	10.0	1.0	m/s
ϕ	Horizontal wind direction	360.0	10.0	Degrees
T_a	Ambient air temperature	288.0	10.0	K
RH	Ambient relative humidity	50.0	5.0	%
BP	Boiling point of the fuel	112.15	16.0	K
D	Diam. Of confined or bounded pool	10.0	1.0	m
H	Module ceiling height	30.0	0.5	m

The sensitivity factors (Eqn.4.25) of the variables in the pool fire model are shown in table 4.5 and figure 4.32. The variables not listed in the table presented below had negligible influence on the uncertainty of the results.

Table 4.5
Sensitivity factors of the variables in the pool fire model

Not depending on the fuel					Depending on the fuel		
T_a	u_w	RH	m	ϕ	$\dot{m}''$	m_w	BP
-0.034	-0.016	-0.006	0.156	0.982	-0.080	-0.007	0.061

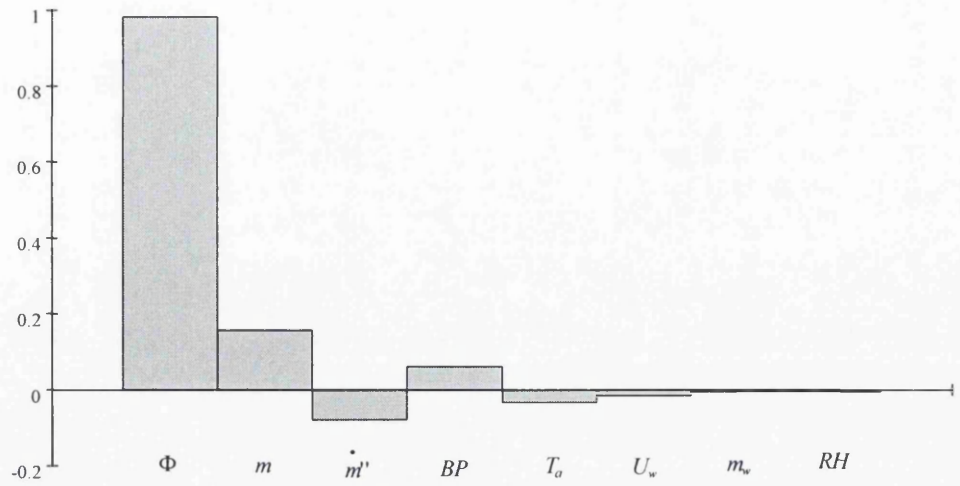

Figure 4.32: Sensitivity factors of the variables in the pool fire model

The analysis of the figure 4.32 (or table 4.5) above, suggests that the most important variables for the pool fire model are:

Table 4.6
Sensitivity and variability of the variables

	Variable	Sensitivity	Variability	Model
ϕ	Horizontal wind direction	High	High	Fire
m	Mass flow rate of spill	High	High	Fire
$\dot{m}''$	Maximum burning rate of the fuel	Medium	Low	Fuel
BP	Boiling point of the fuel	Medium	Low	Fuel
T_a	Ambient air temperature	Low	Medium	Fire
u_w	Ambient wind speed	Low	High	Fire
m_w	Molecular weight of the fuel	Low	Low	Fuel
RH	Ambient relative Humidity	Low	Medium	Fire

The relatively high variability associated with the variables in the fire model means that these factors are difficult to quantify. Additionally, the model is highly sensitive to horizontal wind direction and the mass flow rate of spill, making these two variables especially important in the definition of the fire model. This conclusion allows further studies to concentrate on these variables and their effect.

4.3 RELIABILITY BASED DESIGN OF PASSIVE FIRE PROTECTION IN FIRE WALLS

The ISSC Committee on Structural Design Against Fire and Blast has reviewed recent developments and the current state of the art on design and analysis of ship and offshore structures against fire and blast loading. The first report of the Committee (International Ship and Offshore Structures Congress, 1994) has looked at the work on the use of fibre reinforced plastic materials for offshore platfom topsides and ship structures and also considered the results from the Joint Industry Project in Blast anf Fire Engineering for Topside Structures.

With the advent of fast computers, integrated scenario-based anlyses of accidental fires on offshore structures have been reported in a number of publications as reviewed in the second report of the committee presented in the International Ship and Offshore Structures Congress (1997). These analyses use computational models to calculate the fire process for determination of the heat exposure to adjacent structures, the transient temperature development in the material and the mechanical response of the entire structure.

When unprotected steel is subjected to a design or actual fire it heats up to a dangerous level with a substantial loss of stiffness and strength. This is the reason why many studies have been done during the last few years in the definition and optimisation of fire protection systems.

Active and passive fire protection are the two methods of protection in a fire scenario. An active fire system needs to be activated by detection of the fire using one or more of many types of sensor available. This type of protection relates to the application of water to the structure to provide a cooling effect.

During the last decades significant advancements have been made with particular respect to passive fire protection materials. Passive fire protection (PFP) consist in the methods use the application of an insulative layer to the structural elements or the inclusion of divisions which provide fire protection by their insulative nature.

This type of protection is expensive to apply to steelwork, and is also expensive to maintain once in place. For these reasons, it is advantageous to reduce PFP to the minimum amount necessary.

The various types of passive fire protection materials can be categorised in purely insulative (mineral or ceramic fibre), intumescent (intumescent epoxy), cementitious (vermiculite cement and magnesium oxychloride) and dry fix (panels or mouldings fixed to the substrate by mechanical means, or fabricated panels sandwiching insulative materials between layers of mild steel or stainless steel, which can be used to form fire divisions).

In the definition of the requirements of passive fire protection systems (type of PFP and thickness) factors such as nature of the fire and heat loads, explosion resistance and weatherability should be taken into account.

Using tables of results of fire tests (British Standard Institution: BS5950, 1990), a first estimation of PFP can be obtained. By implementing a computer-based package in which the thermal data is transferred to a structural model of the structure, an estimate of the minimum required thickness of a given insulation material may be obtained.

In (Rogers and Ramsden, 1994) a semi-automated method for optimisation of PFP was described. This method uses a British Gas Code, CHAOS (1993), for determining the characteristics of jet fires, and USFOS (1996) to calculate the thermally induced progressive collapse.

Another computer software package, Global Collapse in Offshore Fires, was developed. Its main purpose is the assessment of the collapse steel core temperature and the margin to progressive collapse module by module as well as for the whole platform (Yngve Anderberg, 1994).

The progressive collapse of structures under time variant thermal loading can also be modelled using RASOS (Gierlinski and Sears, 1994), Reliability Analysis of Fixed Offshore Structures. The software has been produced within the Brite P1270 project "Reliability Methods for Design and Operation of Offshore Structures". The numerical algorithm incorporated into RASOS software comprises two new modules, RASOS_B and RASOS_T which generate the thermal loading from a given accident scenario.

For the optimisation of PFP on firewalls, a computer code OPTIWALL was developed (Jensen and Thoft-Cristensen, 1995). This software for optimisation of non-structural parts was produced jointly by CSR and IST to perform deterministic and reliability based optimisation of the passive fire protection attached to fire walls.

The optimisation problem was defined and formulated by Guedes Soares (1994) and the specifications for interfacing optimisation software with the software for reliability evaluation of fire walls (Teixeira et al., 1995) is described in detail in (Jensen et al., 1995). The OPTIWALL consists of two sets of software; OPTIM01 (CSR ApS, 1994) for optimisation and RTLS (Guedes Soares et al., 1995) for deterministic and reliability based analysis of fire walls. The RTLS software includes three modules: RASOS_B for the heat-flux calculation from pool and jet fires, HOTPLATE (Jensen and Thoft-Cristensen, 1995) for calculation of the temperature in firewalls and RELIAB01 (CSR ApS, 1994) for reliability analysis.

In this section, the reliability formulation used in the software for reliability evaluation of thermally insulated fire walls subjected to a pool is presented. The limit failure criterion is used to calculate the probability of the actual temperature at a given time exceeding a specified random value of the temperature in a plate.

4.3.1 Reliability formulation

It was established in section 4.1.3 that the differential of temperature in a plate will lead to its collapse whenever it reaches the limit value. Therefore, at a specific point in time, one can define the probability of failure as the probability of the temperature in the plate being higher than its limit temperature.

The limit state function is then:

$$g(\bar{x}) = \Delta T_{\text{lim}} - \Delta T_{steel} \tag{4.26}$$

where, ΔT_{lim} is the difference of temperature that leads to plate collapse, and ΔT_{steel} is the actual increase of plate surface temperature.

The change of temperature across an insulation material can be calculated as a function of time by the numerical procedure proposed by Nielsen et al. (1994), as a function of the input thermal radiation intensity, which in turn depends on several fire parameters as described in section 4.2.2.

In the formulation of the reliability problem the input thermal radiation intensity is defined as a stochastic variable which is used as input for the steel temperature evaluation.

Since the temperature increase cannot be described by an analytical expression the limit state equation has to include the numerical scheme that yields the temperature increase as a function of the thickness of the insulation (t_i) the thermal conductivity (k_i), the density (ρ_i) and the specific heat Cp_i of the material, in addition to the input thermal radiation intensity. Thus the limit state equation is written as:

$$g(\underline{x}) = \Delta T_{\text{lim}} - \Delta T_s(\dot{q}'', t_i, \mathrm{k_i}, \rho_i, Cp_i) \tag{4.27}$$

Having established the form of the limit state equation, the reliability can be assessed by any of the available codes based on first order reliability methods. In the present case use was made of RELIAB (CSR ApS, 1994).

The development of a fire is a time dependent problem and so will be the temperature of the steel plate. However, the change of temperature with time is a monotonic function, and this allows the time variant reliability problem to be studied by a series of time independent formulations at different time steps. The problem is solved here by considering different points in time after the start of the fire and calculating the reliability index at those points.

4.3.2 Heat transfer model

Since fire walls are protected by insulation material the prediction of the temperature of the steel plate depends on the heat transfer across the insulation material.

The unknown surface temperature of the plate T_s on the inner side of the fire wall can be calculated from the continuity equations for the heat flux through the insulation. The fire wall, with a total thickness of insulation d, is divided into $n+1$ equidistant subintervals of thickness $\Delta d = \frac{d}{n+1}$ as shown in figure 4.33.

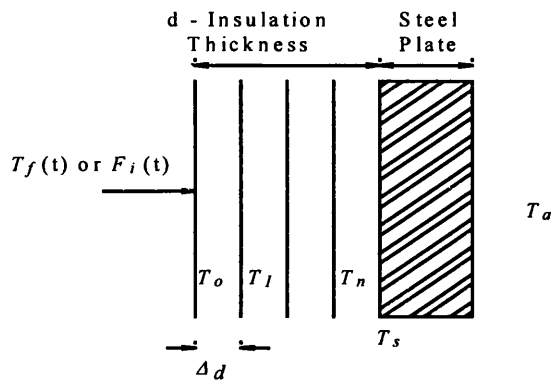

Figure 4.33: Discretisation of the fire wall

The temperature field $T_f(t)$ or flux $F_i(t)$ are assumed to be homogeneous over the exposed side of the fire wall, as is the temperature field $T_a(t)$ at the outward side, which is not exposed to the fire.

The flux into the wall is given as

$$F_i = -k\frac{\partial T_f}{\partial x} \approx \frac{k}{\Delta d}\left(T_f - T_1\right) \tag{4.28}$$

The temperature at layer j, T_j, is given by the following one-dimensional heat equation,

$$\rho_i c_i \frac{\partial T_j(t)}{\partial T} = k_i \frac{\partial^2 T}{\partial x^2} \approx \approx \frac{k_i}{\Delta d_i^2}\left(T_{j-1}(t) - 2T_j(t) + T_{j+1}(t)\right) \tag{4.29}$$

$$\frac{dT_j(t)}{dt} = \alpha\left(T_{j-1} - 2T_j + T_{j+1}\right) \quad j=1\ldots n \tag{4.30}$$

$$\alpha = \frac{k}{\rho c\, \Delta d^2} \tag{4.31}$$

where k, ρ and c represent the thermal conductivity, the mass density and the heat capacity of the firewall, respectively.

This equation can be solved by a finite difference approximation in which the boundary conditions $T_o(t)=T_f(t)$ and $T_{n+1}(t)=T_s$ have been applied, as done by Nielsen, Jensen and Thoft-Cristensen (1994).

Since the plate temperature increases with time, the temperature T_a will also increase, and may be calculated using:

$$F_i = h\left(T_s - T_a\right) \tag{4.32}$$

where h is the average convection heat transfer coefficient of the air.

4.3.3 Limit temperature differential for steel plates

In section 4.1 the elasto-plastic behaviour of plates subjected to heat loads has been studied and curves have shown the stresses as a function of temperature. Table 4.7 summarises the final results for the limit temperature of plates with restrained boundary

conditions, considering three different materials with yield stresses of 235MPa, 300MPa and of 355MPa.

Table 4.7
Limit temperature differentials for plate collapse (°C)

	σ_o=235 (MPa)			σ_o=300 (MPa)		σ_o=355 (MPa)	
b/t	*a/b*=1	*a/b*=2	*a/b*=3	*a/b*=1	*a/b*=3	*a/b*=1	*a/b*=3
20	64	56	56	80	70	128	80
40	68	48	40	88	50	160	80
60	80	56	40	100	56	160	80
80	84	56	48	104	56	160	80
100	84	56	48	100	56	160	80
Mean	76.0	54.4	46.4	94.4	57.6	153.6	80.0
COV	0.123	0.066	0.144	0.106	0.128	0.093	0.0

Inspection of the table shows that there is a clear effect of the three governing parameters. As a general observation, it looks as if the most dominant parameter is the yield stress and the least important is the breadth to thickness ratio.

Table 4.8
Collapse temperature differentials of the different materials (°C)

(MPa)	σ_o=235	σ_o=300	σ_o=355
Mean	58.93	76.00	116.8
COV	0.25	0.28	0.34

Depending on the level of detail desired in the analysis one can either use the collapse temperature for each set of three parameters, or only the average value for each set of σ_0 and a/b, as shown in table 4.7, or even use only σ_0 as the governing parameters as indicated in table 4.8. Note that these values correspond to a differential of temperature, and not to an absolute temperature of collapse.

After attaining the maximum stress at the critical temperature, the plates are still able to carry some load with increasing temperature, but one is generally interested in the maximum load carrying capacity.

In the case of fire walls, even after the collapse, the plate will be in position and as such it will continue to constitute a barrier to the transmission of fire. However, when the plate collapses, it acquires large deformations due to the buckled pattern and it is most likely to cause damage to the adjacent insulation material.

One can expect whenever the passive fire protection becomes ineffective, although in a localised area, that the plate will have a very quick rise of temperature and will collapse rapidly losing any load carrying capacity.

Therefore, taking into account the progression of the damaging situation that will occur after the first plate collapse, it is justifiable to adopt this situation as the reference one to establish the limit state function defining failure.

The validity of adopting the temperature as the governing factor to describe plate collapse can be verified by calculating the displacement induced in a plate by the temperature of collapse and afterwards imposing this edge displacement on a plate without any temperature increase.

The limit temperature of a square plate with a breadth to thickness ratio (*b/t*) equal to 60 and yield stress of 235 MPa. is 80°C (table 4.7). Figure 4.34 shows the increase of longitudinal displacement of a square plate with temperature; it is seen that for a temperature of 80°C the value is 1.121 mm.

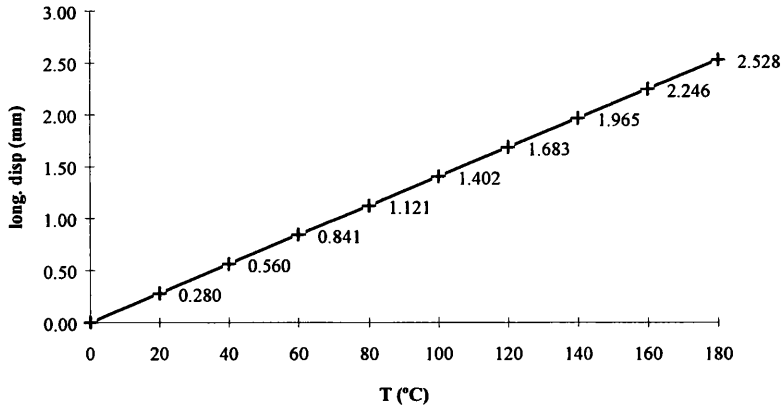

Figure 4.34: Thermal induced in-plane displacement of a square plate (*b/t*=60)

Considering now the same plate without any change of temperature, and imposing a proportional displacement to the edges, leads to the stress-displacement curve shown in figure 4.35.

One can see that the collapse of the plate occurs for a longitudinal displacement of 1.125 mm which is the same as the thermal expansion resulting from an increase of temperature of 80°C.

This clearly demonstrates the equivalence between the two formulations and the adequacy of adopting only the temperature as the governing variable explaining the plate collapse.

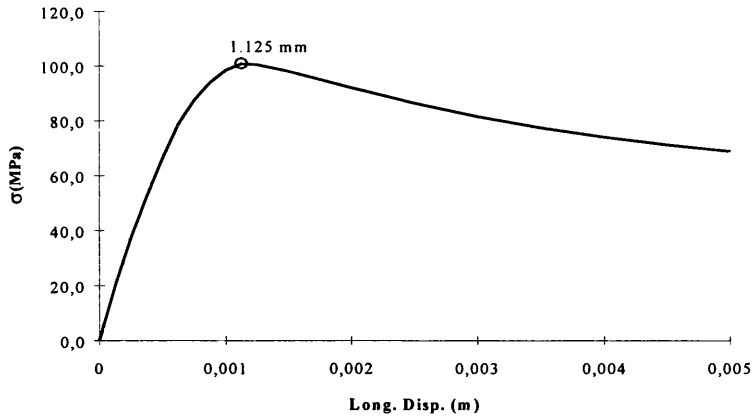

Figure 4.35: Stress-displacement relation (*a/b*=1, *b/t*=60)

4.3.4 Example calculation

The example analysed here is a wall with dimensions representative of the modules in the topsides of offshore platforms, as shown in figure 4.36. The origin of the pool fire was considered to be 10 m away.

Two values for the horizontal wind direction are analysed. The first value of 45° was considered in order to obtain the maximum value of radiation in the centre of the wall (50.9 KW/m^2 - 702 °C). The second value of 80° corresponds to a radiation in the centre of the wall of 13.9 KW/m^2 (436 °C).

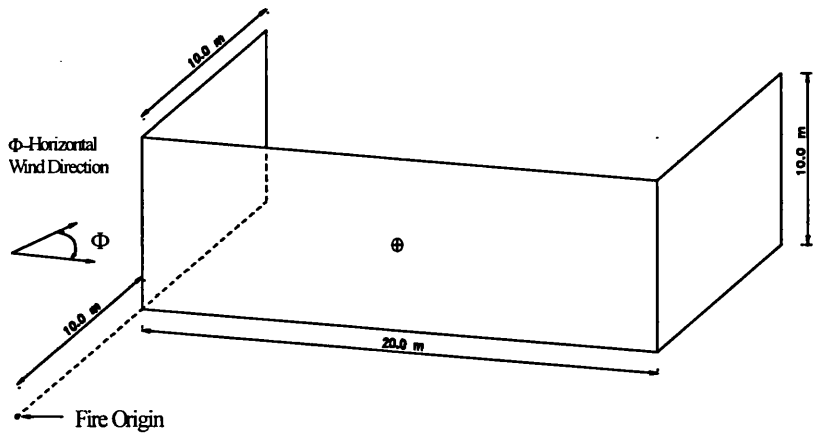

Figure 4.36: Wall model

For the present example all variables are assumed to be normal distributed. Table 4.9 shows the statistical moments of the random variables considered.

Table 4.9
Stochastic variables

	Variables	Mean Value	Std. Dev.
Rad	Radiation	13.9 / 50.9	1.39 / 5.09
t_i	Thick. Of insulation	0.020	0.002
K_i	Thermal conductivity	0.05	0.005
ρ_I	Density	2000.0	200.0
Cp_i	Specific heat	500.0	50.0
T_{lim}	Limit Temperature	58.9	5.89

Figure 4.37 shows the reliability index that was obtained as a function of time for the two mean values of radiation. For the lower radiation value higher values of β were obtained, as was expected.

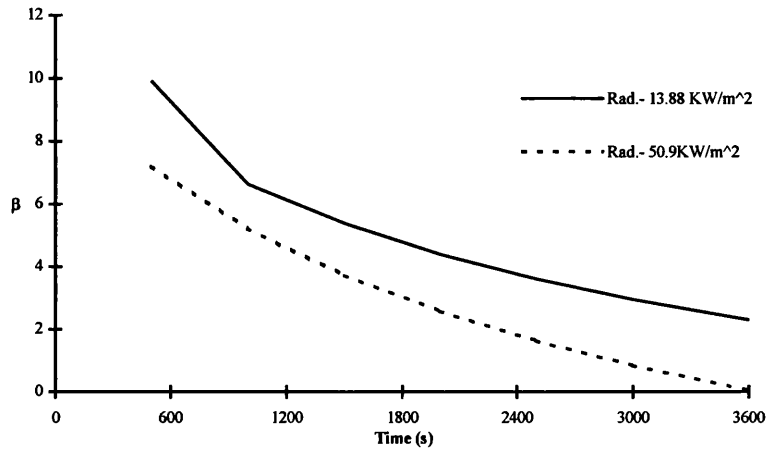

Figure 4.37: Time dependent reliability index for two radiation levels.

Figure 4.38 shows the reliability index obtained with the COV=0.1 and 0.25 to describe the limit temperature. The expected higher values of β were obtained for the curve with COV = 0.1.

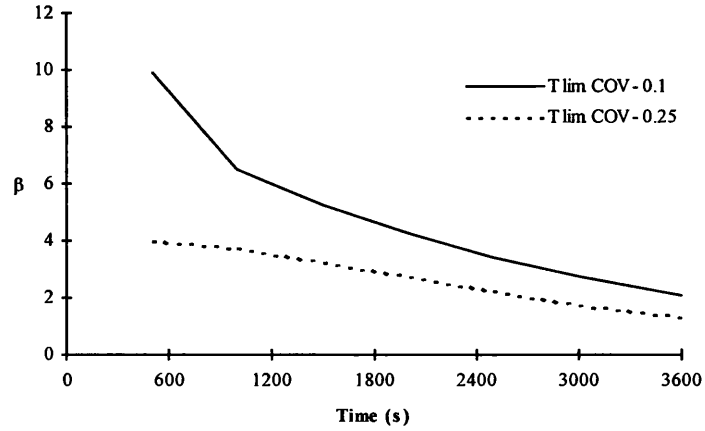

Figure 4.38: Influence of T_{lim} COV in the reliability index β

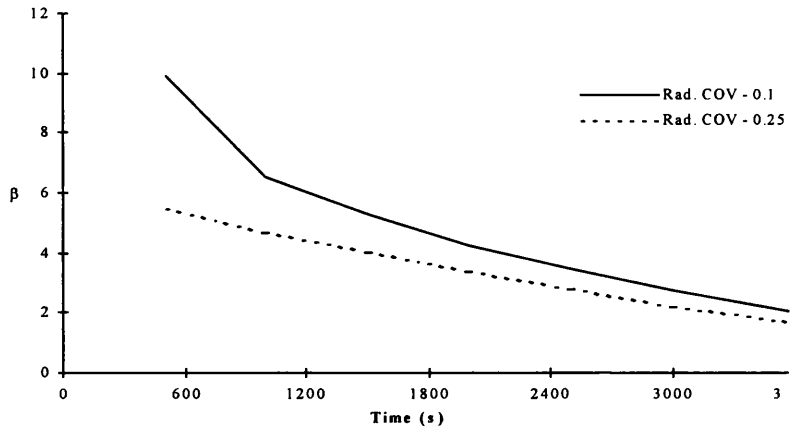

Figure 4.39: Influence of radiation *COV* in the reliability index β

For the radiation a similar result is shown in figure 4.39. The time dependent reliability index is obtained for the values of 0.1 and 0.25 of the coefficient of variation.

Figure 4.40 shows the reliability index obtained for two different materials with yield stress, σ_o=235MPa and σ_o=355 MPa, which correspond to the collapse temperatures values T_{lim} = 58.9°C and T_{lim}=116.8°C, respectively.

The higher values of β were obtained for the curve with higher yield stress, which decreases smoothly with time. The curve obtained with the other yield stress drops quickly with time.

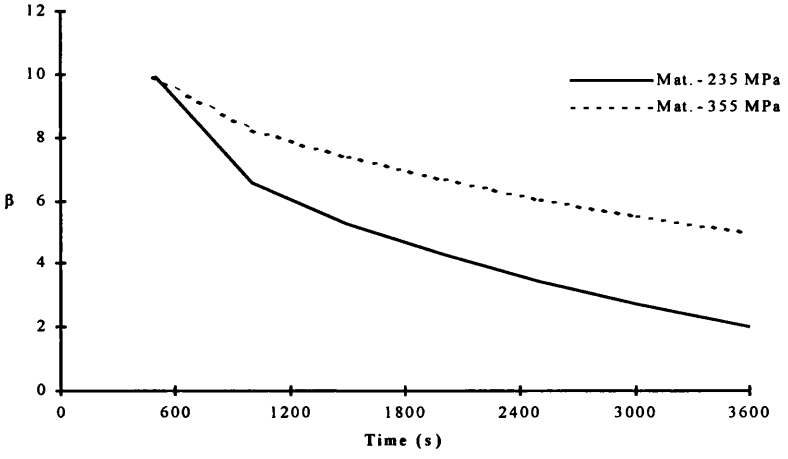

Figure 4.40: Influence of material type in the reliability index

Figure 4.41 shows the reliability index that was obtained for the thickness of insulation with mean value changing from 0.015 to 0.045 mm after 1 hour burning. The curve shows the increase of β with the increase of the thickness of insulation, as was expected.

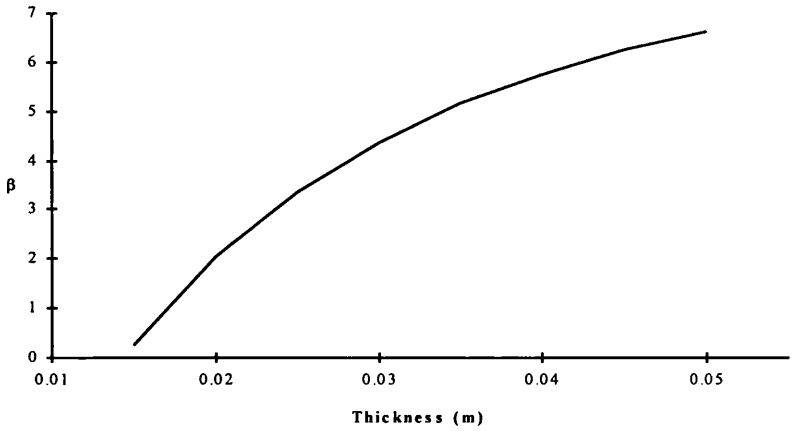

Figure 4.41: Influence of insulation thickness in the reliability index

Table 4.10 presents the elasticities of mean and standard deviation for time 3600s. It is apparent that the important ones are the limit temperature, the thickness of insulation and the thermal conductivity of the insulation.

Table 4.10
Elasticities of mean and standard deviations values for time 3600s

Variable	$\frac{\partial \beta}{\partial \mu}\frac{\mu}{\beta}$	$\frac{\partial \beta}{\partial \sigma}\frac{\sigma}{\beta}$
Radiation	-0.8212	-0.0281
Thickness of insulation	3.5118	-0.5139
Thermal conductivity	-2.1912	-0.2001
Density	0.6250	-0.0163
Specific heat	0.6250	-0.0163
Limit Temperature	2.3235	-0.2251

Figures 4.42 to 4.44 show the sensitivities and time dependent elasticities of the mean and standard deviation values of the reliability index with respect to the different variables. This analysis was made for the higher reliability index curve shown in figure 4.37.

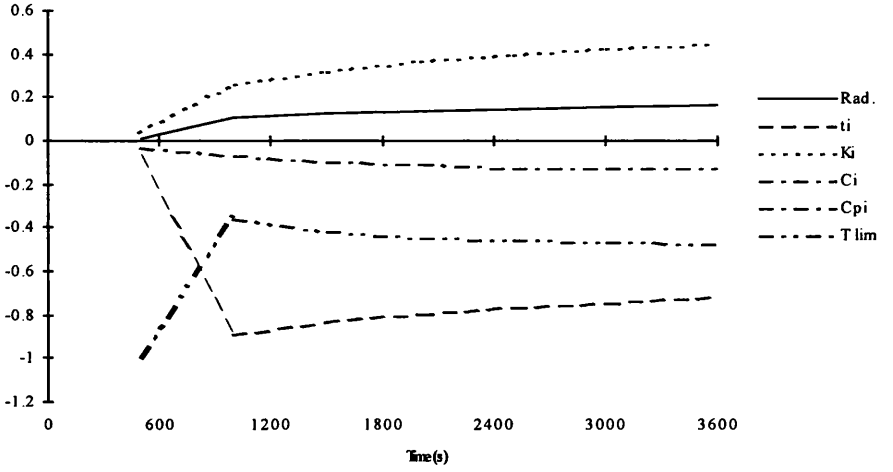

Figure 4.42: Time dependence of sensitivity analysis

The sensitivities show the limit temperature, the thickness of insulation and the thermal conductivity as the more important variables in the determination of the reliability index.

As can be seen in figure 4.43 the elasticities, of the thickness of insulation of the limit temperature and of the thermal conductivity are the largest ones.

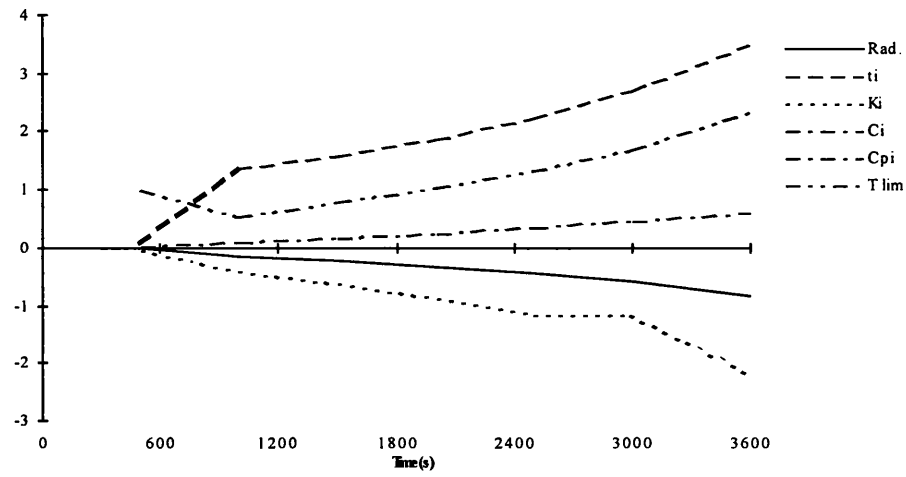

Figure 4.43: Time dependence for elasticity of mean values

The elasticity of standard deviations is presented in figure 4.44. It is observed that the most important variable is the thickness of insulation.

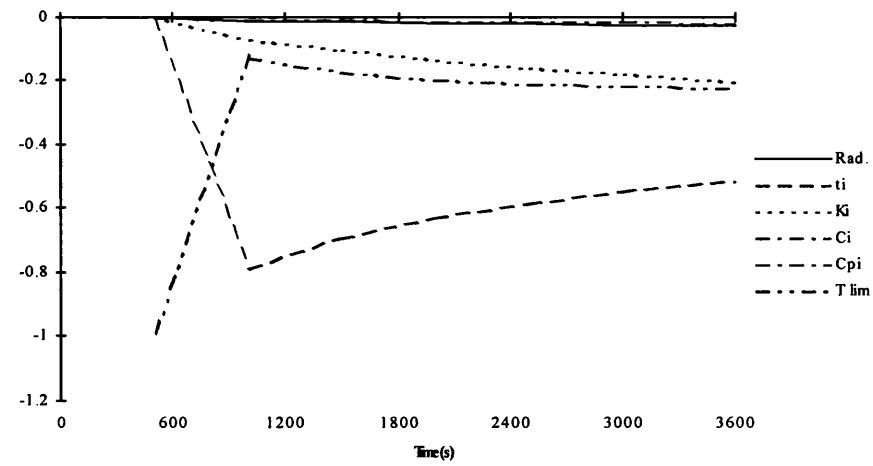

Figure 4.44: Time dependence for elasticity of standard deviation values

4.4 RELIABILITY OF PLATE ELEMENTS UNDER LOCALISED HEAT LOADS

When the heat load is not applied to the whole plate surface, but instead is localised, the strength of the plate will be different, and for some dimensions of the heated zone the plate will not collapse under the exclusive effect of temperature, even if it goes up to 800°.

This implies that plates with localised heat loads are able to sustain additional loads before collapse. Therefore, in this situation it is appropriate to formulate the reliability problem in terms of stresses because this is the condition that will govern collapse. This formulation is adequate whenever one is interested in structural bearing components, which will be subjected to different types of loading. Hence, formulating the problem in terms of stresses gives the possibility of accounting for more than one load effect.

The results of calculations of the collapse load of plate elements with localised heat loads and additional in-plane compressive loads (section 4.1.4) are the basis to define the limit state equation, which is used in the reliability formulations.

Calculations are presented concerning the effect of different parameters on the reliability of plates, and in particular the effect of the size of the heated zone is quantified.

4.4.1 Reliability formulation

The reliability model used is based on the existing formulation for compressive strength of plates subjected to biaxial in-plane loads. This formulation considers the externally applied stresses and the ultimate stresses, which are function of the temperature.

The compressive strength of rectangular plates subjected to biaxial in-plane loads can be determined by the following equation:

$$R_X^2 + R_Y^2 = 1 \tag{4.33}$$

where $R_X = \frac{\sigma_X}{\sigma_{UX}}$, $R_Y = \frac{\sigma_Y}{\sigma_{UY}}$, σ_X and σ_Y are the x and y component of the in plane stress and σ_{UX} and σ_{UY} are the longitudinal and transverse collapse stress.

For square plates equation. (4.33) simplifies once the component x and y of the in plane stress are equal $(\sigma_X = \sigma_Y)$ as well as the longitudinal and the transverse stress $(\sigma_{UX} = \sigma_{UY})$:

$$1 - \sqrt{2R_X^2} = 0 \tag{4.34}$$

$$g = 1 - \sqrt{2\left(\frac{\sigma_X}{\sigma_{UX}}\right)^2} \tag{4.35}$$

The stochastic model used in the reliability analysis considers the normal distribution for both applied and ultimate stresses.

4.4.2 Reliability calculations

The methodology was applied to the study of square plates, and five test cases were considered:

Temperature in the whole plate,

Temperature in 77% of the plate,

Temperature in 56% of the plate,

Temperature in 25% of the plate,

Temperature in 6% of the plate.

The plate is initially loaded from ambient temperature up to the final temperature T_f and is then loaded in-plane, so as to produce the load deflection curves.

The variation of the final temperature considered in the analysis is between 100°C and 800°C, and plates with 5 different breath to thickness ratios were analysed (20, 40, 60, 80 and 100).

The stochastic model of the ultimate stress is defined on the basis of the results of the ultimate stress of plates subjected to localised heat loads presented in appendix 4 and assuming a coefficient of variation of 0.1.

The reliability of the plates is determined assuming no significant in-plane stress. This stress is then taken as a normal distribution with mean value 0.0 MPa. The value assumed for the deviation of the in-plane stress was 10.0 MPa.

Figure 4.45 shows the reliability index as a function of the in-plane stress standard deviation for the different areas considered in the study and for a plate with a breadth to thickness ratio of 60, heated up to a temperature of 800°C.

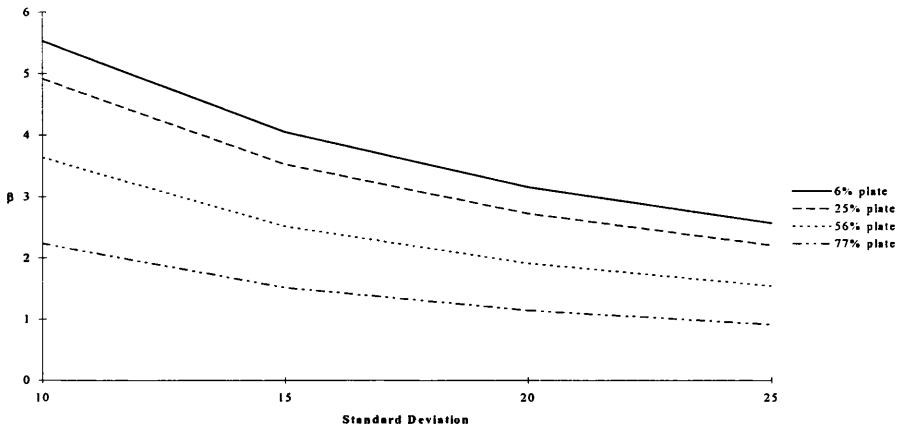

Figure 4.45: Reliability index as function of the applied stress standard deviation (*b/t*=60 ; *T*=800°C)

As one can see, the reliability decreases with the standard deviation, but apparently independently of the area considered in the plate. In the test cases a standard deviation of 10 MPa is considered.

Firstly the behaviour of the reliability index as a function of the plate breadth to thickness ratio (*b/t*) is analysed. Secondly, the *b/t* cases are separated in order to observe how the reliability index varies in the same plate subjected to different conditions (reliability index as function of the heated area and as function of the final temperature).

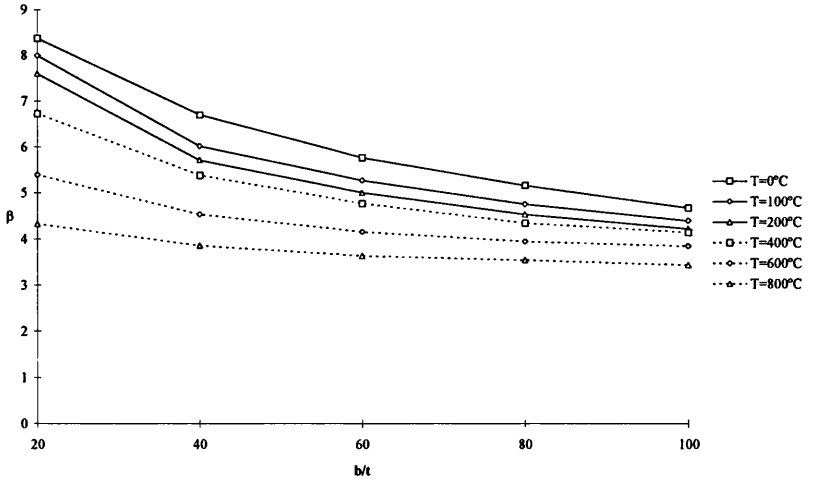

Figure 4.46: Reliability index as function of the breath to thickness ratio for a plate heated in 56% of its area

The previous figure shows the reliability index as a function of the breadth to thickness ratio for a plate heated over 56% of its area. As one can see, the decrease of the reliability index loses significance as *b/t* is increasing, and this happens to all final temperature cases.

Figure 4.47 shows the same kind of curves for the case where 25% of the plate is heated.

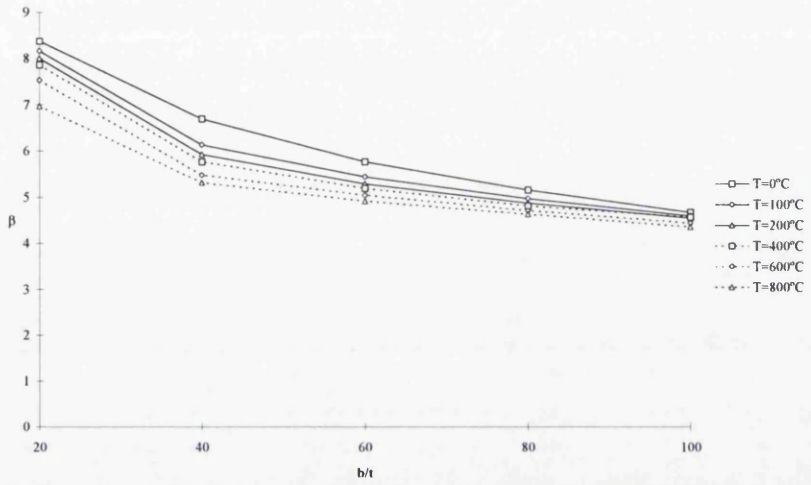

Figure 4.47: Reliability index as function of the breath to thickness ratio for a plate heated in 25% of its area

The comments just made for figure 4.46 are also applied for plate heated over 25% of its area. However it is interesting to notice that the curves from cases where the final temperature is higher, are now closer to those for lower temperatures (The differences between *b/t*=20 and *b/t*=40 become more significant). Figure 4.48 confirms this effect.

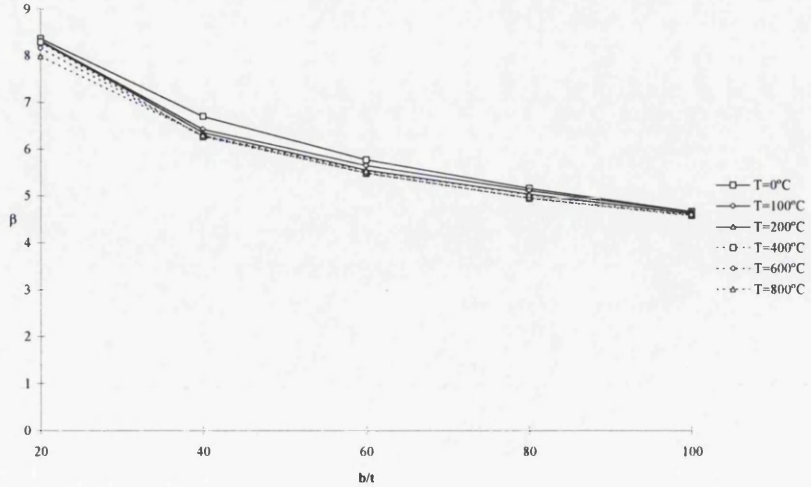

Figure 4.48: Reliability index as function of the breath to thickness ratio for a plate heated in 6% of its area

The different *b/t* cases are now considered separately. Figure 4.49 shows the reliability index as a function of the final temperature for the different heated areas. Only the case with a breadth to thickness ratio of 60 is considered, since the variation of the reliability index with the final temperature is similar for all ratios.

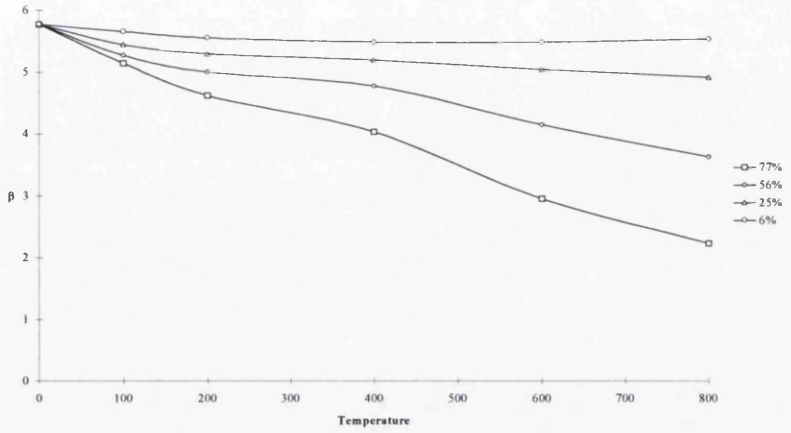

Figure 4.49: Reliability index for the different cases of heated areas in a plate with *b/t*=60 as a function of the final temperature

It should be noticed that the reliability of the plate is more dependent on the final temperature when the area where the temperature is applied is higher (56% of the plate).

CONCLUSIONS

Risk is a probabilistic concept, introduced gradually as a rationale for structural design during the past half century. In marine industry, risk analysis is the designation that has become common to indicate the reliability studies that account for all possible failure modes. This is intended to distinguish them from the structural reliability studies, which consider only structural failures.

The probabilistic theory of structural reliability has a firm theoretical support, and may be implemented at different levels compatible of the importance of the problem to be solve. However it should be considered as one of several means of promoting safety. Risk analysis associated with the results of structural reliability leads to improved solutions and permits the adequate treatment of problems such as design optimisation and safety differentiation. In this context two examples of reliability assesement of marine structures were presented.

Structural reliability of the primary ship structure

A reliability analysis of the primary structure of tankers has been performed, using different formulations of still water and wave induced load effects.

It was shown that different formulations of the reliability problem can be considered and that the results change significantly with the formulation adopted. Therefore, this emphasises that care is required in interpreting the results of any reliability analysis and in comparing different approaches.

It has been shown that the various formulations can be related to each other and the choice of one or other is a matter of standardisation in order to allow the ship structures to be compared with each other.

Load combination

Load combination factors were introduced to combine the still water and the wave induced vertical bending moments. A considerable reduction of the design bending moment was achieved using load combination factors, which range from 0.80 to 0.92 for full and partial load condition, respectively. It was noted that the load factors are dependent on the type of distributions for both still water and wave induced bending moments as well as on the operational profile. However, the values do not change

significantly for different amplitudes of the load variables within the same load condition.

Reliability results for tankers

For any of the formulations, it resulted that the four tankers had clearly different values of the reliability index. It was shown that the failure in sagging has a higher probability for longer ships while hogging is the dominant mode of failure for shorter ships. It was also seen that the still water bending moment has a large effect on the reliability results for ballast load condition. However, the wave induced load effects are by far the most important load variable in full load condition.

Reliability for different ship types

As concerned to the reliability assessment of different ship types, it was shown that there are clear differences on the levels of the basic governing variables as defined in the rules and as they occur in the different ship types. The wave induced load effects in containerships are normally low compared to the influence of the still water loads. However, this is not necessarily so for others type of ships like bulk carriers and tankers. The main conclusion is that having general rule requirements applicable to all types of ships will force different reliability levels. Thus, the present analysis indirectly underlines that modern rules must be separately developed for different ship types.

Partial safety factors

It was demonstrated that the introduction of partial safety factors rationally weights present nominal values of still water and wave induced bending moments in a way that the structure is neither over nor underdesigned with respect to vertical bending loads.

In view of further developments, it is however worth recommending to base the evaluation of target probability of failure on the results of an exhaustive set of reliability calculations carried out on a wide range of existing ships, rather then assuming the outcomes of casualty returns.

Reliability in different ocean areas

Finally, it is important to underline the large influence of the selected scatter diagram on the results of reliability calculations. Based on the evaluation of the wave load effects for different ocean areas it was shown that the probability of structural failure has a significant variability along the sea areas in Northern Europe.

The problem of selecting and defining different scatter diagrams for the purposes of longitudinal strength calculations must be properly solved in order to increase the effectiveness of direct calculation methods in ship design.

Final remark

Structural reliability techniques have been applied to assess the failure probability of the primary hull structure and will be used more often in the future. Therefore, it is necessary to develop tools to perform the different aspects of the analysis, from prediction of load effects to structural collapse and to reliability.

Though, the simplified procedures to calculate the ultimate collapse moment are well established, much research work is needed for the determination of the loads, namely the hydrodynamic calculations and the evaluation of the probability distribution of the extremes. Furthermore, time dependent effects of strength degradation such as fatigue and corrosion need to be seriously taken into account in any further analysis in order quantify the effect of periodic maintenance actions on the reliability levels of ship structures.

Reliability of topside components under fire conditions

A formulation has been presented to determine the reliability of fire walls subjected to a pool fire. The methodology has been developed by integrating models for fire loading, heat transfer and non-linear structural response with the methods of structural reliability.

Probabilistic modelling of offshore pool fires

An approach has been presented based on deterministic models of fire development, which predict the characteristics of the flames and the radiated heat. The number of variables is large and the uncertainty in some of them is also large. Therefore, it is important to identify the ones that contribute the most to the uncertainty of the results.

A probabilistic model was used to quantify the uncertainties of the variables and their contribution to the uncertainty of the model predictions. For the pool fire model studied, the most important variable was by far the wind direction. The other significant variables are the mass flow rate of the spill and two variables dependent on the fuel properties, the maximum burning rate and the boiling point of the fuel. These conclusions allow further studies to concentrate on these variables and their effect.

Strength of plates under heat loads

The study of the strength of plated subjected to uniform heat loads has shown that the maximum load carrying capacity of the plates is often reached at temperature differentials ranging from 100° C to 200° C, a region where the yield stress of the material has not decreased too much yet.

The effect of the elastic supports of the plates is important until the collapse of the plate is reached but afterwards it may be ignored. However the 'ultimate' strength of the plate, i.e., the maximum of the stress - temperature curve decreases with the reduction on the stiffness of the elastic supports.

Reliability of plate elements under heat loads

The reliability of thermally insulated plates was then calculated based on a temperature limit state. An example has shown the applicability of this formulation and it lead to the conclusion that the most important variables in the reliability formulation are the thickness of insulation, the limit temperature of plate collapse and the thermal conductivity of the insulation material.

When the heat load is not applied to whole plate surface, but instead is localised the plate will generally not collapse under the exclusive effect of temperature increase. Therefore the plate can support additional in-plane loads and the limit state equation was defined as a function of stresses.

The results of applying this formulation to square plates showed the effect of the spatial variability of the heat load on the reliability of those plates. It was shown that the reliability index decreases rapidly when the heated area increases beyond 50% of the total area of the plate.

REFERENCES

Abrahamsen, E., (1962), Structural Safety of Ships and Risks to Human Life, *European Shipbuilding*, Vol. 11, pp. 134-146.

Akita, Y., (1982), Lessons Learned from Failure and Damage of Ships, *8th Int. Ship Structures Congress*, In joint session I, Gdansk.

American Gas Association, (1974), LNG Safety Program - Interim Report on Phase II Work, *Report IS 3-1.*

Anderberg, Y, (1983), Behaviour of Steel at High Temperatures, *RILEM Committee*, 44-PHT.

ASASNL, Version 19, (1990), WS Atkins Engineering Sciences Lda, England.

Askadi, A. and Sinai, Y. L., (1992), Advanced CFD Modelling of Practical Jet and Pool Fires, *Proc. Offshore Fire Smoke Hazards: Assessment and Control*, Aberdeen.

Babrauskas, V., (1983), Estimation Large Pool Fire Burning Rates, *Fire Technology 19*, p. 251.

Bitner-Gregersen, E. M Cramer E. H. and Loset, R., (1994), Uncertainties of Load Characteristics and Fatigue Damage of Ship Structures, *Marine Structures*, pp. 97-117.

Breitung, K., (1984), Asymptotic Approximations for Multinormal Integrals, *J. Eng. Mech. Div. ASCE*, Vol. 110, No. 3, pp. 357-366.

Breitung, K. and Hohenbichler, M., (1989), Asymptotic Approximations for Multivariate Integrals With an Application to Multinormal Probabilities, *Journal Multivariate Analysis,* Vol. 30, No. 1.

British Standard Institution: BS5950, (1990), The Structural Use of Steelwork in Buildings, *Code for Practice for Fire Resistance Design*, BSI, part 8, pp. 1-27.

Casella, G., Dogliani M. and Guedes Soares, C., (1996), Reliability Based Design of the Primary Structure of Oil Tankers, *Proceeding of the 15*th International Conference on

Offshore Mechanics and Artic Engineering (OMAE'96), Vol. II, pp. 217-224.

CHAOS, (1993), Consequence and Hazard Assessment of Offshore Structures - User Manuals, *British Gas Research and Development*, Loughborough, UK.

Chen, X and Lind, N. C., (1983), Fast Probability Integration by Three Parameter Normal Tail Approximation, *Structural Safety*, Vol. 1, pp. 269-276.

Chen Y. R. N. and Thayambali, A. K., (1991), Consideration of Global Climatology and Loading Characteristics in Fatigue Damage Assessment of Ship Structures, *Proceedings The Marine Structural Inspection, Maintenance and Monitoring Symposium*, Virginia.

Commission for the European Communities, (1990), Design of Steel Structures, *Eurocode n.3 (EC3)*, Structural Fire Design, part 10.

Cornell, C. A., (1969), A Probability-Based Structural Code, *Journal of American Concrete Institute*, Vol. 66, No. 12, pp. 974-985.

Crisfield, M. A., (1975), Full-Range Analysis of Steel Plates and Stiffened Plating Under Uniaxial Compression, *Inst. of Civil Engrs.-Part 2*, Vol. 59, pp. 595-624.

CSR ApS, (1994), OPTIM01 - Manual+Software, *CSR - software*.

CSR ApS, (1994), RELIAB01 Version 2.0 - Manual+Software, *CSR-software*.

Department of Energy, (1990), The Public Inquiry into the Piper Alpha Disaster (Cullen Report), HMSO, CM 1310.

Ditlevsen, D. and Bjerager, P., (1986), Methods of Structural System Analysis, *Structural Safety*, Vol. 3.

Ditlevsen, O. D., (1979), Generalized Second Moment Reliability Index, *J. Struct. Mech.*, Vol. 7, pp. 435-451.

Ditlevsen, O. D., (1973), Structural Reliability and the Invariance Problem, *Research Report No. 22*, Solid Mechanics Division, University of Waterloo.

Dow, R. S. and Smith, C. S., (1983), Effects of Localised Imperfections on the

Compressive Strength of Long Rectangular Plates, *J. Constructional Steel Research*, Vol. 3, pp. 51-76.

Faulkner, D., (1975), A review of effective plating for use in the analysis of stiffened plating in bending and compression, *Journal of Ship Research*, Vol. 19, pp. 1-17.

Faulkner, D. and Sadden, J. A, (1979), Toward a Unified Approach to Ship Structural Safety, *Transactions Royal Institution of Naval Architects (Rina)*, Vol. 121, pp. 1-38.

Ferry Borges, J., (1991), The Concept of Risk in Building Pathology, *CIB, Was, Building Pathology*, Lisbon.

Ferry Borges, J. Castanheta M., (1971), Structural Safety, *Laboratório Nacional de Engenharia Civil*, Lisboa.

Fiessler, B., Neumann, H. and Rackwitz, R., (1980), Quadratic Limit States In Structural Reliability, *J. Eng. Mech. Div., ASCE*, Vol. 105, No. EM4, pp. 661-676.

Freudenthal, A. M., Garrelts, J. M. and Shinozuka, M., (1966), The Analysis of Structural Safety, *J. Struct. Div*, American Society of Civil Engineers (ASCE), Vol. 92, pp. 235-246.

Frieze, P. A., Dowling, P. J. and Hobbs, R. H., (1977), Ultimate Load Behaviour of Plates in Compression, *Steel Plated Structures*, Crosby Lockwood Staples, ed. P. J. Dowling *et al.*, pp. 24-50, London.

Fukuda, J., (1967), Theoretical Determination of Design Wave Bending Moment, *Japan Shipbuilding and Marine Engineering*, Vol. 2, No. 3, pp. 13-22.

Gierlinski, J. T. and Sears, R. J., (1994), Methodology for Collapse Analysis Under Combined Thermal and Force Loading Using V.D.M., implemented in Rasos , *Report TEC-C024-01*, 14.

Gollwitzer, S., Abdo, T. and Rackwitz, R., (1988), Form Program Manual, Munich.

Goodman, L. E. et al., (1954), Aseismic Design of Firmly Founded Elastic Structures, *Trans ASCE*, Proc paper 2762.

Gordo, J. M. and Guedes Soares, C., (1993), Approximate Load Shortening Curves for

Stiffened Plates Under Uniaxial Compression, *Integrity of Offshore Structures - 5*, EMAS, pp. 189-211, U.K.

Gordo, J. M. and Guedes Soares, C., (1996), Approximate Method to Evaluate the Hull Girder Collapse Strength, *Marine Structures*, Vol. 9, 1, 449-470.

Gordo, J. M. and Guedes Soares, C., (1995), Collapse of Ship Hulls Under Combined Vertical and Horizontal Bending Moments, *Proceedings of the 6th International Symposium on Practical Design of Ships and Mobile Units (PRADS'95)*, Vol. II, pp. 808-819, Korea.

Gordo, J. M., Guedes Soares, C. and Faulkner, D., (1996), Approximate Assessment of the Ultimate Longitudinal Strength of the Hull Girder, *Journal of Ship Research*, Vol. 40, N. 1, pp. 60-69.

Grigoriu, M. and Lind, N. C., (1980), Optimal Estimation of Convolution Integrals, *J. Eng. Mech. Div., ASCE*, Vol. 106, pp. 1349-1364.

Guedes Soares, C., (1992), Combination of Primary Load Effects in Ship Structures, *Probabilistic Engineering Mechanics*, Vol. 7, pp. 103-111.

Guedes Soares, C., (1994), Definition of the Optimisation Problem for Fire Walls, *CEC-BRITE/EURAM 4359 Report TEC-C041-03(1)* .

Guedes Soares, C., (1991), Effect of Transfer Function Uncertainty on Short Term Ship Responses , *Ocean Engineering*, Vol. 18, pp. 329-362.

Guedes Soares, C., (1990), Influence of Human Control on the Probability Distribution of Maximum Still-water Load Effects in Ships, *Marine Structures*, Vol. 3, pp. 319-339.

Guedes Soares, C., (1993), Mechanical Properties of Steel at Elevated Temperatures, *CEC-BRITE/EURAM 4359 Report TEC-C021-02.*

Guedes Soares, C., (1996), On The Definition of Rule Requirements for Wave Induced Vertical Bending Moments, *Marine Structures*, Vol. 9, pp. 409-425.

Guedes Soares, C., (1985), Probabilistic Models for Load Effects in Ship Structures,

Division of Marine Structures, The Norwegian Institute of Technology, Report UR-84-38.

Guedes Soares, C., (1993), Review of Modelling Techniques for Hydrocarbon Fires, *Report TEC-C013-01*, OFSOS Project, Instituto Superior Técnico.

Guedes Soares, C., (1990), Stochastic Modelling of Maximum Still-Water Load Effects in Ship Structures, *Journal of Ship Research*, Vol. 34, N°. 3, pp. 199-205.

Guedes Soares, C. and Dogliani, M., (1995), Probabilistic Modelling of Still-Water Load Effects in Tankers, *SHIPREL Report 1.1-07(0)*.

Guedes Soares, C., Dogliani., M., Ostergaard, C., Parmentier, G. and Pedersen, P. T., (1996), Reliability Based Ship Structural Design, *SNAME 1996 Annual Meeting*, New York.

Guedes Soares, C. and Gordo, J. M., (1996), Compressive Strength of Rectangular Plates Under Biaxial Load and Lateral Pressure, *Thin-Walled Structures*, Elsevier Science Limited, Vol. 22, pp. 231-259.

Guedes Soares, C. and Ivanov, L. D., (1989), Time-Dependent Reliability of the Primary Ship Structure, *Reliability Engineering and System Safety*, Vol. 26, pp. 59-71.

Guedes Soares, C. and Moan, T., (1991), Model Uncertainty in the Long Term Distribution of Wave Induced Bending Moments for Fatigue Design of Ship Structures, *Marine Structures*, Vol. 4, pp. 295-315.

Guedes Soares, C. and Moan, T., (1988), Statistical Analysis of Still Water Load Effects in Ship Structures, *Transactions of the Society of Naval Architects and Marine Engineers*, Vol. 96, No. 4, pp. 129-156, New York.

Guedes Soares, C., Teixeira, A. P., Neves, L and Lopes, B., (1995), Reliability Formulation for Plates under Heat Loads with Temperature Limit-State, *CEC-BRITE/EURAM 4359 Report TEC-C031-01A*.

Guedes Soares, C. and Trovão, M. F. S., (1991), Influence of Wave Climate Modelling on the Long-Term Prediction of Wave Induced Responses of Ship Structures, *Dynamics of Marine Vehicles and Structures in Waves*, W.G. Price, P. Temarel and

A.J. Keane (Eds), Elsevier Science Publishers, pp. 1-10, Amsterdam.

Guedes Soares, C. and Viana, P. C., (1988), Sensitivity of the Response of Marine Structures to Wave Climatology, *Computer Modelling in Ocean Engineering*, B.A. Schreffler and O.C. Zienkiewicz (Eds), A.A. Balkema Pub., pp. 487-492, Rotterdam.

Harding, J. E., Hobbs, R. E. and Neal, B. G., (1977), The Elasto-Plastic Analysis of Imperfect Square Plates Under In-Plane Loading, *Proc. Inst. of Civil Engrs.-Part 2*, 63, pp. 137-158.

Hasofer, A. M. and Lind, N. C., (1974), An Exact and Invariant First-Order Reliability Format, *J. Eng. Mech. Div. (ASCE)*, Vol. 100, pp. 111-121.

Hogben, N., Da Cuna, L. F. and Ollivier, H. N., (1986), Global Wave Statistics, *British Marine Tecnology*, Publishing Urwin Brothers Limited, London.

Hohenbichler, M., Gollwitzer, S., Kruse, W. and Rackwitz, R., (1989), New Light on First and Second-Order Reliability Methods, *Structural Safety*, Vol. 4, pp. 267-284.

Hulbert, W. G., (1993), Rasos B Theoretical Manual, *Report TEC-C013-03A*, OFSOS Project, W.S. Atkins.

IACS, (1993), Requirement S11 on Longitudinal Strength Standard, Revision 1.

International Ship and Offshore Structures Congress, (1994), Proc. of 12th Edition, *Report of Committee V.3, Design of Structures Against Fire and Blast*, N.E. Jeffrey and A.M. Kendrick (Eds.), Vol. 2, pp. 115-162, Canada.

International Ship and Offshore Structures Congress, (1997), Proc. of 13th Edition, *Report of Committee V.2, Structural Design Against Fire and Blast*, T. Moan and S. Berge (Eds.), Vol. 2, pp. 43-77, Norway.

Ivanov, L. D. and Minchev, A. D., (1979), Comparative Analysis of the Hull Section Modulus on the Basis of the Theory of Reliability, *Budownictwo Okretowe*, Vol. 34, No. 11, pp. 16-19.

Ivanov, L. Madjarov H., (1975), The Statistical Estimation of SWBM (Still Water Bending Moment) for Cargo Ships, *Shipping World and Shipbuilder*, Vol. 168, pp.

759-762.

Janss, J. and Minne, R., (1981), Buckling of Steel Columns in Fire Conditions, *Fire Safety J.*, Vol. 4, pp. 227-235.

Jensen, F. M and Thoft-Cristensen, P., (1995), OPTIWALL (Software and Documentation) for Optimisation of Non-Structural Parts Based on Optim and RTLS (RELIAB, HOTPLATE and RASOS_B, *CEC-BRITE/EURAM 4359 Report TEC-C041-05C.*

Jensen, F. M, Thoft-Cristensen, P. and Guedes Soares, C., (1995), Specifications for Interfacing Optimisation of Fire/Blast Walls Using RELOFS, OPTIM and RELIAB, *CEC-BRITE/EURAM 4359 Report WOR-C051-05C.*

Kaplan, M. Benatar M. Bentson J. Achtarides T. A., (1984), Analysis and Assessment of Major Uncertainties Associated With Ship Hull Ultimate Failure, *Report No. SSC-322*, Ship Structure Committee, Washington, DC, USA.

Kirby, B. R. and Preston, R. R., (1988), High Temperature Properties of Hot Rolled Steel for Use in Fire Engineering Design Studies, *Fire Safety J.*, Vol. 13, pp.27-37.

Larrabee, R. D. Cornell C. A., (1981), Combination of Various Load Processes, *J. of Structural Division*, ASCE, Vol. 107, pp. 223-238.

Lewis, E. V. *et al.*, (1975), Load Criteria For Ship Structural Design, *Ship Structure Committee*, Report No. SSC-224, Washington, DC, USA.

Little, G. H., (1980), The Collapse of Rectangular Steel Plates Under Uniaxial Compression, *The Structural Engineer*, Vol. 58B, pp. 45-60.

Longuet-Higgins, M. S., (1952), The Statistical Distribution of the Height of Sea Waves, *J. Marine Research*, Vol. 11, pp. 245-266.

Mano, H. Kawabe H. Iwakawa K. Mitsumune N., (1977), Statistical Character of the Demande on Longitudinal Strength (second report) - Long Term Distribution of Still Water Bending Moment, *J. Soc. Naval Architects of Japan*, Vol. 142, pp. 255-263.

Mansour, A. E., (1974), Approximate Probabilistic Methods of Calculating Ship

Longitudinal Strength, *Journal of Ship Research*, Vol. 18, pp. 203-213.

Mansour, A. E, (1984), Implementation of Reliability Methods to Marine Structures, Vol. 92, pp. 353-382.

Mansour, A. E., (1972), Probabilistic Design Concepts in Ship Structural Safety and Reliability, *Transactions of the Society of Naval Architects and Marine Engineers*, Vol. 80, pp. 64-97.

Mansour, A. E. and Faulkner, D., (1973), On Applying the Statistical Approach to Extreme Sea Loads and Ship Hull Strength, *Transactions Royal Institution of Naval Architects (Rina)*, Vol. 115, pp. 277-314.

Marley, M. J. and Moan, T., (1992), Time Variant Formulation for Fatigue Reliability, *Proceedings Offshore Mechanics and Arctic Engineering Conference*, Vol. II, Safety and Reliability ASME.

McCaffrey, B. J. and Evans, D. D., (1986), Very Large Methane Jet Diffusion Flames, *Center of Fire Research*, NBS Rep. MD 208899, Gaithersburg.

Mudan, K. S. and Croce, P. A, (1988), Fire Hazard Calculations for Open Hydrocarbon Fires, *in The SFPE Handbook of Fire Protection Engineering, P.J. DiNenno et al (Eds)*, National Fire Protection Association, section 2, pp. 45-97, Quincy.

Murotsu, H., Okada, H., Matsuzaki and Katsura, S., (1986), On the Reliability Assessment of Marine Structures, *Proc. 5th International Conference on Offshore Mechanical Arctic Engineering*, ASME.

Murotsu, Y., Okada, H., Masoaka, K., Hibi, S., Niho, O. and Kaminaga, H., (1993), A System for Collapse and Reliability of Ship Structures Using a Spatial Element Model, *J. Offshore Mechanics Artic Engineering*, pp. 305-312.

Najjar, S. R. and Burgess, I. W., (1996), A Non-linear Analysis for Three-dimensional Steel Frames in Fire Conditions, *Engineering Structures*, Vol. 18, N°. 1, pp. 77-89.

Nielsen, S. R. K, Jensen, F. M. and Thoft-Cristensen, P., (1994), Heat Transfer Through Firewalls, *Report TEC-C022-03*, OFSOS Project, CSR.

Nitta, A., (1976), Reliability Analysis of the Fatigue Strength of Ship Structures, *Trans. Nippon Kaiji Kyokai*, Vol. 155, pp. 1-6.

Nordenstrom, N., (1971), Methods for Predicting Long-Term Distributions of Wave Load and Probability of Failure for Ships, *Report No. 71-2-S*, Det norske Veritas.

Offshore Installations (Safety Case) Regulations, (1992), *HMSO*, London.

Okada, H., Masoaka, K., Hibi, S., Kuroda, H., Kiyokawa, W. and Murotsu, Y., (1995), Comparative Studies on Structural Reliability of Ship's Hull Structures Based On Collapse Mode Analysis, *The Sixth International Symposium on Practical Design of Ships and Mobile Units (PRADS'95)*, Vol. 2, pp. 783-794.

Opstad, K., Wighus, R., Holen, J., Hekkelstrand, B. and Stensaas, J. P, (1991), Modelling of Hydrocarbon Fires Offshore - Final Report, *Report STF25 - A91029*, SINTEF.

Ostergaard, C., (1992), Partial Safety Factors for Vertical Bending Loads on Containerships, *Journal of Offshore Mechanics and Arctic Engineering*, Vol. 114, pp.129-136.

Parkinson, D. B., (1980), Four-Moment Reliability Analysis for Static and Time-Dependent Problems, *Reliability Engineering*, Vol. 1, pp. 29-42.

Rackwitz, R. and Fiessler, B., (1978), Structural Reliability Under Combined Random Load Sequences, *Computers & Structures*, Vol. 9, pp. 486-494.

Rew, P. J. and Deaves, D. M, (1992), POOL, A computer Model for the Calculation of Heat Fluxes from Pool Fires, *Internal report*, W.S. Atkins.

Rogers, C. P. and Ramsden, M., (1994), Optimisation Of Passive Fire Protection For Offshore Structures Using Progressive Collapse Techniques, *Proc. International Conf. on Offshore Structural Design-Hazards, Safety and Engineering*, Paper 3, pp. 4.3.1-4.3.10, UK.

Rutherford, S. E. and Caldwell, J. B, (1990), Ultimate Longitudinal Strength of Ships: A Case Study, *Transactions SNAME*, Vol. 98, pp. 441-471.

Saab, H. A. and Nethercot, D. A., (1991), Modelling Steel Frames Behaviour Under Fire

Conditions, *Engineering Structures*, Vol. 13, pp.371-382.

Shellin, T., Östergaard, C., and Guedes Soares, C., (1996), Uncertainty Assessment of Low Frequency Wave Induced Load Effects for Containerships, *Marine Structures*, Vol. 9, n. 3-4, pp. 313-332.

Shetty, N. K., Deaves, D. M., Gierlinski, J. T. and Dogliani, M., (1996), Unified Methodology for Fire Design, *Proceedings 15th Int. Conference on Offshore Mechanics and Artic Engineering*, Vol. II, pp. 359-369.

Söding, H., (1971), Calculation of Stresses on Ships in a Seaway, *Schiff und Hafen*, Vol. 23, pp. 752-762.

Stanzak, W. W. and Lie, T. T., (1973), Fire Resistance of Unprotected Steel Columns, *J. Struct. Div. ASCE*, Vol. 99, pp. 837-852.

Teixeira, A. P., Neves, L and Lopes, J. B, (1995), Software for Reliability Evaluation of Plated Elements, *CEC-BRITE/EURAM 4359 Report SOF-C031-03C.*

Thomas, P. H., (1963), The Size of Flames from Natural Fires, *9th International Combustion Symposium*, Academic Press, pp. 844-859.

Turkstra, C. J., (1970), Theory of Structural Design Decisions Study No. 2, *Solid Mechanics Division*, University of Waterloo, Ontario.

Twilt, L., (1991), Stress-Strain Relations of Structural Steel at Elevated Temperatures: Analysis of Various Options & European Proposal, *TNO Report BI-91-015.*

Ueda, Y. and Yao, T., (1985), The Influence of Complex Initial Deflection Modes on the Behaviour and Ultimate Strength of Rectangular Plates in Compression, *J. Constructional Steel Research*, Vol. 5, pp. 265-302.

USFOS, (1996), Ultimate Strength For Offshore Structures - User Manuals, *SINTEF Structures and Concrete*, Trondheim, Norway.

Wang, W. and Moan, T., (1996), Stochastic and Deterministic Combinations of Still and Wave Bending Moments in Ships, *Marine Structures*, Elsevier, Vol. 9, pp. 787-810.

Wang, X. and Moan, T., (1995), Reliability Based Design Of Stiffened Panels in

Production Ships Under Biaxial and Lateral Loading, *Proceedings of the 6th International Symposium on Practical Design of Ships and Mobile Units (PRADS'95)*, Vol. 2, pp. 795-807.

Wang, X., Moan, T. and Jiao, G., (1994), Reliability Analysis of Production Ships, *International Journal of Offshore and Polar Engineering*, Vol.4, No 4, pp. 302-311.

Wang, Y. C., (1997), The Effects of Frame Continuity on the Behaviour of Steel Columns Under Fire Conditions and Fire Resistant Design Proposals, *J. Construct. Steel Res.*, Vol. 41, No. 1, pp. 93-111.

Warnsinck, W. H., (1964), Environmental Conditions, Report of the Committee 1, *Proc. 2nd International Ship Structures Congress*, Oslo.

Wen, Y. K., (1977), Statistical Combination of Extreme Loads, *J. Structural Division*, ASCE, Vol. 103, pp. 1079-1093.

Witteveen, J. and Twilt, L., (1975), Behaviour of Steel Columns Under Fire Action, *Int. Conf. on Column Strength*, Vol. 23, Proc. IABSE, Paris.

Yim, S. J., Yang, Y. S. and Kim, J. H., (1992), Probabilistic Structural Analysis for the Web Frame of Tankers, *Practical design of Ships and Mobile Units*, Elsevier Applied Science, Vol. 12.

Yngve Anderberg, (1994), Computer Methods For Optimising Passive Fire Protection On Offshore Platforms, *Proc. International Conf. on Offshore Structural Design-Hazards, Safety and Engineering*, Paper 4, pp. 4.4.1-4.4.11, UK.

APPENDIX 1

Midship sections

TK1

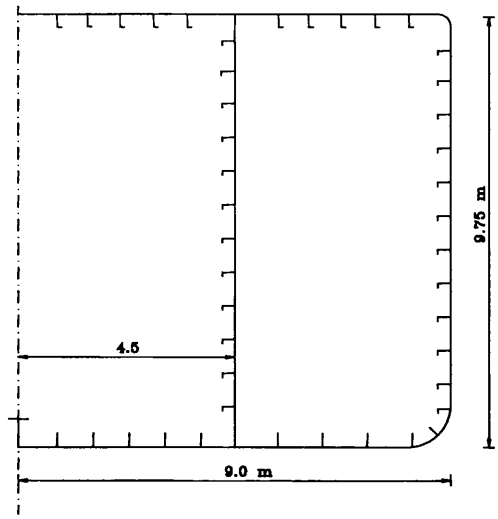

TK2

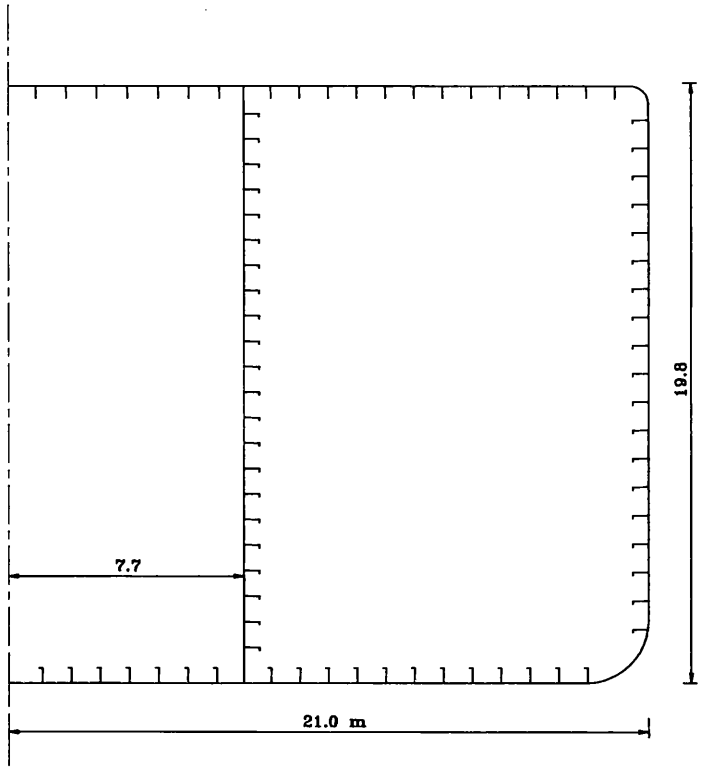

TK3

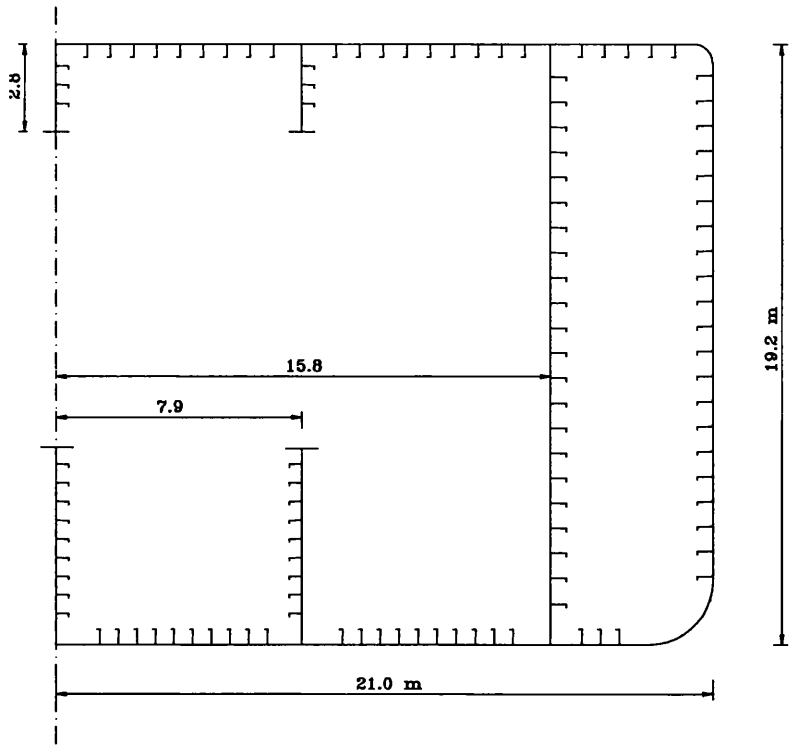
2.8
15.8
7.9
19.2 m
21.0 m

TK4

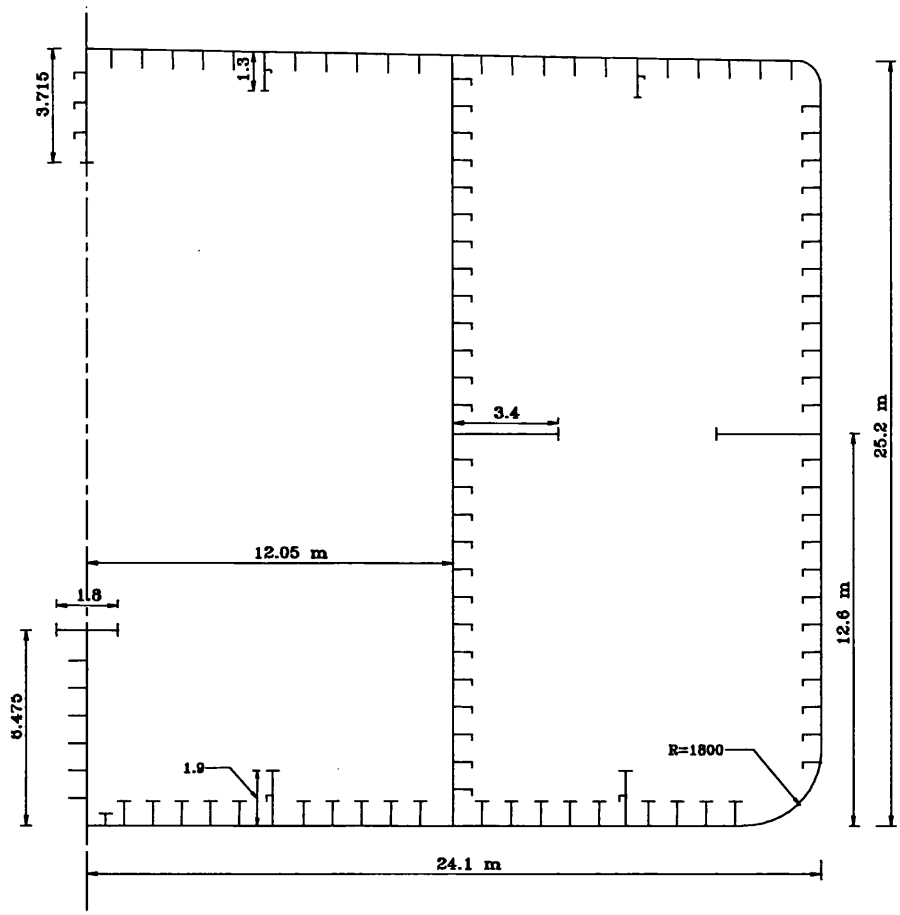
3.715
1.3
3.4
25.2 m
12.05 m
1.8
12.6 m
0.475
1.9
R=1800
24.1 m

BSH

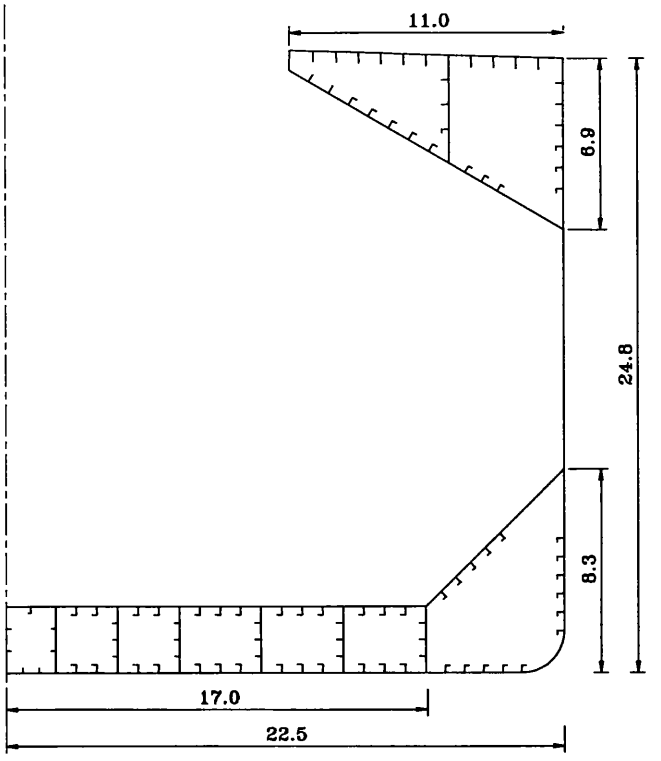

BDH

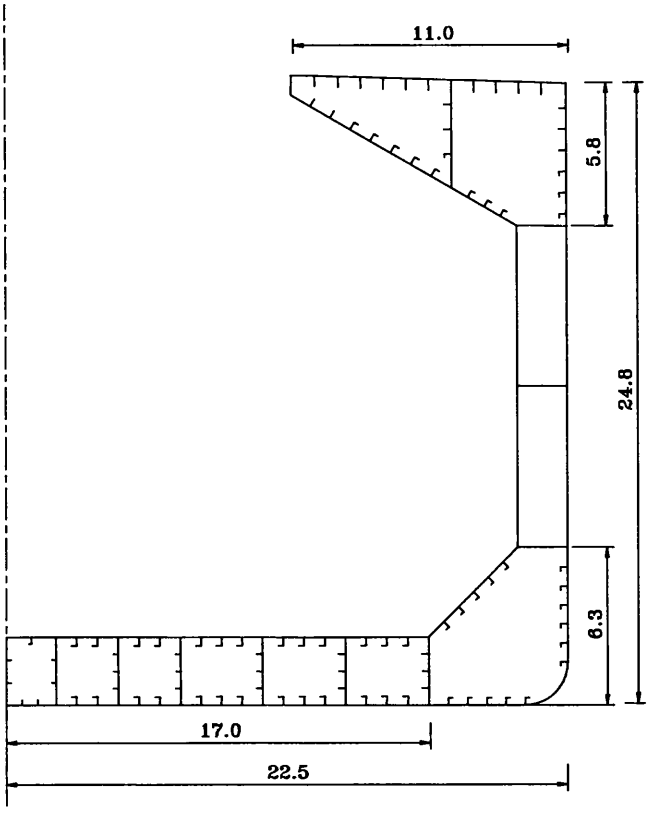

CT

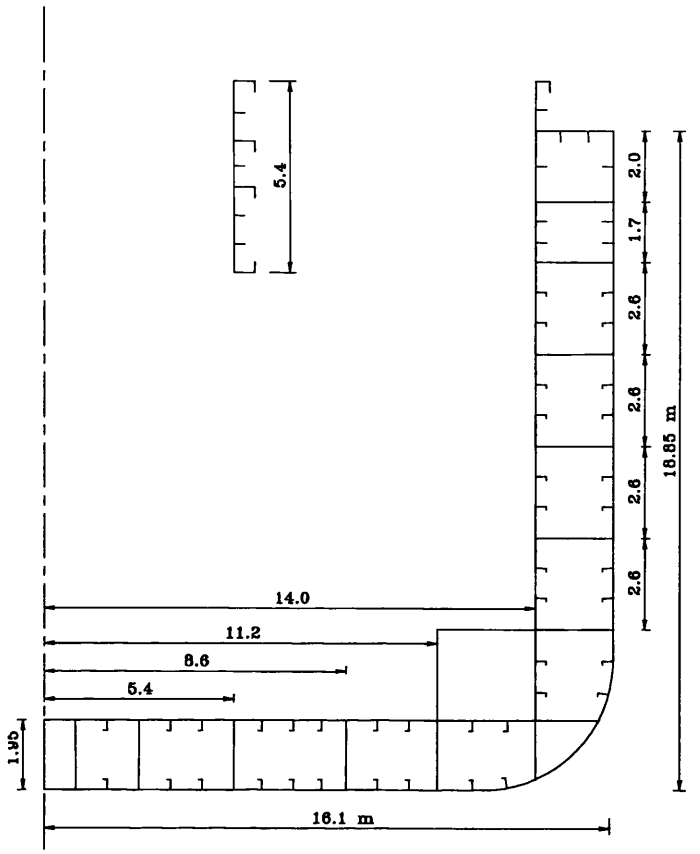

APPENDIX 2

Hydrodynamic calculations (TK3)

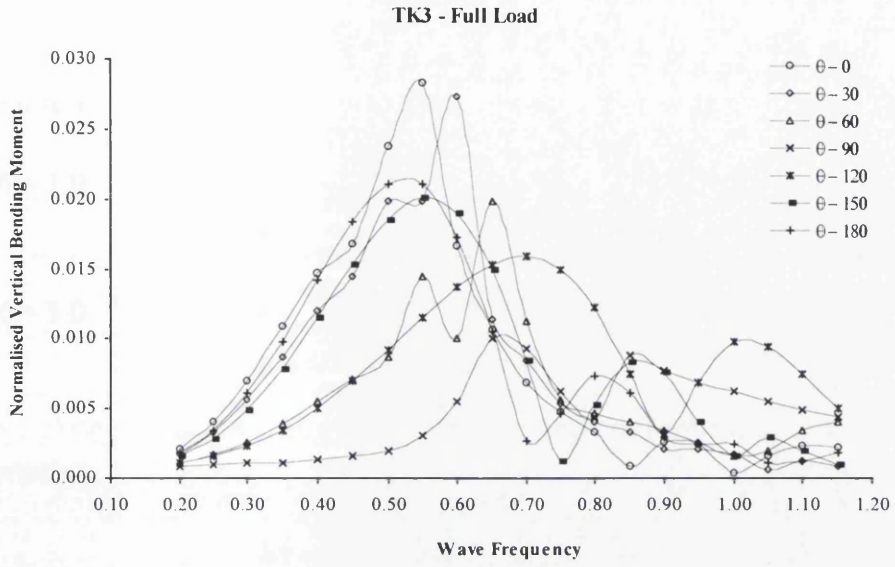

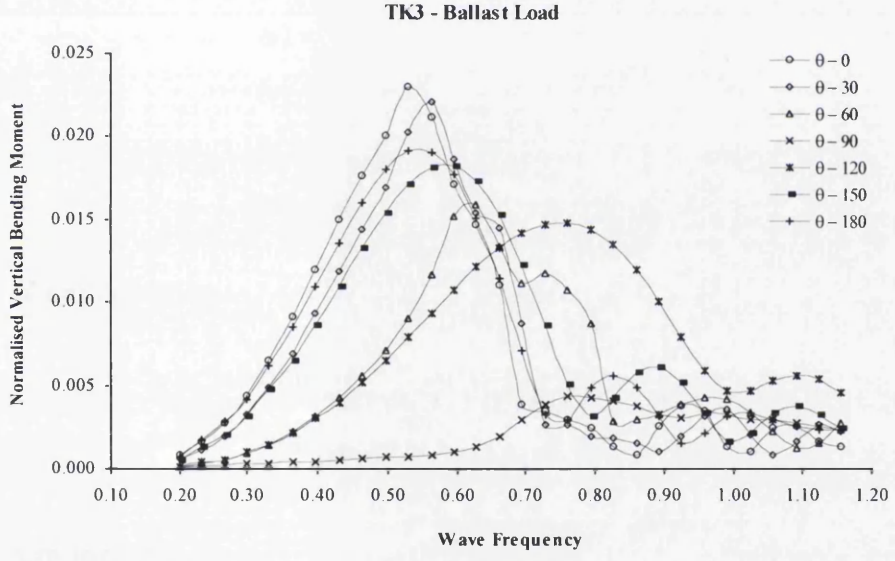

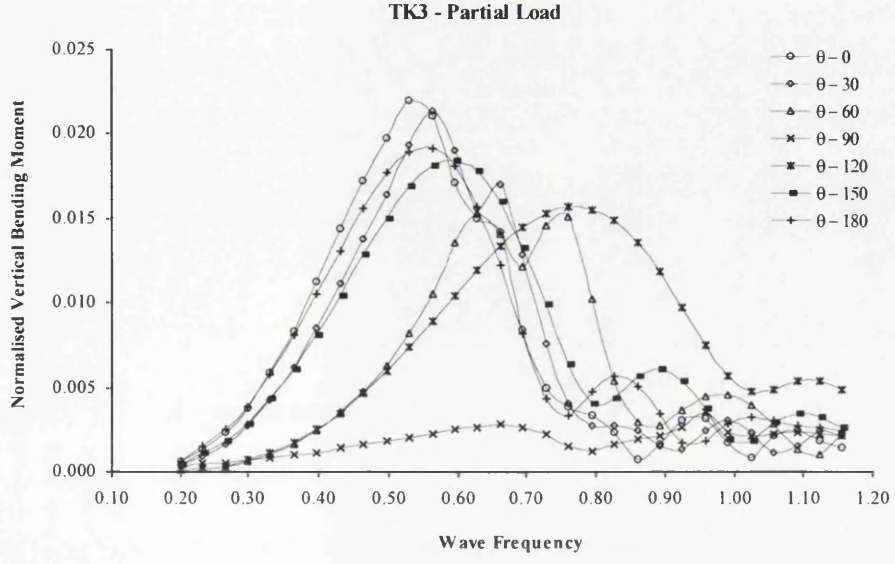

APPENDIX 3

Strength of plates subjected to uniform heat loads

Plate models

$a/b = 1.0$	$a = 1000$ mm
	$b = 1000$ mm
$a/b = 3.0$	$a = 1000$ mm
	$b = 3000$ mm

Slenderness

$b/t = 20$	$\Rightarrow$	$t = 50$ mm
$b/t = 40$	$\Rightarrow$	$t = 25$ mm
$b/t = 60$	$\Rightarrow$	$t = 16.67$ mm
$b/t = 80$	$\Rightarrow$	$t = 12.5$ mm
$b/t = 100$	$\Rightarrow$	$t = 10$ mm

Levels of imperfection

Imp A	$\delta = 0.001$ mm
Imp C	$\delta/t = 0.10\ \beta^2$

Elastic supports $K \neq \infty$

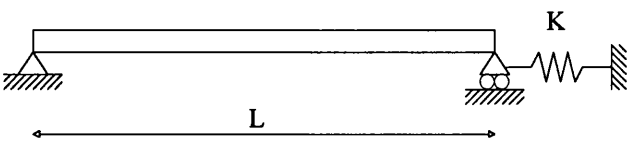

$$K = \frac{EA}{L}$$

where A – cross sectional area ($A=b.t$)

L – length of the plate

High Strength Steel (HSS) - σ_o = 355 MPa

a/b = 1

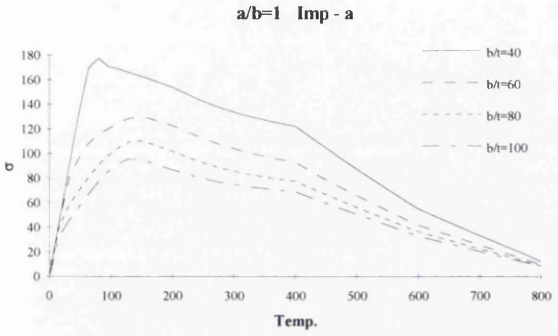

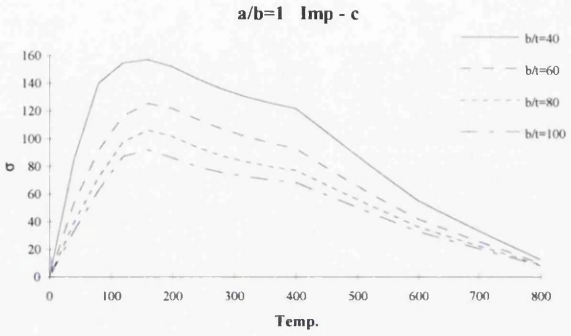

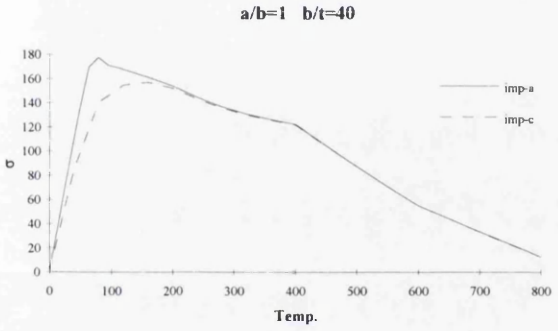

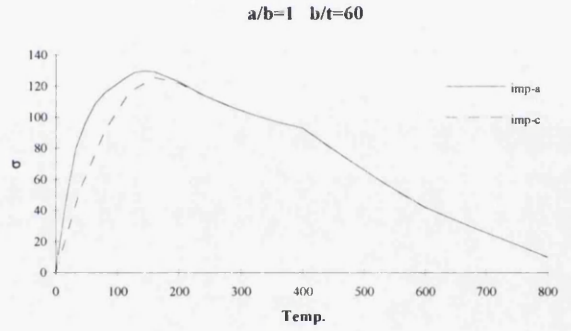

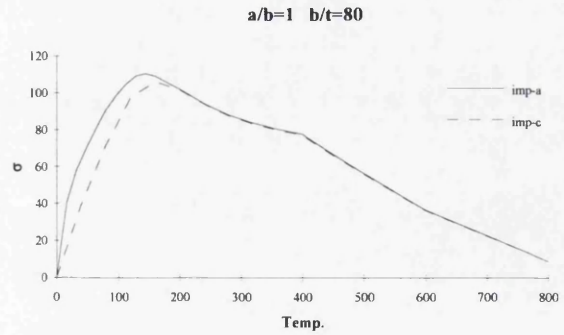

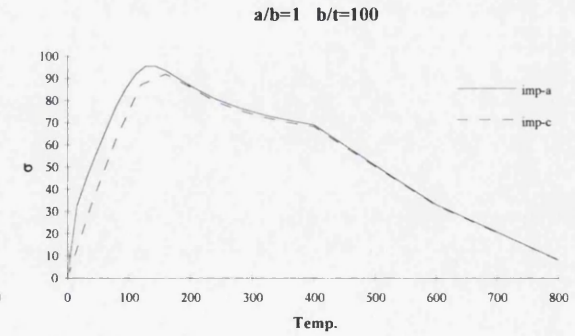

a/b = 3

a/b=3 Imp - a Long.

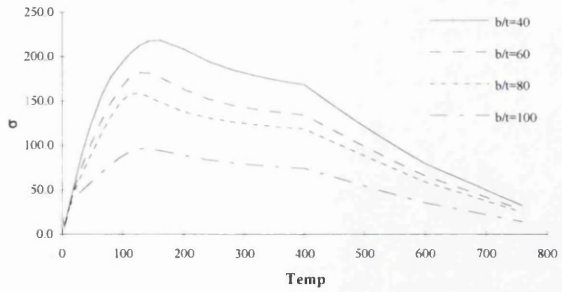

a/b=3 Imp - a Transv.

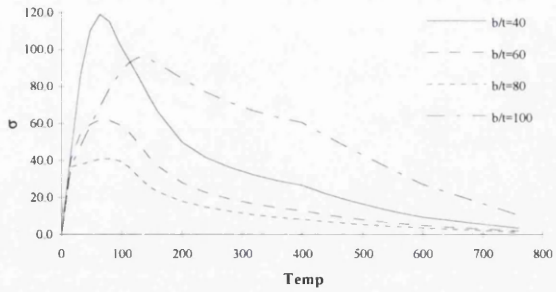

a/b=3 Imp - c Transv.

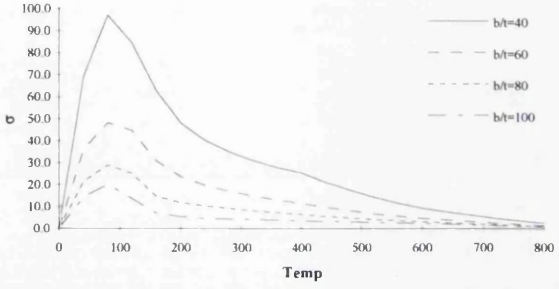

a/b=3 Imp - c Long.

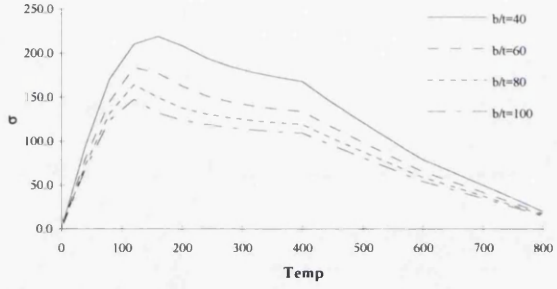

a/b=3 b/t=40 Imp - c

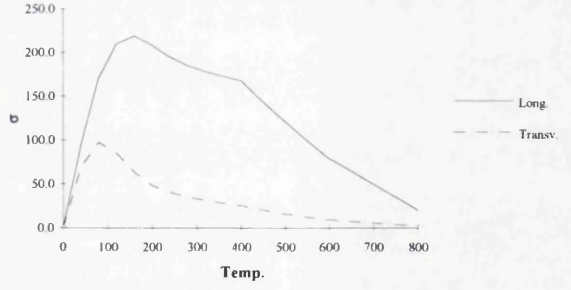

a/b=3 b/t=60 Imp - c

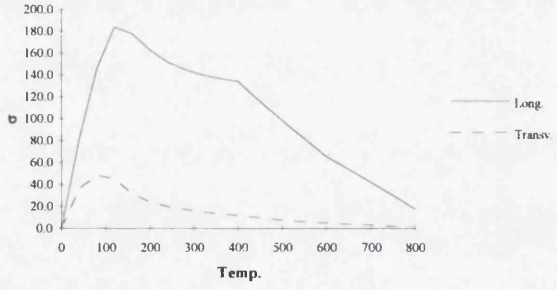

a/b=3 b/t=80 Imp - c

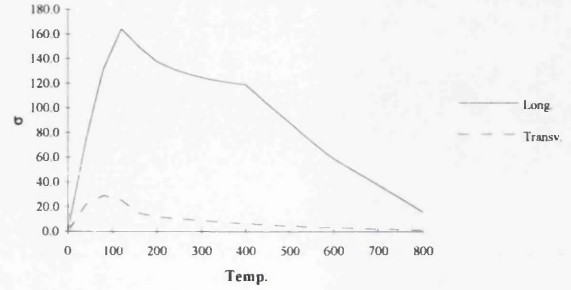

a/b=3 b/t=100 Imp - c

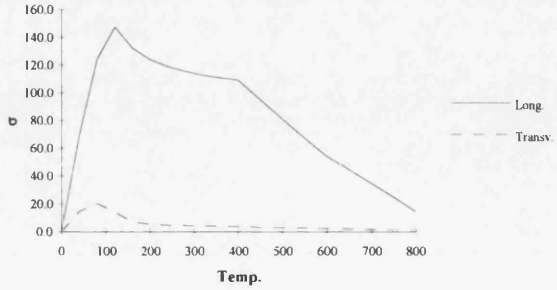

a/b=3 b/t=40

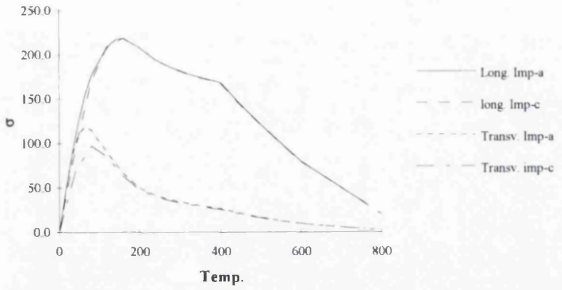

a/b=3 b/t=60

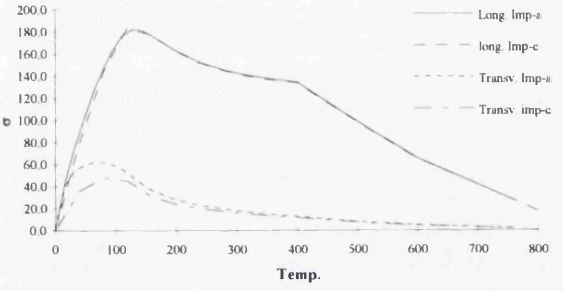

a/b=3 b/t=80

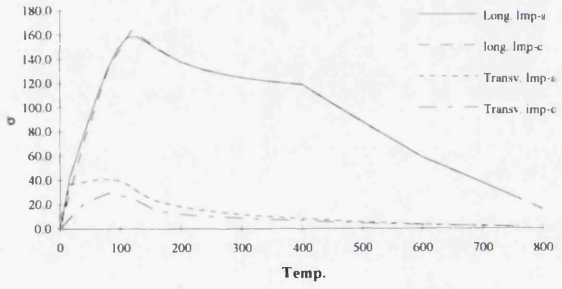

a/b=3 b/t=100

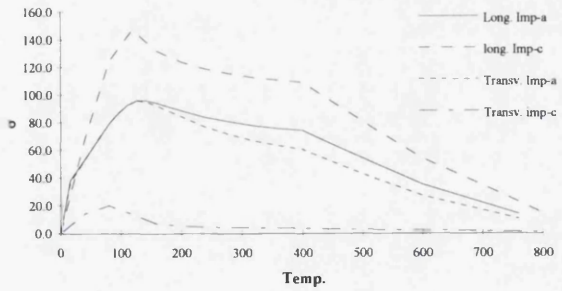

Mild Steel (NS) - σ_o = 235 MPa

Normal Steel a/b =1 K = inf.

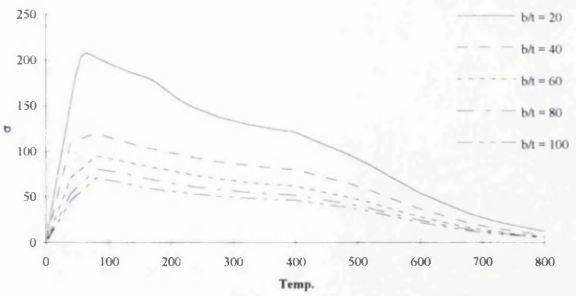

Normal Steel a/b =1 K = E

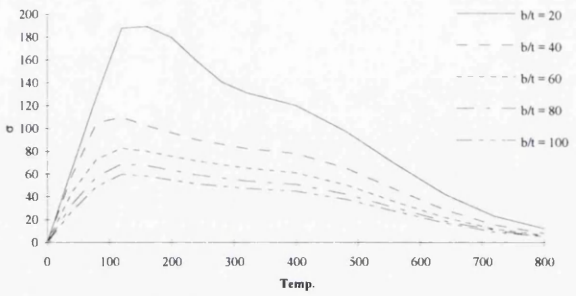

Normal Steel a/b =1 K = 0.5 E

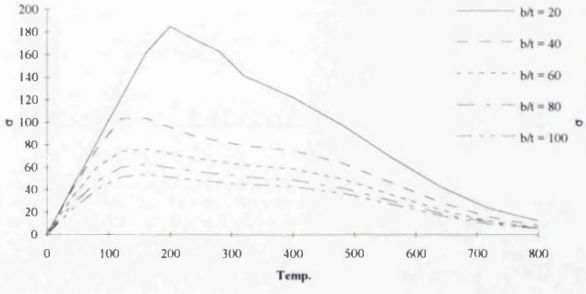

Normal Steel b/t = 20

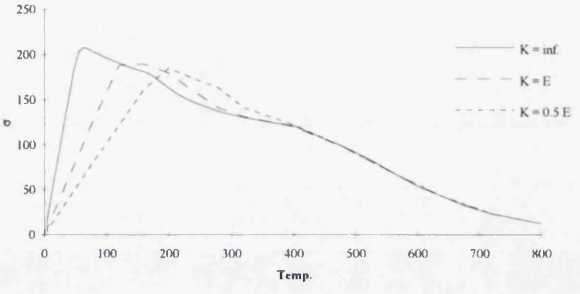

Normal Steel b/t = 40

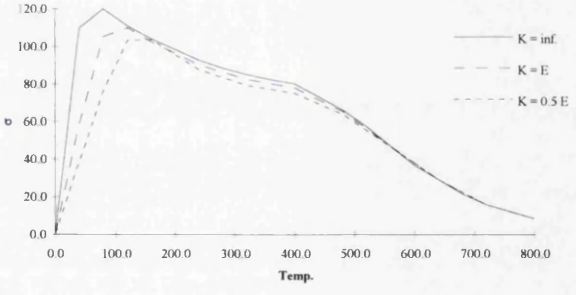

Normal Steel b/t = 60

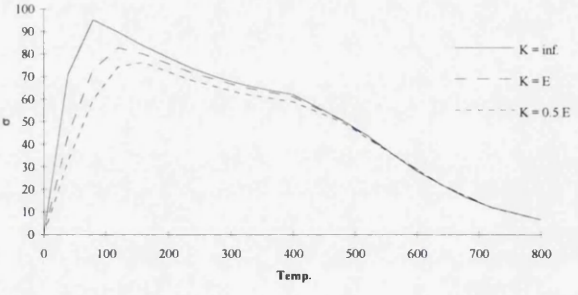

Normal Steel b/t = 80

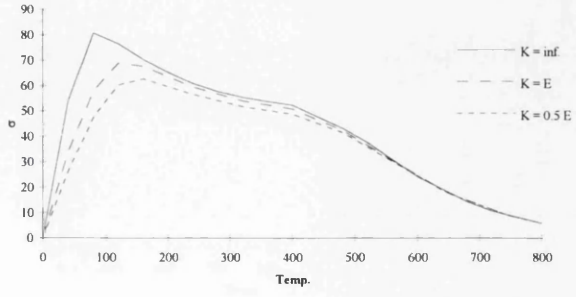

Normal Steel b/t = 100

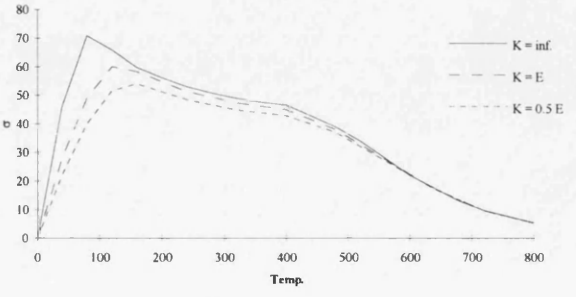

a/b = 3

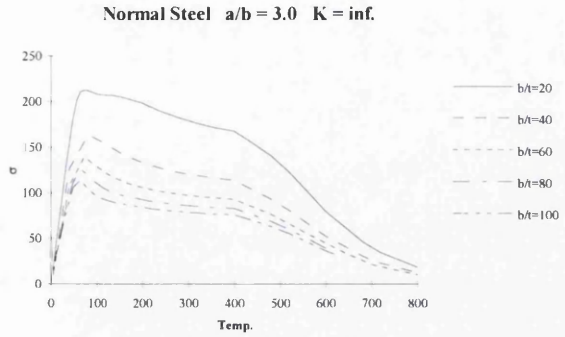
Normal Steel a/b = 3.0 K = inf.
σ
Temp.
b/t=20
b/t=40
b/t=60
b/t=80
b/t=100

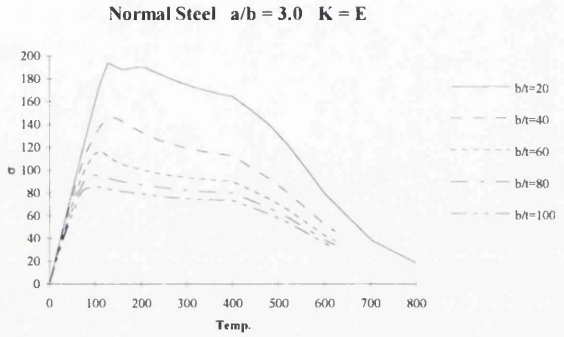
Normal Steel a/b = 3.0 K = E
σ
Temp.
b/t=20
b/t=40
b/t=60
b/t=80
b/t=100

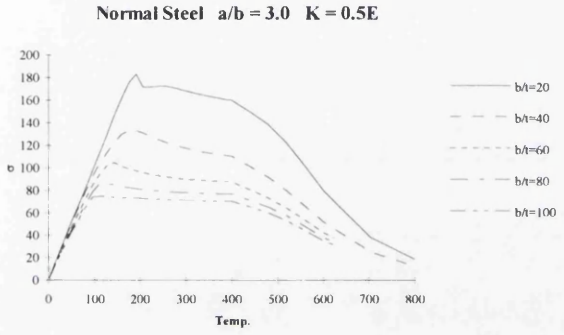
Normal Steel a/b = 3.0 K = 0.5E
σ
Temp.
b/t=20
b/t=40
b/t=60
b/t=80
b/t=100

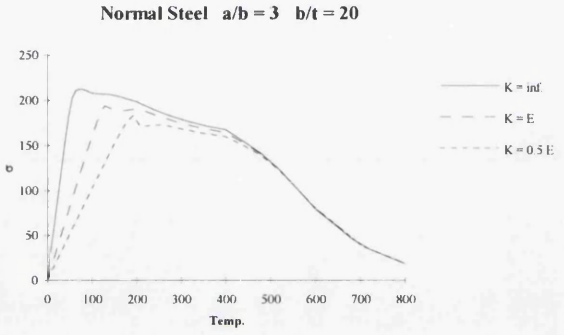
Normal Steel a/b = 3 b/t = 20
σ
Temp.
K = inf.
K = E
K = 0.5 E

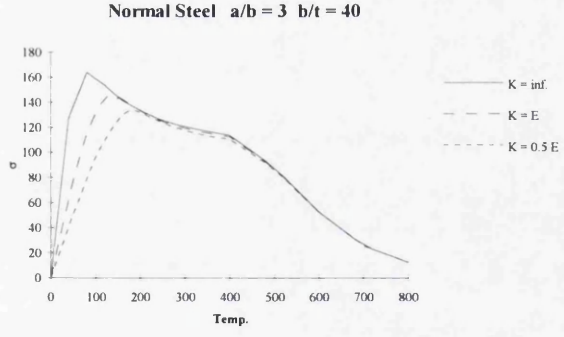
Normal Steel a/b = 3 b/t = 40
σ
Temp.
K = inf.
K = E
K = 0.5 E

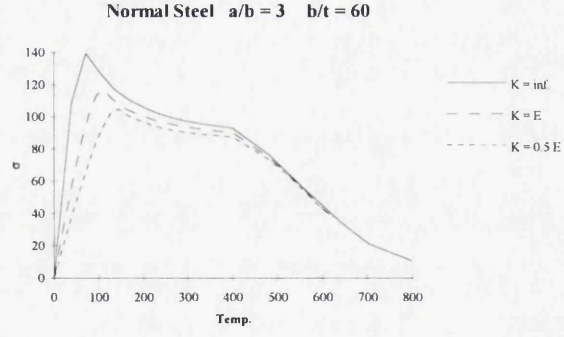
Normal Steel a/b = 3 b/t = 60
σ
Temp.
K = inf.
K = E
K = 0.5 E

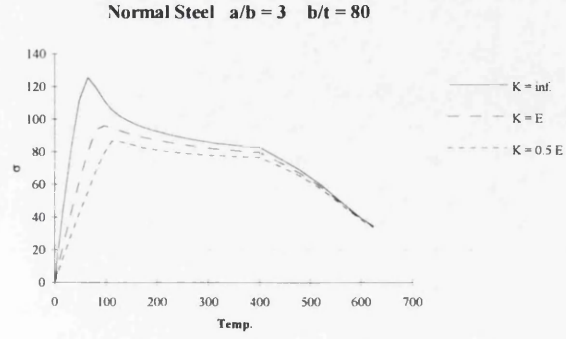
Normal Steel a/b = 3 b/t = 80
σ
Temp.
K = inf.
K = E
K = 0.5 E

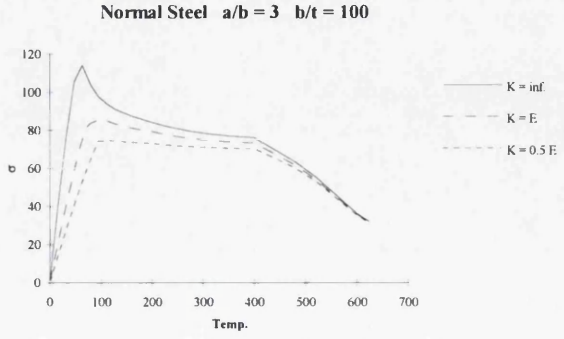
Normal Steel a/b = 3 b/t = 100
σ
Temp.
K = inf.
K = E
K = 0.5 E

APPENDIX 4

Strength of plates under localised heat loads

A total of 125 different models were analysed. The models differ in the dimension of the heated area and in the maximum value of the temperature applied. The curves with stresses as a function of the imposed in plane displacement are presented in the following figures.

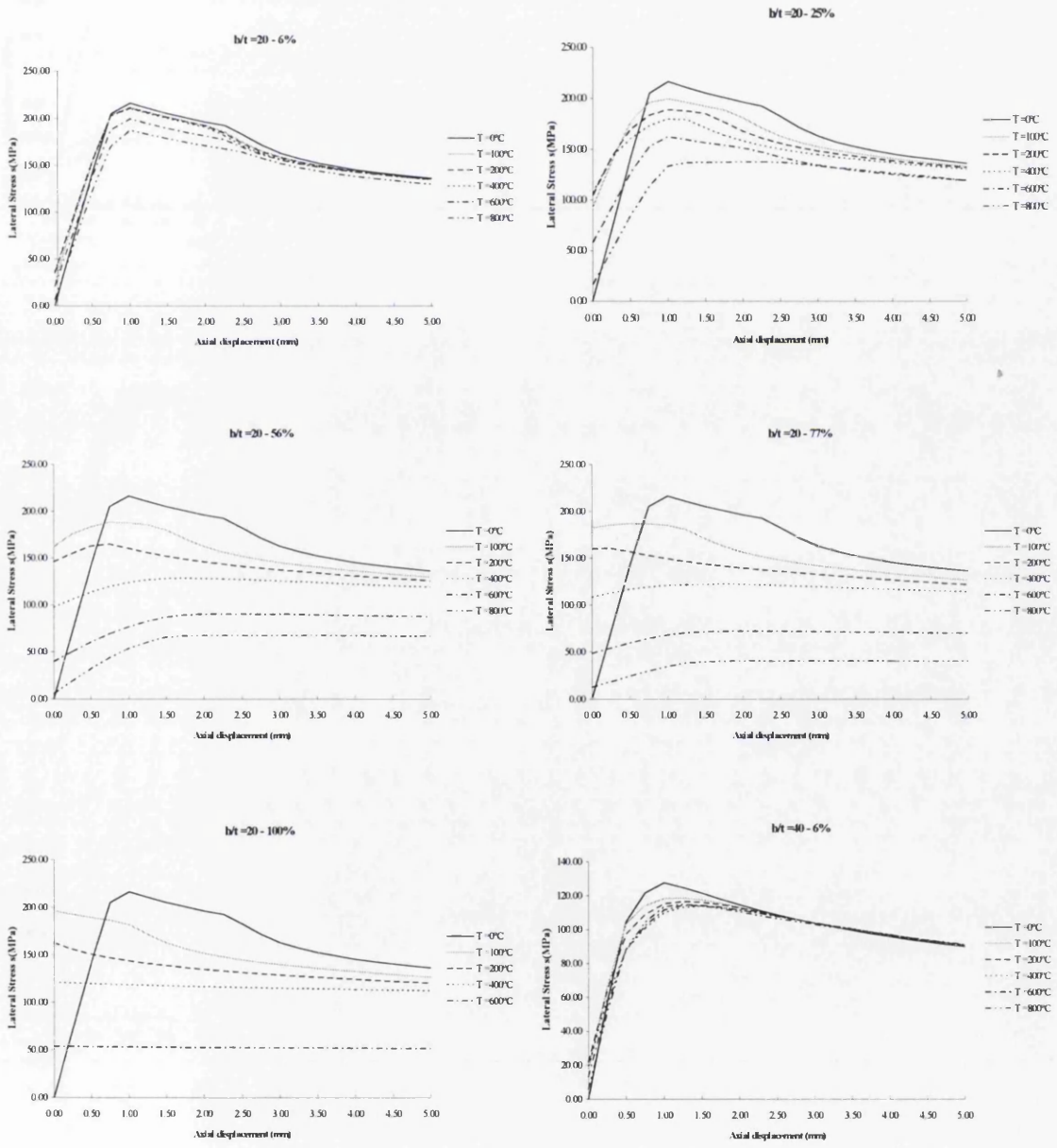

b/t =40 - 25%

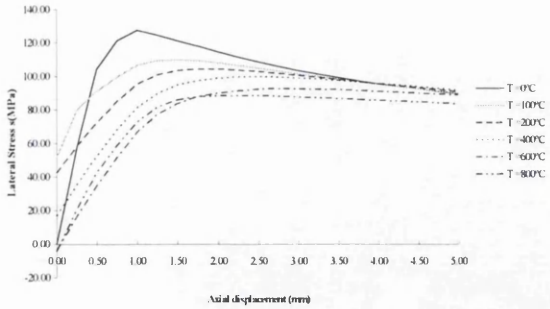

b/t =40 - 56%

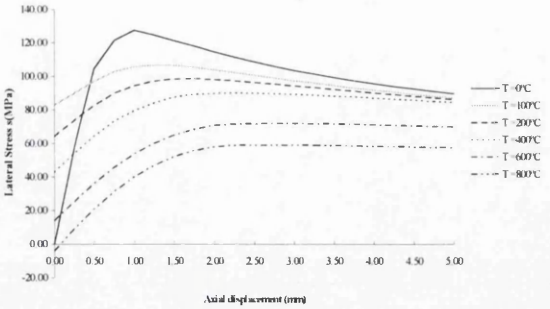

b/t =40 - 77%

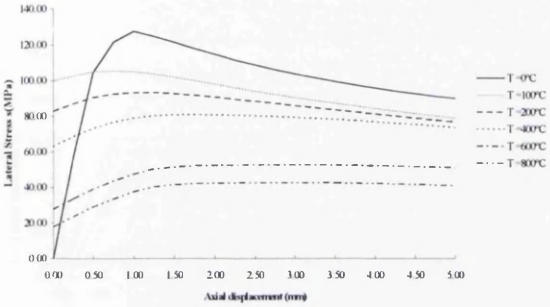

b/t =40 - 100%

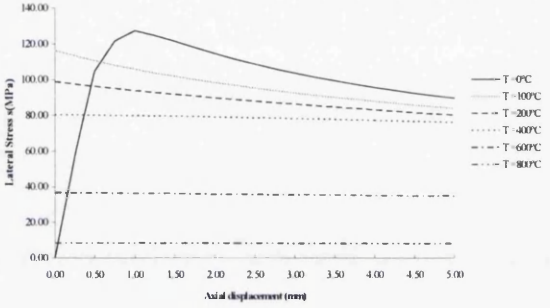

b/t =60 - 6%

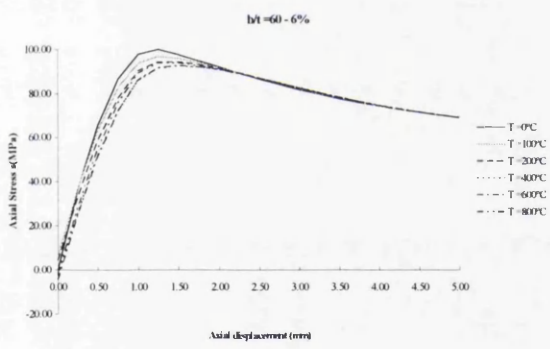

b/t =60 - 25%

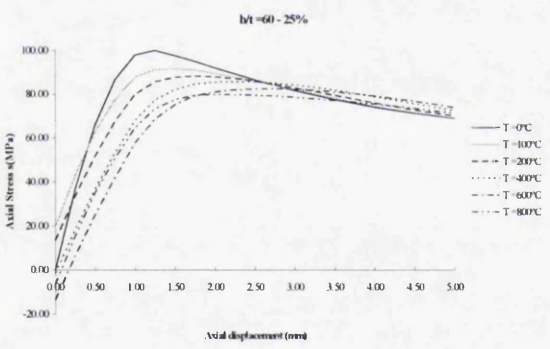

b/t =60 - 56%

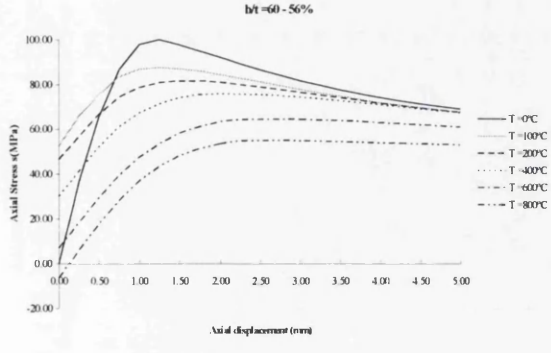

b/t =60 - 77%

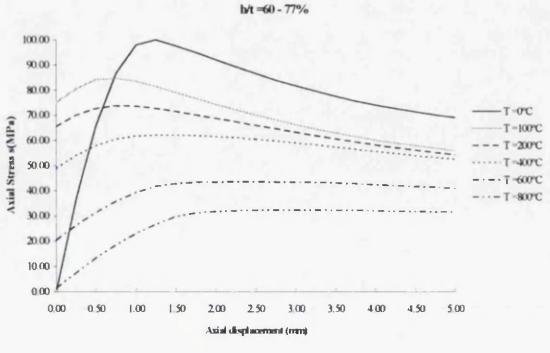

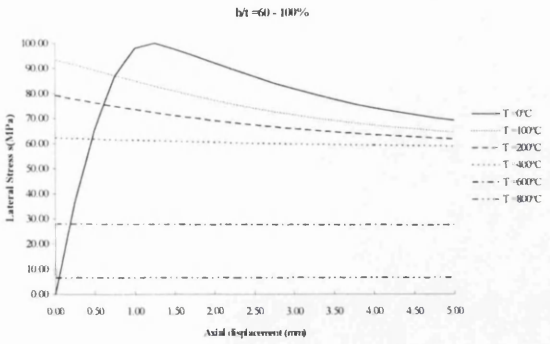
b/t =60 - 100%
Lateral Stress s(MPa)
Axial displacement (mm)
T =0°C
T =100°C
T =200°C
T =400°C
T =600°C
T =800°C

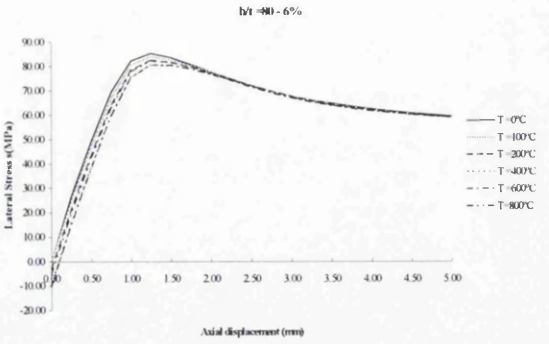
b/t =80 - 6%
Lateral Stress s(MPa)
Axial displacement (mm)
T =0°C
T =100°C
T =200°C
T =400°C
T =600°C
T =800°C

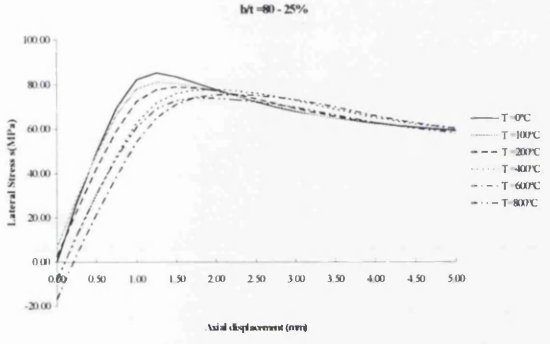
b/t =80 - 25%
Lateral Stress s(MPa)
Axial displacement (mm)
T =0°C
T =100°C
T =200°C
T =400°C
T =600°C
T =800°C

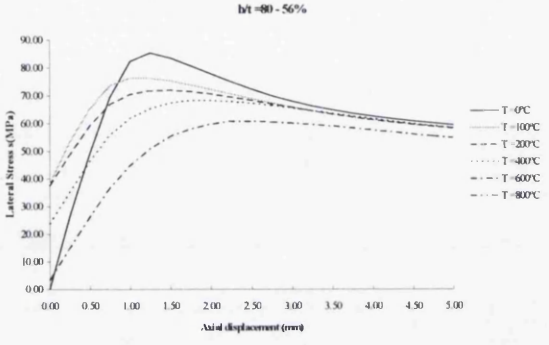
b/t =80 - 56%
Lateral Stress s(MPa)
Axial displacement (mm)
T =0°C
T =100°C
T =200°C
T =400°C
T =600°C
T =800°C

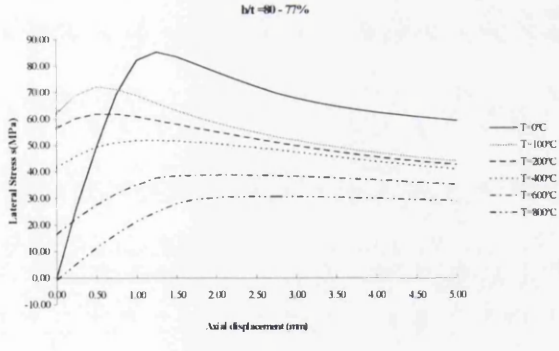
b/t =80 - 77%
Lateral Stress s(MPa)
Axial displacement (mm)
T =0°C
T =100°C
T =200°C
T =400°C
T =600°C
T =800°C

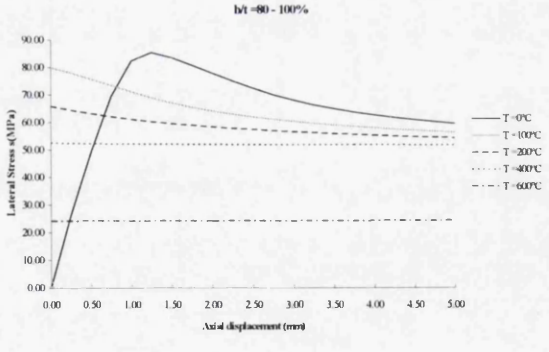
b/t =80 - 100%
Lateral Stress s(MPa)
Axial displacement (mm)
T =0°C
T =100°C
T =200°C
T =400°C
T =600°C

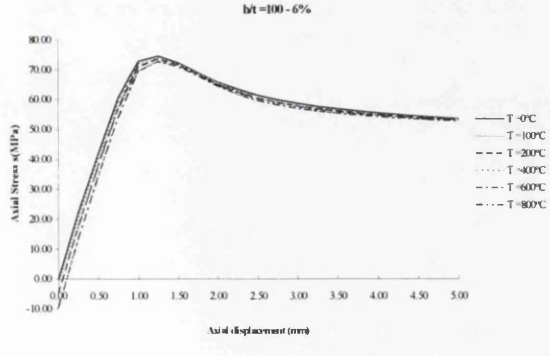
b/t =100 - 6%
Axial Stress s(MPa)
Axial displacement (mm)
T =0°C
T =100°C
T =200°C
T =400°C
T =600°C
T =800°C

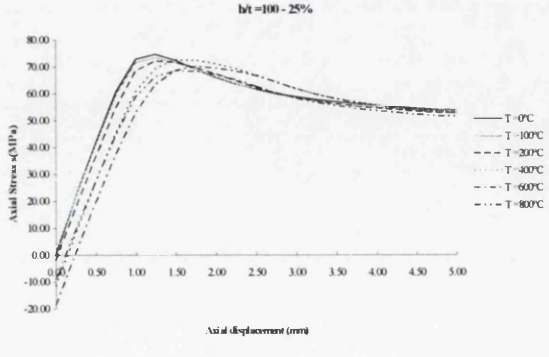
b/t =100 - 25%
Axial Stress s(MPa)
Axial displacement (mm)
T =0°C
T =100°C
T =200°C
T =400°C
T =600°C
T =800°C

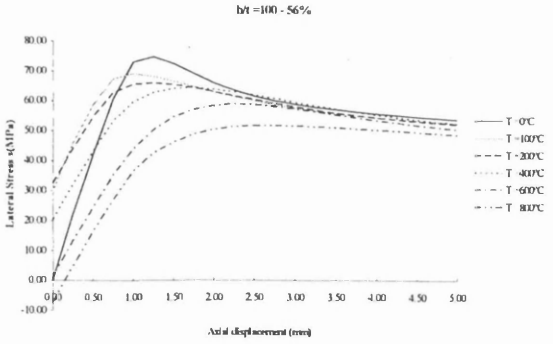
b/t =100 - 56%
Lateral Stress s(MPa)
Axial displacement (mm)
T =0°C
T =100°C
T =200°C
T =400°C
T =600°C
T =800°C

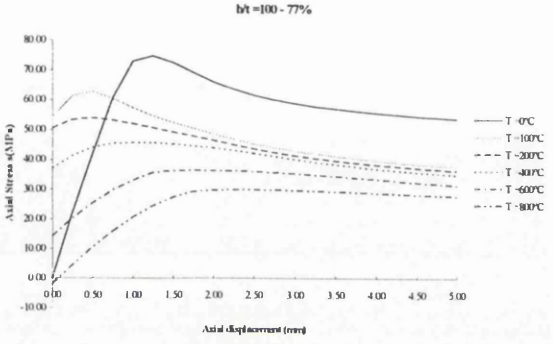
b/t =100 - 77%
Axial Stress s(MPa)
Axial displacement (mm)
T =0°C
T =100°C
T =200°C
T =400°C
T =600°C
T =800°C

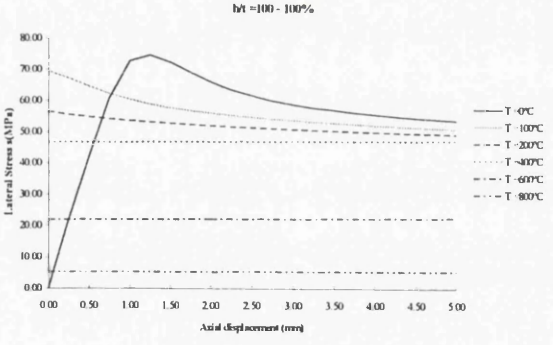
b/t =100 - 100%
Lateral Stress s(MPa)
Axial displacement (mm)
T =0°C
T =100°C
T =200°C
T =400°C
T =600°C
T =800°C

Normalised Collapse loads of plates under localised heat loads

b/t = 20					
T. (°C)	6%	25%	56%	77%	100%
0	1.00 (216.1 MPa)				
100	0.98	0.92	0.87	0.86	0.0
200	0.98	0.87	0.76	0.74	0.0
400	0.97	0.83	0.59	0.57	0.0
600	0.92	0.75	0.42	0.33	0.0
800	0.87	0.64	0.31	0.19	0.0

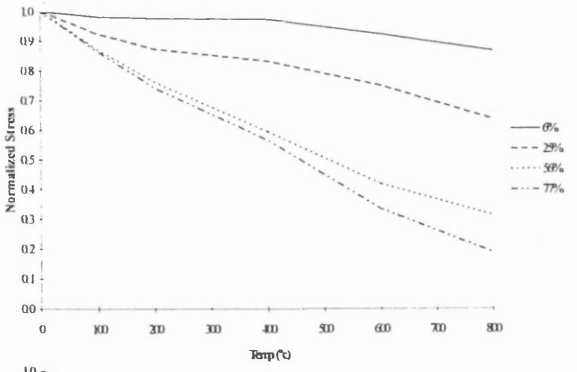

b/t = 40					
T. (°C)	6%	25%	56%	77%	100%
0	1.00 (127.5 MPa)				
100	0.93	0.86	0.84	0.83	0.0
200	0.91	0.82	0.77	0.73	0.0
400	0.89	0.78	0.71	0.63	0.0
600	0.89	0.73	0.56	0.41	0.0
800	0.90	0.69	0.46	0.26	0.0

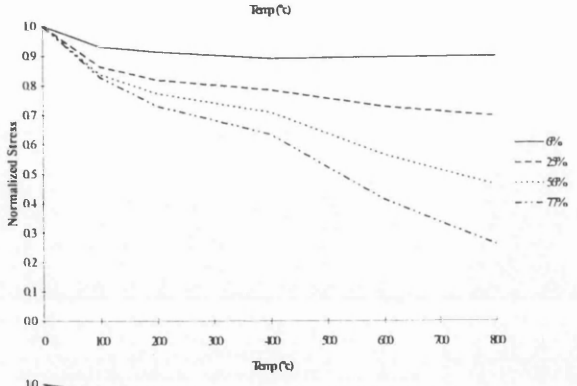

b/t = 60					
T. (°C)	6%	25%	56%	77%	100%
0	1.00 (100.0 MPa)				
100	0.97	0.92	0.88	0.85	0.0
200	0.94	0.88	0.82	0.74	0.0
400	0.93	0.86	0.77	0.62	0.0
600	0.93	0.83	0.65	0.44	0.0
800	0.94	0.80	0.55	0.32	0.0

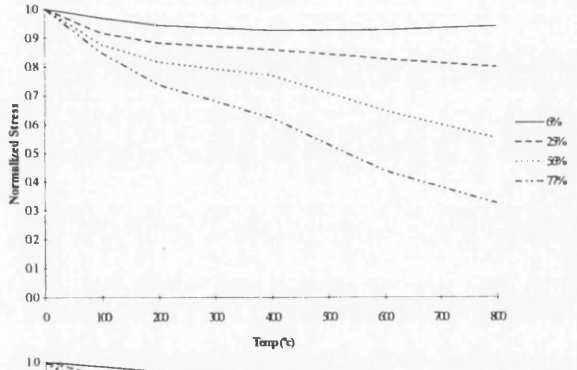

b/t = 80					
T. (°C)	6%	25%	56%	77%	100%
0	1.00 (85.3 MPa)				
100	0.98	0.95	0.89	0.85	0.0
200	0.97	0.92	0.84	0.72	0.0
400	0.94	0.91	0.80	0.61	0.0
600	0.94	0.89	0.71	0.46	0.0
800	0.96	0.87	0.62	0.36	0.0

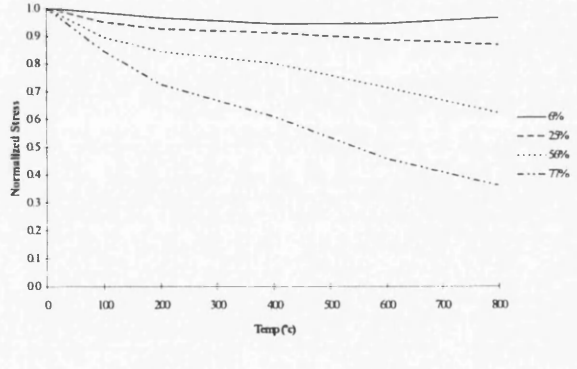

b/t = 100					
T. (°C)	6%	25%	56%	77%	100%
0	1.00 (74.6 MPa)				
100	0.99	0.98	0.93	0.84	0.0
200	0.99	0.97	0.88	0.72	0.0
400	0.98	0.97	0.86	0.61	0.0
600	0.97	0.94	0.79	0.49	0.0
800	0.99	0.92	0.69	0.40	0.0